UCLA
UCLA Electronic Theses and Dissertations

Title
The Role of the Huntingtin N17 Domain and its Modifications in Modulating Protein-Protein Interactions and Huntington's Disease Pathogenesis

Permalink
https://escholarship.org/uc/item/8ks1115h

Author
Greiner, Erin Rochelle

Publication Date
2012

Supplemental Material
https://escholarship.org/uc/item/8ks1115h#supplemental

Peer reviewed|Thesis/dissertation

eScholarship.org Powered by the California Digital Library
University of California

UNIVERSITY OF CALIFORNIA

Los Angeles

The Role of the Huntingtin N17 Domain and its Modifications in Modulating Protein-Protein Interactions and Huntington's Disease Pathogenesis

A dissertation submitted in partial satisfaction of the

requirements for the degree Doctor of Philosophy

in Biochemistry and Molecular Biology

by

Erin Rochelle Greiner

2012

ABSTRACT OF THE DISSERTATION

The Role of the Huntingtin N17 Domain and its Modifications in Modulating Protein-Protein Interactions and Huntington's Disease Pathogenesis

by

Erin Rochelle Greiner

Doctor of Philosophy in Biochemistry and Molecular Biology

University of California, Los Angeles, 2012

Professor Joseph A. Loo, Chair

Huntington's disease (HD) is an autosomal dominant, fatal neurodegenerative disorder characterized by movement disorders, cognitive impairment, and psychiatric deficits. Despite the discovery of the *huntingtin (htt)* gene more than 19 years ago, the biological function of normal and mutant huntingtin (Htt) protein still remain unclear in HD pathogenesis. We performed a spatiotemporal proteomic profiling of proteins co-immunoprecipitated with full-length Htt in BACHD and wildtype mouse brains to identify 747 Htt-interacting proteins that are highly enriched with known Htt interactors. In order to obtain an unbiased interpretation of this Htt interactome, we applied Weighted Gene Correlation Network Analyses (WGCNA) to define protein correlation relationships among the Htt interactors across 30 independent tissue (cortex, striatum, cerebellum), genotype (Wt *vs* BACHD), and age (2m *vs* 12m) conditions. The analysis established a verifiable rank of proteins based on their correlation strength with Htt, and also revealed the organization of Htt-interacting protein networks, with one such network containing Htt itself, 19 known Htt interactors, and 12 novel genetic modifiers of HD. Our study

demonstrates a novel systems biology approach to interpret *in vivo* proteomic interactomes derived from complex tissues such as the brain, and the value of such an approach in illuminating known and novel molecular targets for HD.

Recent studies suggest that the N-terminal 17 amino acids of Htt (N17 domain) immediately preceding the polyQ domain may constitute a critical domain for Htt function and HD pathogenesis. Biochemical characterization, proteomic profiling, and WGCNA network analysis of the full-length Htt interactomes from novel BAC transgenic mouse models of HD expressing human huntingtin with 97 glutamines, with 1) phosphomimetic Ser13 and Ser16 mutations (SD mice), 2) phosphoresistant Ser13 and Ser16 mutations (SA mice), and 3) deletion of Htt aa 2-16 (BACHD-ΔN17 mice) reveal critical insights into how this domain regulates Htt nuclear toxicity, protein aggregation, and protein-protein interactions.

The dissertation of Erin Rochelle Greiner is approved.

Catherine F. Clarke

James A. Wohlschlegel

Robert T. Clubb

X. William Yang

Joseph A. Loo, Committee Co-Chair

University of California, Los Angeles

2012

DEDICATION

This dissertation is dedicated to my loving parents, Mark and Deborah Greiner.

TABLE OF CONTENTS

LIST OF FIGURES ix

LIST OF TABLES xi

LIST OF SUPPLEMENTARY MATERIAL xii

ACKNOWLEDGMENTS xvi

VITA xx

CHAPTER 1: Introduction 1

1.1. Huntington's Disease 1

1.2. The Huntington Protein: Structure and Function 2

1.3. Huntingtin Post-Translational Modifications 4

1.4. Huntingtin Aggregation 6

1.5. Huntingtin N17 Domain 8

1.6. Summary 13

CHAPTER 2: Network Organization of the Full-length Huntingtin Interactome in Mammalian Brain 15

2.1. Abstract 16

2.2. Introduction 16

2.3. Results 18

2.3.1. Building an *In Vivo* Spatiotemporal Full-length Htt Interactome in BACHD and Wildtype Mouse Brains 18

2.3.2. The *In Vivo* fl-Htt Interactome Is Enriched With Known Htt Interactors and Proteins Involved in Pathways Relevant to HD 20

2.3.3. Semi-Quantitative Measures of Protein Abundance Allow Ranking of Candidate Interactors Based on Correlation With Fl-Htt 23

2.3.4. Weighted Gene Correlation Network Analyses (WGCNA) Organizes the *In Vivo* fl-Htt Interactome into Network 26

2.3.5. Enrichment of Htt Interactome Modules and Meta-Networks in Specific Sample Conditions 29

2.3.6. WGCNA Modules Are Related With Distinct Aspects of Htt Biology 31

2.3.7. Experimental Validation of Red Module Proteins as Huntingtin Interactors and Genetic Modifiers of Functional Deficit in a Fly Model of HD 36

2.4. Discussion 40

2.5. Experimental Methods 45

CHAPTER 3: Biochemical Characterization of BAC Transgenic Mouse Models of HD with Htt N17 Mutations 52

I: Biochemical Characterization of the SD and SA Mouse Models 53

II: Biochemical Characterization of the BACHD-ΔN17 and BACWT-ΔN17 Mouse Models 66

3.1. Introduction 66

3.2. Results 67

3.2.1. Generation and Characterization of BACHD-ΔN17 and BACWT-ΔN17 Models 67

3.2.2. BACHD-ΔN17 Transgene Can Rescue Murine htt Knockout Lethality 67

3.2.3. Western Blot Analysis of Relative Fl-mHtt Levels in BACHD-ΔN17 and BACWT-ΔN17 Mouse Models 69

3.2.4. Mutant Htt Nuclear Localization and Aggregation in BACHD-ΔN17 Mice 71

3.2.5. Solubilization of HMW mHtt Nuclear Aggregates in BACHD-ΔN17 Mice Reveals Accumulation of a ~55 to 71 kDa N-terminal mHtt Fragment 73

3.2.6. Mass Spectrometry Analysis of BACHD-ΔN17 mHtt HMW Species and Solubilized Fragments 76

3.3. Discussion 84

3.4. Experimental Methods 84

CHAPTER 4: Building the Huntingtin N17-Dependent and Phosphorylation-State-Dependent Proteomic Interactome 89

4.1. Introduction 89

4.2. Results 90

4.2.1. Confirmation of an N17-Dependent Interacting Protein: Tcp1/Cct1 90

4.2.2. Identification of Htt N17-Dependent Interacting Proteins 91

4.2.3. Building the Phosphorylation-State-Dependent Interactome 94

4.2.4. Comparison of Reproducible Htt Interactors Identified in the BACHD, BACHD-ΔN17, SD, and SA Mouse Models of HD Reveals Potential Interesting N17 Htt Biology 98

4.2.5. Functional Annotation of the N17- and Phosphorylation-State-Dependent Interactome 102

4.2.6. Preliminary Weighted Gene Correlation Network Analysis of the Htt N17- and Phosphorylation-State-Dependent Interactome 104

4.2.7. WGCNA Modules Reveal Distinct Htt N17 Biology 106

4.3. Discussion 108

4.4. Experimental Methods 110

CHAPTER 5: Conclusions and Future Directions 112

5.1. Overview 112

5.2. WGCNA of Fl-Htt Interactome Reveals New Htt Biology and Genetic Modifiers of HD 113

5.3. Phosphorylation at Htt Ser13 and Ser16 Acts as a Neuroprotective Molecular Switch *In Vivo* 114

5.4. The Htt N17 Domain Acts as a Cytoplasmic Retention Signal *In Vivo* 114

5.5. Htt N17- and Phosphorylation-State-Dependent Interactors Reveal New Htt N17 Biology and Disease Implications 116

5.6. Concluding Remarks 118

REFERENCES 120

LIST OF FIGURES

Figure 2.1. Generation and characterization of a full-length Htt interactome from wildtype and BACHD mouse brain 22

Figure 2.2. Brain regional and age-specific protein interactions revealed in Htt interactome 23

Figure 2.3. Unique peptide counts as a measure of relative protein abundance reveals proteins most correlated with Htt 25

Figure 2.4. Weighted Gene Correlation Network Analysis (WGCNA) of fl-Htt interactome 28

Figure 2.5. Top Htt-correlated modules reveal spatiotemporal protein relationships 30

Figure 2.6. Functional annotation of top Htt-correlated modules 35

Figure 2.7. Validation of Red Module proteins in Htt interactome uncovers Htt-interacting proteins in WT and BACHD mice and novel genetic modifiers of disease in a fly model of HD 38

Figure 3.1. Generation and initial biochemical characterization of BACHD-ΔN17 transgenic mice 68

Figure 3.2. Western blot analysis of the fl-mHtt levels in BACHD, BACHD-ΔN17-97Q-N, BACHD-ΔN17-97Q-L, BACHD-ΔN17-97Q-A, and BACWT-ΔN17-31Q-C transgenic mouse models of HD 70

Figure 3.3. Soluble fl-mHtt protein levels in BACHD and BACHD-ΔN17-97Q-N mice do not change between 2- and 12-months of age 71

Figure 3.4. Age-dependent N-terminal mHtt HMW nuclear accumulation in BACHDΔN17 mice 72

Figure 3.5. Solubilization treatments of BACHD-ΔN17 nuclear mHtt aggregates 74

Figure 3.6. Disaggregation of BACHD-ΔN17 nuclear aggregates with formic acid treatment results in a N-terminal ~55 to 71 kDa mHtt fragment 75

Figure 3.7. Isolation of mHtt HMW species from 10-month old wildtype and BACHD-ΔN17 pure cytosolic and nuclear fractions 77

Figure 3.8. Formic acid solubilization of mHtt HMW species from 10-month old wildtype and BACHD-ΔN17 pure nuclear fractions 78

Figure 3.9. Western blot analysis of 1C2-enrichment of N-terminal mHtt fragments in 12-month BACHD-ΔN17 mice 81

Figure 3.10. 1C2-enrichment of formic acid solubilized 12-month wildtype, BACHD, and BACHD-ΔN17 pure nuclear fractions 82

Figure 4.1. Validation of Tcp1 as an Htt N17-dependent interaction 90

Figure 4.2. A proteomic strategy to profile Htt N17-dependent interactions 92

Figure 4.3. Validation of Tuba1a as an N17-dependent Htt interactor *in vivo* 93

Figure 4.4. Htt N17-binding proteins identified by comparing BACHD anti-N17 and anti-HDB4E10 immunoprecipitations 94

Figure 4.5. Optimization of anti-HDB4E10 immunoprecipitation of fl-mHtt from SD and SA mouse models 96

Figure 4.6. Experimental overview of the Htt N17- and phosphorylation-state-dependent interactome 97

Figure 4.7. Venn diagram comparison of the reproducible fl-Htt interactors identified in the BACHD, BACHD-ΔN17, SD, and SA IP samples 98

Figure 4.8. IPA canonical pathway comparison of the reproducible proteins identified in the BACHD, BACHD-ΔN17, SA, and SD IP samples 103

Figure 4.9. Weighted Gene Correlation Network Analysis of the Htt N17- and phosphorylation-state-dependent interactome 105

Figure 5.1. A schematic diagram illustrating the putative neuroprotective or toxic roles of the Htt N17 domain in HD pathogenesis 119

LIST OF TABLES

Table 2.1. Summary of Top 50 Red Module Membership Proteins 39

Table 3.1. HMW proteins identified in the 10-month old wildtype and BACHD-ΔN17 cytosolic and nuclear fraction 77

Table 3.2. Human Htt tryptic peptides identified in solubilized BACHD-ΔN17 nuclear Fraction 79

Table 4.1. The most significant GO terms and IPA canonical pathways enriched for the reproducible proteins identified in the BACHD, BACHD-ΔN17, SA, SD, and WT IP samples 102

Table 4.2. A summary of the top IPA canonical pathways for each WGCNA color module and their potential implications in HD pathogenesis 107

LIST OF SUPPLEMENTARY MATERIALS

CHAPTER 2

Supplemental Table 2.1. The complete MudPIT mass spectrometry information of the 747 Htt-interacting proteins identified in this study. The IP conditions are represented by age (2 or 12-months), sample (BACHD = Q, wildtype = W, no Htt antibody IP control = Blk), brain region (cortex = Ctx, striatum = Str, cerebellum = Crb), and biological replicates (either 1 or 2).

Supplemental Table 2.2. A complete list of the huntingtin (Htt) peptides identified in this study. The human Htt peptides (HD) and mouse Htt peptides (HDh) are indicated. Htt peptides modified by post-translational modifications are listed in a separate tab.

Supplemental Table 2.3. A comparison of the Htt-interacting proteins identified in this study to curated Htt protein interactions and the ataxia protein interaction network.

Supplemental Table 2.4. Gene ontology (DAVID Bioinformatics Resource 6.7) was performed on the entire dataset of 747 Htt-interacting proteins identified in this study. The GO term enrichment with associated p-values (GO_Fat category) for biological processes, cellular compartments, and molecular functions are provided in separate tabs.

Supplemental Table 2.5. Ingenuity Pathway Analysis (IPA) was performed on the entire dataset of 747 Htt-interacting proteins identified in this study. The IPA canonical pathways, networks, functions, and molecules enriched in the dataset are provided in separate tabs.

Supplemental Table 2.6. A comparison of the brain regional (cortex, striatum, and cerebellum), age (2- and 12-months), and genotype (BACHD, wildtype, and no Htt antibody blank) specific Htt protein-protein interactions identified in this study.

Supplemental Table 2.7. The unique tryptic peptide counts of the 747 Htt-interacting proteins identified in this study across the 30 experimental IP conditions. Note the human Htt (HD), murine Htt (HDh), and combined Htt peptides in both human and murine (HTT) are indicated (751 total proteins in list; the HTT peptides are used for further analyses).

Supplemental Table 2.8. A Pearson's pairwise correlation was calculated for the 747 Htt-interacting proteins identified in this study to the Htt protein. A p-value significance is provided for each correlation value.

Supplemental Table 2.9. Our dataset of 747 Htt-interacting proteins were grouped into Htt correlation bins (each consisting of 125 proteins) and submitted to IPA. The top 125 proteins most significantly correlated with Htt are in bin 1 (1-125), whereas the proteins least correlated with Htt are in bin 6 (628-747). The IPA canonical pathways, networks, and functions enriched in each correlation bin are provided in separate tabs.

Supplemental Table 2.10. Weighted Correlation Network Analysis (WGCNA) of Htt interactome identifies eight modules of proteins with high topological overlap (blue, brown, cyan, green, navy, pink, red, and yellow). Proteins that were not assigned to any module were colored grey. The color module membership (MM) and color module membership p-values (Pvalue.MM) are provided for each of the 411 Htt-interacting proteins in the dataset (proteins had peptides identified in at least three independent IP conditions).

Supplemental Table 2.11. Correlation of WGCNA color modules with Htt protein. A p-value is provided for each correlation value.

Supplemental Table 2.12. A comparison of the previously identified Htt-interacting proteins present in each WGCNA color module. The names of the curated Htt proteins identified in each color module are listed in separate tabs.

Supplemental Table 2.13. IPA was performed on each WGCNA color module. The IPA canonical pathways, networks, and functions enriched in each color module are provided in separate tabs.

Supplemental Table 2.14. Gene ontology was performed on each WGCNA color module. The GO term enrichment (GO_Fat category) for biological processes, cellular compartments, and molecular functions are provided in separate tabs.

Supplemental Figure 2.1. Unique tryptic BSA peptide counts correlates well with relative protein abundance level in BACHD cortical lysate.

Supplemental Figure 2.2. Htt correlation versus WGCNA module membership values.

Supplemental Figure 2.3. Htt-containing Red Module is enriched for proteins involved in human neurological and genetic disorders.

Supplemental Figure 2.4. Validation of Red Module proteins in an HD fly model.

References for Table 2.1.

CHAPTER 3

Supplemental Material for Gu et al, 2009 manuscript

Supplemental Table 3.1. The complete list of peptides identified from the formic acid solubilized 12m WT and BACHD-ΔN17 pure nuclear fractions using the ProteinLynx Global Server (PLGS, version 2.4) and queried against the Swiss-Prot mouse database (with the addition of BSA, human huntingtin, and keratin sequences). Only proteins with a PLGS score >100 are listed.

Supplemental Table 3.2. The complete list of the proteins identified in the 1C2-enriched formic acid solubilized nuclear fractions as searched by PLGS. Only proteins with a PLGS score >100 are listed.

Supplemental Table 3.3. A comparison of the proteins identified in the formic acid solubilized 12m BACHD-ΔN17 nuclear fraction versus the proteins identified in the 1C2-enrichment formic acid solubilized 12m BACHD-ΔN17 nuclear fraction. 16 proteins are shared between the two datasets.

CHAPTER 4

Supplemental Table 4.1. The complete list of proteins (PLGS score > 100) and the number of unique tryptic peptides identified from each of the 20 IP (anti-Htt, HDB4E10) sample conditions performed to generate the Htt N17- and phosphorylation-state-dependent interactome. The IP conditions are represented by age (2 -months), sample (BACHD = B, wildtype = W, SAA = A, CH = D, BACHD-ΔN17 = NT), brain region (cortex = Ctx or striatum = Str) and biological replicates (either 1 or 2). Note that 1.6x more IP input was used to generate the 2-month SD cortical IP conditions (labeled 2m2D1Ctx and 2m2D2Ctx). The proteins with peptides identified in one, two, or three IP sample conditions are provided in separate tabs.

Supplemental Table 4.2. A comparison of the proteins identified in the anti-HDB4E10 2-month BACHD and BACHD-ΔN17 cortical samples to reveal Htt N17- and HDΔN17-specific interactors. As an example of how to classify a protein as a Htt N17 interactor, a protein must be identified in both BACHD IP conditions (>5 unique tryptic peptides/condition), and not identified in any of the HDΔN17 cortical IP conditions.

Supplemental Table 4.3. A comparison of the proteins identified in the anti-HDB4E10 2-month BACHD versus the anti-PW0595 (N17) 2-month BACHD cortical samples to reveal Htt N17- and more C-terminal Htt specific interactors. As an example of how to classify a protein as a Htt N17 interactor, a protein must be identified in both BACHD IP conditions (> 2 unique tryptic peptides/condition), and not identified in any of the anti-PW0595 cortical IP conditions.

Supplemental Table 4.4. A comparison of the reproducible 2-month anti-HDB4E10 WT, BACHD, SD, SA, and BACHD-ΔN17 cortical and striatal proteins identified in both biological duplicates, with a intersection and union provided for each dataset.

Supplemental Table 4.5. The highly reproducible 2-month anti-HDB4E10 WT, BACHD, SD, SA, and BACHD-ΔN17 proteins identified in both cortical and striatal biological duplicates (4 conditions). A comparison between the highly reproducible interactors from the BACHD, SD, SA, and BACHD-ΔN17 IP samples (with shared WT proteins removed) is also provided.

Supplemental Table 4.6. Gene ontology (DAVID Bioinformatics Resource 6.7) was performed on the highly reproducible 2-month anti-HDB4E10 WT, BACHD, SD, SA, and BACHD-ΔN17 proteins identified in this study. The GO term enrichment with associated p-values (GO_Fat category) for biological processes, cellular compartments, and molecular functions are provided in separate tabs.

Supplemental Table 4.7. Ingenuity Pathway Analysis (IPA) was performed on the highly reproducible 2-month anti-HDB4E10 WT, BACHD, SD, SA, and BACHD-ΔN17 proteins identified in this study. The IPA canonical pathways, networks, functions, transcription factors, and molecules enriched in the dataset are provided in separate tabs.

Supplemental Table 4.8. A Pearson's pairwise correlation was calculated for the 626 Htt-interacting proteins identified in this study to the Htt protein. A p-value significance is provided for each correlation value.

Supplemental Table 4.9. Weighted Correlation Network Analysis (WGCNA) of Htt interactome identifies eight modules of proteins with high topological overlap (black, blue, brown, green, navy, purple, red, yellow) for the 336 Htt-interacting proteins identified in at least three independent IP conditions. Proteins that were not assigned to any module were colored grey.

Supplemental Table 4.10. The WGCNA color module membership (MM) and color module membership p-values (MM.Pvalue) are provided for each of the 336 Htt-interacting proteins in the dataset (proteins had peptides identified in at least three independent IP conditions).

Supplemental Table 4.11. Gene ontology was performed on each WGCNA color module. The GO term enrichment (GO_Fat category) for biological processes, cellular compartments, and molecular functions for each color module are provided in separate tabs.

Supplemental Table 4.12. IPA was performed on each WGCNA color module. The IPA canonical pathways, networks, and functions enriched in each color module are provided in separate tabs.

Supplemental Figure 4.1. The complete WGCNA report including the cluster dendrograms, modueprotein (MP) meta-network organization, and heat map profiles for each color module.

ACKNOWLEDGEMENTS

I would first like to thank my parents, Mark and Deborah Greiner, and siblings, Katie and Patrick Greiner, for their continuous love and support throughout my Ph.D. career. They believed in me at times when I no longer believed in myself.

I would also like to thank my advisors, Dr. X. William Yang and Dr. Joseph A. Loo, for their continuous support throughout my doctoral training. I appreciate the overall experience and opportunities I've had here at UCLA, and hope that our careers continue to cross paths in the future.

William - thank you for always pushing me to reach my full potential. I am much more confident in myself than when I first started my graduate career, and know that you and your motivational speeches are the reason for this transformation. I will always admire your scientific inquiry and intensity, and look forward to the new findings that the Yang lab will discover. Thank you for providing me with an exciting thesis project and a stimulating laboratory environment to work in everyday.

Joe – thank you for always providing me with great scientific, career, and life advice. I always found that after meeting with you, I was more relaxed and focused to continue with my work. Thank you giving me the opportunity to help set-up and maintain the Waters Xevo-QTof MS instrument - I've gained hands-on experience and have learned so much from working with the Waters engineers. I would also like to thank Joe's other-half, Dr. Rachel Ogorzalek Loo – she is beyond knowledgeable and helpful, and can always bring a smile to my face!

Many thanks to my other committee members: Dr. James Wohlschlegel, Dr. Robert Clubb, and Dr. Catherine Clarke. Thank you for providing wonderful advice and guidance throughout my graduate career.

Thank you to Dr. Giovanni Coppola for his continuous support with our on-going WGCNA collaborations.

I would like to thank all the current and former members of the Loo laboratory, more specifically my friends and mentors Dr. Catherine S. Kaddis, Dr. Deborah Francoleon, Dr. Jimmy Ytterberg, Dr. Dyna Shirasaki, Dr. Scott Hsieh, Jonathan Erde, and Carly Ferguson.

I would especially like to thank Dr. Dyna Shirasaki, who pioneered the full-length huntingtin interactome study. I credit most of my skill-set and scientific training to Dyna. Her motivation and passion to work on Huntington's disease (HD) was the reason I joined the Loo laboratory in collaboration with the Yang laboratory. She fights for what she believes in, and taught me to stand up for myself.

I would like to thank all the current and former members of the Yang laboratory and "Team HD": Dr. Dyna Shirasaki, Dr. Tara M. Weitz, Dr. Mary Kay Lobo, Dr. Brian Wilburn, Dr. Michelle Gray, Dr. Xiaofeng Gu, Dr. Xiaohong Lu, Dr. Nan Wang, Dr. Yijun Cui, Chris Park, Jeff Cantle, Anthony Daggett, Susie Sandoval, and Richard Zhang. A very special thanks to our administrative assistants Margaret Chu, Helena Tran, and Binh Voung – your hard work does not go unnoticed. You each have made my graduate career a more memorable experience, and had the ability to make a workday no longer seem like work.

I would especially like to thank Dr. Xiaofeng Gu for creating and characterizing the SD, SA, BACHD-ΔN17, BACWT-ΔN17 mouse models. I have always considered Xiaofeng my “Lab Dad” – his patience, warm heart, kindness, and generosity have taught me how to be a better person both inside and outside of lab. He is the first person I say “Hi” to and the last person I say “Goodbye” to in lab, and he is the first person I want to share my exciting data with – I will miss working next to him everyday. We really did make a great team together.

Many thanks to Dr. Joan Steffan (UC Irvine) for providing the phosphospecific antibodies described Chapter 3. She has also been a wonderful mentor and friend throughout my graduate career.

I am beyond grateful for the wonderful girlfriends and support network I’ve made in the UCLA Biochemistry Department: Dr. Catherine S. Kaddis, Dr. Valerie Villareal, Dr. Tracy M. Blois, and Dr. Deborah Francoleon. Thank you for taking me under your wings and providing your constant friendship and support – I always looked forward to our lunches, coffee breaks, and daily interactions in Boyer Hall. You are all wonderful examples of women scientists, and what I strive to become.

I would not have been able to survive graduate school if it were not for my best friends outside of the laboratory: Colleen Burkett, Aimee Workman, Susie Sandoval, Erica Hess, and Biljana Rolih. Thank you for always being there to provide moral support, making me laugh, and being the much-needed distraction away from the laboratory! Weenie – I was dependent on your daily phone calls and texts; thank you for being my friend every step throughout this journey. Pony – I looked forward to our daily lunches at noon and coming into lab to work side-by-side my best friend.

I would like to formally acknowledge Nature Publishing Group for allowing me to reprint the *Nature Chemical Biology* article, “Huntington’s disease: Flipping a switch on huntingtin,” published on June 17, 2011 in Chapter 1 of my dissertation. I would also like to acknowledge Elsevier for providing copyright access to reprint the *Neuron* manuscript, “Serines 13 and 16 Are Critical Determinants of Full-Length Human Mutant Huntingtin Induced Pathogenesis in HD Mice,” published on December 24, 2009 in Chapter 3 of my dissertation.

Lastly, I would like to thank CHDI for funding the research performed in Chapter 4 and the 2011-2012 UCLA Dissertation Year Fellowship for supporting my final year of research.

VITA

2006	Bachelor of Arts, Chemistry College of Wooster Wooster, OH
2007-2010	Teaching Assistant Department of Chemistry & Biochemistry University of California, Los Angeles Los Angeles, CA
2007 – 2012	Graduate Research Assistant Department of Chemistry & Biochemistry & Semel Institute University of California, Los Angeles Los Angeles, CA

HONORS AND AWARDS

2011-2012	UCLA Dissertation Year Fellowship
2011	The Journal of Biological Chemistry Herbert Tabor Young Investigator Award (presented at the GRC CAG Triplet Repeat Disorders)
2003	College of Wooster Chemistry Department Award for Excellence in Undergraduate Organic Chemistry

PUBLICATIONS AND PRESENTATIONS

Journal Articles

1) Shirasaki DI#, Greiner ER#, Al-Ramahi I, Gray M, Boontheung P, Botas J, Coppola G, Horvath S, Loo JA*, Yang XW*. "Network Organization of the Huntingtin Proteomic Interactome in Mammalian Brain." In press at *Neuron*. (# authors contributed equally to this manuscript; * co-corresponding authors)

2) Greiner, ER & Yang, XY. "Huntington's disease: Flipping a switch on huntingtin." Nat Chem Biol 2011; 7: 412-4.

3) Wilburn B, Rudnicki DD, Zhao J, Weitz TM, Gu X, Greiner ER, Park CS, Wang N, Sopher BL, La Spada AR, Osmand A, Margolis RL, Sun YE, Yang XW. "An Antisense CAG Repeat Transcript at JPH3 Locus Mediates Expanded Polyglutamine Protein Toxicity in Huntington's Disease-Like 2 Mice." Neuron 2011; 70(3): 727-40.

4) Gu, X, Greiner ER, Mishra, R, Kodali R, Osmand A, Finkbeiner S, Steffan JS, Thompson LM, Wetzel R, Yang XW. "Serines 13 and 16 Are Critical Determinants of Full-Length Human Mutant Huntingtin Induced Disease Pathogenesis in HD Mice." Neuron 2009; 64(6): 828-40.

Oral Presentations

Shirasaki, DI, Greiner ER, Al-Ramahi I, Weitz TM, Gray M, Boontheung P, Botas J, Coppola G, Horvath S, Loo JA, Yang XW. "A Novel Systems Biology Approach to Uncover In Vivo Full-length Huntingtin Protein Interaction Networks in the Brain." Presented at the UCLA Department of Biological Chemist, Los Angeles, CA, April 30, 2010.

Shirasaki DI, Greiner ER, Al-Ramahi I, Weitz TM, Gray M, Boontheung P, Botas J, Coppola G, Horvath S, Loo JA, Yang XW. "A Novel Systems Biology Approach to Uncover In Vivo Full-length Huntingtin Protein Interaction Networks in the Brain." Presented at the UCLA Synapse to Circuit Journal Club, Los Angeles, CA, March 17, 2010.

Poster Presentations (presenter underlined)

Greiner ER, Shirasaki DI, Al-Ramahi I, Gray M, Gu, X, Boontheung P, Botas J, Coppola G, Horvath S, Loo JA, Yang XW. "Network Organization of the Full-Lenth Huntingtin Interactome & Preliminary Investigation of the Huntingtin N17-Dependent Proteomic Interactome in Mammalian Brain." Presented at the CHDI 7th Annual HD Therapeutics Conference, Palm Springs, CA, Feb 27-Mar 1, 2012.

Greiner ER, Shirasaki DI, Ramahi I, Boontheung P, Gray M, Botas J, Coppola G, Horvath S, Loo JA, Yang XW. "Deciphering the In Vivo Huntingtin Interactome in the Mammalian Brain by Affinity-Purification-Mass Spectrometry and Weighted Gene Correlation Network Analysis." Presented at the Gordon Research Conference CAG Triplet Repeat Disorders Conference, Barga (Lucca), Italy, Jun 5-10, 2011.

Greiner ER, Yang XW, Loo JA. "Evaluation of Data-Dependent versus Data-Independent Proteomic Approaches for Identification of Huntingtin Protein Networks in BACHD Mice." Presented at the 58th ASMS Conference on Mass Spectrometry and Allied Topics, Salt Lake City, UT, May 23-27, 2010.

Shirasaki DI, Greiner ER, Al-Ramahi I, Weitz TM, Gray M, Boontheung P, Botas J, Coppola G, Horvath S, Loo JA, Yang XW. "A Novel Systems Biology Approach to Uncover In Vivo Full-length Huntingtin Protein Interaction Networks in the Brain." Presented at the CHDI 5th Annual HD Therapeutics Conference, Palm Springs, CA, Feb 8-11, 2010.

Shirasaki, DI, Greiner ER, Boontheung P, Horvath S, Yang XW, Loo JA. "An Integrative Proteomic Approach to Identify Huntingtin Protein Networks Using a Novel BAC Transgenic Mouse Model of Huntington's Disease." Presented at the 57th ASMS Conference on Mass Spectrometry and Allied Topics, Philadelphia, PA, May 31-Jun 4, 2009.

CHAPTER 1

Introduction

This chapter includes the reprint of the News and Views article:
Greiner, ER & Yang, XY. (2011). Huntington's disease: Flipping a switch on huntingtin. Nat Chem Biol *7*, 412-414.

1.1. Huntington's Disease

Huntington's disease (HD) is one of the most common inherited fatal, autosomal dominant neurodegenerative disorders affecting 30,000 Americans with another 150,000 who are at risk (The Huntington's Disease Collaborative Research Group, 1993). Currently there is no cure or treatment for this devastating disease. HD manifests as a triad of clinical symptoms including involuntary movements (*e.g.,* chorea, gait abnormalities), personality changes, and cognitive deficits (Bates and Harper, 2002). The most common age of adult-onset HD is between 30-50 years of age, after which the disease becomes progressively worse for 10-20 years until death.

HD is one of nine inherited neurodegenerative diseases caused by expansion of CAG encoding for a polyQ tract, including dentatorubralpallidoluysianatrophy (DRPLA), spinobulbar muscular atrophy (SBMA), and spinocerebellar ataxia (SCA) types 1–3, 6, 7 and 17 (Zoghbi and Orr, 2000). HD is caused by a CAG repeat expansion in exon 1 of the IT15 or 'huntingtin' gene, which is translated into an elongated polyglutamine (polyQ) tract near the N-terminus of the huntingtin protein (Htt). Individuals with less than 35 CAG repeats remain unaffected, while those with greater than 40 CAG repeats will develop HD within a normal lifespan. There is an inverse correlation between the age at onset in HD patients and the number of glutamines, as

individuals with greater than 70 CAG repeats are typically associated with juvenile-onset HD (The Huntington's Disease Collaborative Research Group, 1993). Even though the mutant Htt (mHtt) protein is ubiquitously expressed in all tissues, HD neuropathology is characterized by selective degeneration of the pyramidal neurons in the cortex and the medium spiny neurons in the stratum (Vonsattel and Difiglia, 1998). While the mechanism of mHtt selective neurodegeneration is poorly understood, several studies suggest that N-terminal mHtt fragments accumulate in nuclear aggregates in these affected regions to alter transcription and induce neuronal dysfunction (Davies et al., 1997; Difiglia et al., 1997).

1.2. The Huntingtin Protein: Structure and Function

Human huntingtin is a very large, single chain 350 kDa protein comprised of 3144 amino acids. Htt consists of 67 exons, in which exon-1 (aa 1-82) contains the N17 domain, polyQ mutation, and polyproline regions. The N-terminus of Htt consists of 17 highly conserved amino acids in vertebrates and has been termed the Htt N17 domain (Atwal et al., 2007; Rockabrand et al., 2007). The polyQ domain begins at the 18^{th} amino acid and is directly followed by two proline-rich domains, which consist of 11 and 10 prolines. Unlike the N17 domain, the polyQ and polyP domains are not highly conserved across vertebrate species. For example, human Htt typically has 11-34 glutamines in the polyQ domain, whereas zebrafish and pufferfish Htt only have 4 glutamines and lack a polyP region (Harjes and Wanker, 2003).

The polyproline (polyP) region of Htt is known to be important in the gain of toxic mHtt function as it is a binding sequence capable of interactions with proteins that have Src homology 3 (SH3) (Liu et al, 1997; Sittler et al., 1998) and WW domains (Faber et al., 1998; Passani et al., 2000). Targeted intrabody therapies against the proline-rich domain were able to reduce mHtt toxicity and aggregation in a mHtt exon-1 model *in vitro* (Southwell et al., 2008). It is proposed that the polyP domain is able to provide structural stability to the N-terminal region of Htt

through its abnormal binding protein interactions.

A highly conserved region further downstream the Htt protein starting at amino acid 205 are four clusters of structural HEAT repeats (named according to first four proteins identified with this motif; **H**tt, **E**longation factor 3, regulatory A subunit of protein phosphatase 2**A**, and **T**OR1) (Andrade and Bork, 1995). HEAT repeats are approximately 40 amino acids with a helix-loop-helix motif and serve as a platform for a variety of Htt protein-protein interactions.

Considering the Htt protein is ubiquitously expressed in all tissues and has been associated with nearly all of the organelles in the cell including the nucleus, mitochondria, Golgi complex, microtubules, and vesicles (Caviston et al, 2007; Choo et al, 2004; Hoffner et al, 2002), it has been difficult for the HD field to define the exact biological function of normal and mutant Htt. There is sufficient evidence to suggest HD results from both a loss of normal Htt function, and a gain of mutant Htt toxicity. Normal Htt plays an essential role in embryonic development, since homozygous knockout mice die at embryonic day 7.5 (Zeitlin et al., 1995). Furthermore, conditional deletion of Htt from the forebrain and testis in adult mice led to late-onset degeneration in these tissues (Dragatsis et al., 2000). HD, as a disease with almost pure genetic dominance, is presumed to result from a gain of toxic mutant Htt function. This is evident in mouse models expressing N-terminal mutant Htt fragments or full-length mutant Htt (fl-mHtt), which exhibit HD neuropathology and symptoms even in the presence of endogenous Htt (Davies et al., 1997; Gray et al., 2008; Hodgson et al., 1999; G. Schilling et al., 1999).

To better understand the function of Htt, many studies have identified proteins that interact with Htt using yeast-two hybrid experiments, affinity chromatography, and immunoprecipitation experiments (Goehler et al., 2004; Harjes and Wanker, 2003; Kaltenbach et al., 2007). These studies have provided significant insight into the role of Htt as a scaffolding protein involved in intracellular signaling, trafficking, apoptosis, gene transcription, endocytosis, and metabolism. A caveat to the above studies is that Htt-interacting proteins were identified

using *ex-vivo* methods and an N-terminal fragment of Htt as bait. In Chapter 2 of my dissertation, I present a novel spatiotemporal proteomic approach to profile endogenous full-length Htt interactors from mammalian brain.

1.3. Huntingtin Post-Translational Modifications

Previous studies have demonstrated that Htt undergoes numerous post-translational modifications (PTMs) including phosphorylation (Aiken et al., 2009; Humbert et al., 2002; Rangone et al., 2004; Schilling et al., 2006; Thompson et al., 2009), acetylation (Cong et al., 2011; Jeong et al., 2009), ubiquitination (Kalchman et al., 1996), SUMOylation (Steffan et al., 2004), palmitoylation (Huang et al., 2004), and proteolysis (Graham et al., 2006; Kim et al., 2001; Lunkes et al., 2002; Mende-Mueller et al., 2001; Wellington et al., 2002), and these have been shown to regulate mHtt localization, conformation, and toxicity.

Ubiquitinated mutant Htt has been associated with nuclear accumulation and aggregation in both human and HD mouse brain (Davies et al., 1997; Difiglia et al., 1997), and is considered a common protective mechanism in polyQ disorders to target the mutant protein to the proteasome for degradation. However, the addition of SUMO-1 (small ubiquitin-like modifiers) to Htt has been shown to stabilize the mutant protein and prevent proteasomal degradation to result in increased aggregation, nuclear localization, and toxicity (Steffan et al., 2004). The Htt protein can undergo both SUMOylation and ubiquitination at lysines 6, 9, and 15, where SUMOylation exacerbates Htt exon-1 neurodegeneration and ubiquitination abrogates Htt exon-1 neurodegeneration in a fly model of HD (Steffan et al., 2004). The ubiquitin ligase E3-25K has been shown to interact with Htt and mediate Htt ubiquitination to direct mHtt for degradation by the proteasome (Kalchman et al., 1996), whereas the striatal-enriched E3 ligase Rhes catalyzes the SUMOylation of Htt at K6, K9, and K15 to increase mHtt nuclear localization and cytotoxicity (Subramaniam et al., 2009). These two studies reveal possible mechanistic and

therapeutic insights into balancing the opposing effects of these PTMs.

Htt has several known sites of phosphorylation including: T3, S13, and S16 at the N-terminus, S421, S434, S536, S1181, S1201, S2076, S2653, and S2657 (Aiken et al., 2009; Humbert et al., 2002; Rangone et al., 2004; Schilling et al., 2006; Thompson et al., 2009). At all known sites, Htt phosphorylation is associated with reduced mutant Htt toxicity and neuroprotective effects. Chapter 3 of my dissertation will focus on the neuroprotective effects of "mimicking" Ser13 and Ser16 phosphorylation *in vivo* (Gu et al., 2009). Acetylation of Htt at K444 has recently been identified as a PTM that facilitates mHtt clearance by trafficking Htt to autophagosomes for degradation (Jeong et al., 2009). In addition, Htt can be palmitolyated at C214 by the palmitoyl transferases HIP14 and HIP14L to enhance membrane association, and a mutation rendering the protein resistant to palmitoylation was shown to increase Htt nuclear localization and toxicity (Yanai et al., 2006).

Htt is also subject to proteolytic cleavage events by a number of caspases, calpains, matrix metalloproteinase 10 (MMP-10), and cathepsins. Cleavage of Htt into small N-terminal fragments is believed to contribute to HD pathogenesis. Htt caspase cleavage sites include caspase-3 (D513, D552), caspase-2 (D552), and caspase-6 (D586) (Wellington and Hayden, 2000). The most well characterized cleavage site of Htt is at amino acid 586 mediated by caspase-6. A caspase-6 resistant mutation in the YAC128 mouse model ameliorates HD phenotype (Graham et al., 2006), while a transgenic mouse model expressing N-terminal Htt (N586-82Q) has a progressive behavioral and neuropathological HD phenotype (Waldron-Roby et al., 2012). These *in vivo* studies suggest caspase-6 is a critical cleavage site in the generation of a toxic N-terminal fragment of Htt. Calpains (1, 5, 7, and 10) have also been shown to cleave Htt generating small N-terminal fragments, and inhibition of calpain cleavage at Htt amino acids 469 and 536 was able to reduce toxicity in cell culture models (Gafni et al., 2004). The matrix metalloproteinase 10 (MMP-10) has recently been linked to cleavage at Htt

amino acid 402, and knock-down of MMP-10 results in rescued striatal neurons from mHtt-induced cell death (J. P. Miller et al., 2010). Lastly, the aspartyl proteases cathepsins are responsible for Htt cleavage at the following sites: cp-A (104-114), cp-B (205-214), cp-1 (81-129), and cp-2 (R167) (Kim et al., 2006; Lunkes et al., 2002). These very small N-terminal fragments of Htt are the major component of nuclear and cytoplasmic inclusions found in post-mortem HD brain tissue, and R6/2 and N171-82Q mouse models (Difiglia et al., 1997; Landles et al., 2010; Schilling et al., 2007).

1.4. Huntingtin Aggregation

A biochemical hallmark of HD pathogenesis is the presence of intranuclear inclusion bodies, which are large insoluble aggregates of mutant Htt in neuronal nuclei that have been observed in mammalian cell lines, in fragment and full-length transgenic Htt mouse models, and in post-mortem brain tissues from HD patients (Davies et al., 1997; Difiglia et al., 1997; Gray et al., 2008; Lunkes and Mandel, 1998). Inclusions containing mutant Htt are present in brain regions that degenerate (cortex and striatum), but this does not directly correspond to the neurons that degenerate (Kuemmerle et al., 1999; Vonsattel et al., 1985). While it remains under debate whether the mutant Htt aggregates are the toxic species in HD pathogenesis, a neutral byproduct of the disease, or rather a neuroprotective mechanism - the formation of insoluble mutant Htt aggregates is a marker of neuronal dysfunction leading to HD pathology (Gutekunst et al., 1999).

The current hypothesis in HD is that an N-terminal fragment of Htt is the “pathogenic or toxic” species that can translocate into the nucleus, form nuclear inclusions, and cause neuronal dysfunction based on the following lines of evidence: 1) nuclear inclusions in the HD patient brains are only detected by N-terminal Htt antibodies (close to the polyQ domain), and not by C-terminal Htt antibodies (Difiglia et al., 1997; Sieradzan et al., 1999), 2) N-terminal fragments of

Htt aggregate much more readily *in vitro* (Scherzinger et al., 1997) and in cell models (Martindale et al., 1998), 3) mouse models expressing exon-1 alone (R6/2) (Mangiarini et al., 1996) or a N-terminal fragment of Htt (N171-82Q) recapitulate several key aspects of HD pathogenesis (Schilling et al., 1999), and 4) Htt contains multiple N-terminal proteolytic cleavage sites to generate small N-terminal pathogenic fragments that have been identified in HD post-mortem brain and other HD mouse model systems (Kim et al., 2006; Lunkes et al., 2002; Ratovitski et al., 2009; 2007; Schilling et al., 2007; Tanaka et al., 2006). The smallest fragment that has been identified is Htt exon-1 Htt, which accumulates in neuronal nuclei in the form of a detergent insoluble high molecular weight species (Landles et al., 2010). In Chapter 3 of my dissertation, I reveal critical insight into the N-terminal fragment mHtt nuclear aggregation process by performing biochemical characterization on the novel BACHD-ΔN17 mouse model of HD.

Considerable evidence supports that the polyQ expansion in the Htt protein results in a toxic, more compact β-sheet protein conformation, which acts as a precursor to trigger a pathogenic aggregation cascade during disease (soluble monomer → abnormal conformation → oligomers → protofibrils → fibrils → toxic amyloid fibrils) (Ross and Poirier, 2004; Wetzel, 2012). To gain insight into the mechanism of mHtt aggregation, many studies have identified proteins sequestered in the polyQ aggregates (Doi et al., 2004; 2008; Mitsui et al., 2002; Suhr et al., 2001). These aggregate-interacting proteins (AIPs) include ubiquitin, members of the heat shock proteins (Hsp) 40, 70, and 90 families, transcription factors, and components of the ubiquitin-proteasome system. Considering that many of these proteins are involved with protein folding, degradation, and maintaining homeostasis, the depletion of these proteins from the cell may enhance HD pathology (Sherman and Goldberg, 2001). In Chapter 3 of my dissertation, I use a proteomic strategy to identify mHtt nuclear aggregates and AIPs from BACHD-ΔN17 mouse brains.

1.5. Huntingtin N17 Domain

One approach to study the pathogenesis of HD and other polyQ disorders is to identify other critical protein contexts beyond the polyQ domain (*e.g.,* structural elements or PTMs) that can modify or even abolish the disease pathogenesis *in vivo* (Orr and Zoghbi, 2007). On the 3144 amino acid Htt protein, the highly conserved N-terminal 17 amino acid residues (N17 domain) has recently been described as a Htt cytoplasmic-retention signal that targets Htt to membranous structures including the endoplasmic reticulum (ER), Golgi, mitochondria, endosomes, and autophagic vesicles (Atwal et al., 2007; Rockabrand et al., 2007). The N17 domain is subject to many PTMs and is modified by SUMOylation (Steffan et al., 2004), phosphorylation (Aiken et al., 2009; Thompson et al., 2009), and acetylation (Thompson et al., 2009), all of which modulate the toxicity of mHtt. Chapter 3 of my dissertation provides *in vivo* evidence that phosphomimetic mutations at Serines 13 and 16 of N17 domain can abolish fl-mHtt induced disease pathogenesis in BAC mice, and phosphomimetic mutants can block mHtt aggregation *in vitro* (Gu et al., 2009). A recent high-content screening for kinase inhibitors that modulate Htt N17 phosphorylation, localization, and toxicity revealed casein kinase-2 (CK2) inhibitors as a potential small-molecule therapeutic target for HD (Atwal et al., 2011). A reprint of the News & Views review article highlighting this study is shown below (Greiner and Yang, 2011).

Converging evidence shows that the alpha-helical structure of the Htt N17 domain can dramatically accelerate mHtt aggregation (Atwal et al., 2007; Tam et al., 2009; Thakur et al., 2009). In the context of mHtt fragments, deletion of this N17 domain, disruption of the alpha-helical structure (*i.e.,* M8P mutation), or certain deleterious PTMs of this domain (*i.e.,* SUMOylation) lead to enhanced nuclear entry and toxicity in cellular and fly models of HD (Atwal et al., 2007; Rockabrand et al., 2007; Steffan et al., 2004). One protein thus far (*i.e.,* chaperonin Tcp1) has been shown to bind to the Htt N17 domain and suppress mHtt fragment

aggregation (Tam et al., 2009). Furthermore, N-terminal Htt intrabody therapies that target this domain have shown to reduce mHtt aggregation *in vitro* (Lecerf et al., 2001) and improve HD pathology in a toxic N-terminal Htt fragment mouse model of HD (R6/1) (Snyder-Keller et al., 2010). However, whether N17 could mediate mHtt cytoplasmic retention in a mammalian model and the significance of such function in mHtt-induced disease pathogenesis remains elusive. In Chapter 3 of my dissertation, I perform biochemical characterization on the novel BACHD-ΔN17 mouse model of HD, which strives to address the function of the N17 domain *in vivo*.

domain connected by a highly conserved hydrophobic linker. Although the central role of this linker in coupling the activity of the nucleotide-binding and substrate-binding sites has been know for a long time, the detailed mechanism by which it operates has remained elusive. Through the work of Zhuravleva and Gierasch, part of the story is now becoming clear. By a careful analysis of the chemical shift changes observed in a series of constructs comprising the nucleotide-binding domain and the flexible linker, they identified a group of residues that make up an allosteric network extending from the ATP binding site in the nucleotide-binding domain to the interdomain linker[7]. Although further studies will be needed to complete the picture for full-length Hsp70, the work by Zhuravleva and Gierasch[7] offers a vivid illustration of the great potential of chemical-shift based approaches.

In a related study, Melacini and co-workers[8] introduced a method in which coupled residues were identified through a covariance analysis of the chemical shift changes caused by a series of covalently modified analogs of the allosteric effectors. They illustrated this approach on the multidomain protein EPAC, which is a guanine nucleotide exchange factor representative of a class of proteins that function as molecular switches and signal transducers, finding also in this case that the change in the state of the protein is associated with a modulation in the structure and dynamics of residues within an extended network. The nub of the method is to identify residue pairs that, following a perturbation, show correlated chemical shifts changes, and then to cluster the residues in groups to obtain the cooperative units that are responsible for giving rise to an allosteric transition. Application of this approach to other systems will undoubtedly enable optimization of technical aspects of the method and full exploitation of the opportunities it offers.

These two studies[7,8], together with a series of other recent equally notable ones[3–6], show that the goal of accurately describing allosteric mechanisms can be achieved by adopting the view that proteins constantly undergo conformational fluctuations and that such fluctuations can be modulated through specific binding events. Indeed, the accumulated evidence indicates that many aspects of protein behavior, including folding, function and regulation can be effectively explained by statistical theories. This type of conceptual framework in combination with new methods that are emerging in NMR spectroscopy[3–8], in particular those that enable the use of chemical shifts for structure determination[9,10], provides excellent chances for obtaining detailed descriptions of the ways in which proteins are regulated. These advances will increase our understanding of at least some of the processes responsible for protein homeostasis and create new opportunities to target proteins for therapeutic intervention. ■

Michele Vendruscolo is at the Department of Chemistry, University of Cambridge, Cambridge, UK.
e-mail: mv245@cam.ac.uk

References
1. Monod, J. *et al. J. Mol. Biol.* **12**, 88–118 (1965).
2. Cui, Q. & Karplus, M. *Protein Sci.* **17**, 1295–1307 (2008).
3. Boehr, D.D. *et al. Nat. Chem. Biol.* **5**, 789–796 (2009).
4. Kalodimos, C.G. *Protein Sci.* **20**, 773–782 (2011).
5. Mittermaier, A. & Kay, L.E. *Science* **312**, 224–228 (2006).
6. Masterson, L.R. *et al. Nat. Chem. Biol.* **6**, 821–828 (2010).
7. Zhuravleva, A. & Gierasch, L.M. *Proc. Natl. Acad. Sci. USA* **108**, 6987–6992 (2011).
8. Selvaratnam, R. *et al. Proc. Natl. Acad. Sci. USA* **108**, 6133–6138 (2011).
9. Cavalli, A. *et al. Proc. Natl. Acad. Sci. USA* **104**, 9615–9620 (2007).
10. Shen, Y. *et al. Proc. Natl. Acad. Sci. USA* **105**, 4685–4690 (2008).

Competing financial interests
The author declares no competing financial interests.

© 2011 Nature America, Inc. All rights reserved.

HUNTINGTON'S DISEASE

Flipping a switch on huntingtin

Phosphomimetic mutations at huntingtin (Htt) Ser13 and Ser16 within the conserved N-terminal 17-amino-acid domain profoundly suppresses its toxicity in cell and mouse models of Huntington's disease. New research reveals that cell stress acts as a stimulus for double phosphorylation of endogenous Htt, causing its nuclear translocation, and shows that certain chemicals can target such molecular processes in Huntington's disease cell models.

Erin R Greiner & X William Yang

Huntington's disease is caused by the expansion of a polyglutamine (polyQ) repeat near the amino terminus of the mutant huntingtin (mHtt) protein. Despite its monogenetic etiology, the precise molecular pathogenic mechanisms remain poorly understood, and disease-modifying therapies are not yet available. Recent converging evidence reveals that an evolutionarily conserved N terminus of Htt, consisting of only 17 amino acids (N17), is a substantial contributor to a variety of mHtt-associated properties, from subcellular localization and aggregation to toxicity in cells and mice. The impact of the N17 domain in Huntington's disease pathogenesis was highlighted by recent findings that mimicry of physiological phosphorylation at Ser13 and Ser16 could suppress mHtt toxicity in Huntington's disease cells and mice[1,2]. However, the physiological pathways that lead to N17 phosphorylation and the potential for such pathways to be modified by small chemicals remain unclear. In this issue, Atwal *et al.*[3] provide evidence that cellular stress leads to Htt Ser13 and Ser16 double phosphorylation, which in turn triggers subnuclear targeting of Htt. They also identify several proof-of-concept chemical compounds that can boost neuroprotective Htt modifications in cellular models of Huntington's disease.

Several independent lines of evidence converge on the crucial role of the Htt N17 domain in Huntington's disease pathogenesis. Cell biological studies reveal this small N terminus of Htt as a cytoplasmic retention signal, as it can keep fragmented or full-length mHtt in the cytoplasm, physically associate Htt to membranous structures such as the endoplasmic reticulum and mitochondria[4,5], and facilitate Htt nuclear export[6]. Also, an *in vitro* study unexpectedly showed that the presence of N17 can accelerate the mHtt exon1 peptide aggregation[7], and such aggregation process can be suppressed by an N17 interacting protein, the chaperonin Tcp1 (also known as CCT1)[8]. Thus, N17 seems to be a small *cis*-domain that can play a big part in influencing the misfolding and

aggregation of the adjacent polyQ domain on mHtt fragments.

The study of proteolysis of full-length mHtt to more toxic N-terminal polyQ fragments (**Fig. 1**) remains a key area of research in understanding the molecular mechanisms that directly impinge on mHtt itself. Additionally, emerging evidence suggests that mHtt post-translational modifications (PTMs) and pathways modifying such PTMs contain unique molecular targets that can considerably modify the disease[4]. N17 spans only 0.5% of the protein and can be modified by SUMOylation or ubiquitination at Lys6, Lys9 and Lys15, acetylation at Lys9, and phosphorylation at Thr3, Ser13 and Ser16 (refs. 1,9). SUMO and ubiquitin modification of N17 has been shown to induce opposing effects on mHtt exon 1 toxicity in fly models[9]. In bacterial artificial chromosome–transgenic mice, expression of full-length mHtt with phosphomimetic mutations at Ser13 and Ser16 (S13D and S16D), but not phosphoresistant mutations (S13A and S16A), can abolish disease pathogenesis, as observed by multiple behavioral and neuropathological readouts[2]. Moreover, the phosphomimetic mutations can prevent mHtt aggregation *in vivo* and suppress amyloid fibril formation of an mHtt peptide *in vitro*[2]. This latter study validated mHtt N17 PTMs as key modifiers of Huntington's disease pathogenesis in mammalian models, hence providing a strong rationale to further elucidate the detailed signaling mechanisms leading to Htt N17 phosphorylation and to search for chemicals that could alter such a disease-relevant molecular switch.

Now, Truant and colleagues first address the question of cause and effect of Htt Ser13 and Ser16 double phosphorylation in Huntington's disease cell models[3]. First, they showed that mimicking Ser13 and Ser16 phosphorylation in the context of N17 alone or small mHtt N-terminal fragments could enhance nuclear entry, a finding consistent with recent data demonstrating that Ser16 phosphorylation alone is sufficient to mediate nuclear entry of small mHtt fragments[10]. An important advance of the current study is the development of a new, carefully validated antibody to detect Ser13 and Ser16 double phosphorylation on the endogenously expressed full-length Htt. Using this reagent, Atwal *et al.*[3] were able to shed light on several new properties of double phosphorylated endogenous Htt in the striatal cell lines derived from wild-type and a Huntington's disease mouse model. First, unlike the vast majority of Htt that is membrane bound via N17 (for example, to the endoplasmic reticulum

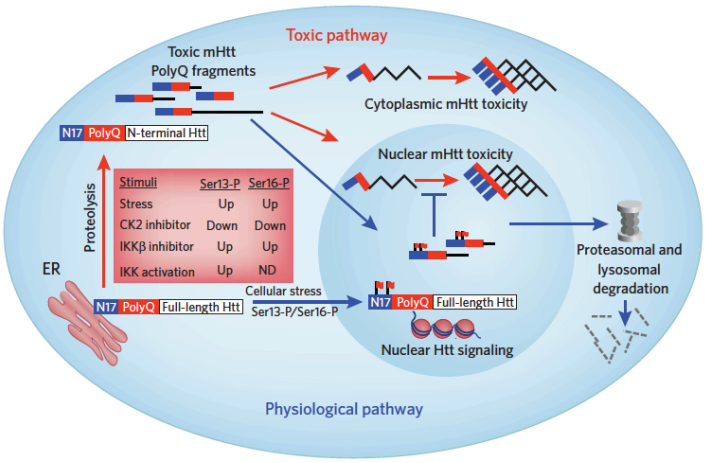


Figure 1 | A schematic of Htt N17-mediated physiological and pathological pathways in Huntington's disease. The toxic (red arrows) and physiological (blue arrows) fates of mHtt and its proteolytic N-terminal fragments in Huntington's disease pathogenesis are illustrated. The N17 domain normally functions as a cytoplasmic retention signal and mediates the association of Htt to cytoplasmic membranous structures such as the endoplasmic reticulum, Golgi and mitochondria. Under cellular stress (for example, heat shock), Ser13 and Ser16 in N17 can be double phosphorylated, which targets Htt to subregions in the nucleus. This double-phosphorylated form of mHtt can be readily cleared by the proteasome and lysosome and hence does not lead to increased nuclear aggregation. In disease conditions, the neuroprotective function of N17 or the mHtt clearance mechanism is compromised, which leads to misfolding and aggregation of mHtt in the cytoplasm and nucleus. The Ser13 and Ser16 double phosphorylation on Htt N17 is shown to be modifiable by genetic or chemical manipulation of CK2 and IKKβ. ND, not determined.

or mitochondria), phospho-N17 Htt is perinuclear or in distinct nuclear puncta. Interestingly, the latter localization seems to be chromatin dependent, as disruption of chromatin structure reduced the number of phospho-Htt nuclear puncta. The authors also found that cellular stress, elicited by heat shock, results in dramatically increased nuclear phospho-Htt signals, supporting a physiological role of Htt in handling cellular stress[3]. N17 phosphorylation could be a functional switch to relieve Htt from its normal cytoplasmic function, thereby allowing Htt to enter the nucleus to facilitate the stress response through a mechanism that remains to be defined.

Atwal *et al.*[3] went on to identify small molecules that can modulate N17-mediated cytoplasmic localization. They found four compounds that could reduce and another four that could enhance Htt cytoplasmic localization[3]. Among the latter group were the casein kinase 2 (CK2) inhibitors DMAT and quinalizarin, which reduce Htt N17 double phosphorylation and nuclear targeting. Interestingly, the very specific CK2 inhibitor, DMAT, enhanced the targeting of mHtt to the endoplasmic reticulum and increased cellular toxicity caused by a mHtt fragment in a Ser13- and Ser16-dependent manner. Intriguingly, the current study also revealed that the IKKβ kinase inhibitor, BMS-345541, as well as RNAi against IKKβ, enhances mHtt N17 Ser13 and Ser16 double phosphorylation and facilitates its nuclear entry, presumably due to enhanced activities of other Ser13 and Ser16 kinases. The latter finding is seemingly contradictory to the prior study demonstrating that activation of IKK complex can stimulate Ser13 phosphorylation[1]. These results are not mutually exclusive, and they provide the impetus to validate IKK as a modifier of Huntington's disease pathogenesis in mammalian models of Huntington's disease.

With an ever-increasing interest in the Huntington's disease field to study the Htt N17 domain and its phosphorylation as an avenue toward deeper understanding of disease mechanisms and discovering new therapeutic targets, many key questions still need to be answered. Because the current study suggests N17 phosphorylation may be a signal for Htt to participate in the nuclear stress response, does Htt normally have such a role in the brain during aging? What is the precise nuclear function of Htt during stress response? Is this function

© 2011 Nature America, Inc. All rights reserved.

related to the cytoplasmic function of Htt? One also has to wonder how such physiological N17-mediated Htt nuclear entry is compromised in Huntington's disease to result in a pathological pathway of nuclear accumulation of mHtt fragments and nuclear toxicity (**Fig. 1**). Finally, although enhanced mHtt Ser13 and Ser16 phosphorylation in principle should be beneficial in Huntington's disease, the manipulation of a kinase with additional targets other than Htt may carry toxicity of its own and requires validation in an animal model. Hence, the kinases and their chemical inhibitors identified in the current study should be considered as tools for probing N17 biology *in vitro* and *in vivo* rather than immediate preclinical candidates. Elucidating the biological underpinnings of the Htt N17 molecular switch may lead to better understanding of Huntington's disease pathogenesis and hopefully a disease-modifying therapy. ■

Erin R. Greiner is in the Semel Institute & Department of Psychiatry & Biobehavioral Sciences and the Department of Chemistry & Biochemistry, University of California at Los Angeles, Los Angeles, California, USA. X. William Yang is in the Semel Institute & Department of Psychiatry & Biobehavioral Sciences, University of California at Los Angeles, Los Angeles, California, USA.
e-mail: xwyang@mednet.ucla.edu.

References

1. Thompson, L.M. *et al. J. Cell Biol.* **187**, 1083–1099 (2009).
2. Gu, X. *et al. Neuron* **64**, 828–840 (2009).
3. Atwal, R.S. *et al. Nat. Chem. Biol.* **7**, 453–460 (2011).
4. Atwal, R.S. *et al. Hum. Mol. Genet.* **16**, 2600–2615 (2007).
5. Rockabrand, E. *et al. Hum. Mol. Genet.* **16**, 61–77 (2007).
6. Cornett, J. *et al. Nat. Genet.* **37**, 198–204 (2005).
7. Thakur, A.K. *et al. Nat. Struct. Mol. Biol.* **16**, 380–389 (2009).
8. Tam, S. *et al. Nat. Struct. Mol. Biol.* **16**, 1279–1285 (2009).
9. Steffan, J.S. *et al. Science* **304**, 100–104 (2004).
10. Havel, L.S. *et al. Hum. Mol. Genet.* **20**, 1424–1437 (2011).

Competing financial interests

The authors declare no competing financial interests.

© 2011 Nature America, Inc. All rights reserved.

1.6. Summary

The N17 domain of Htt and its role in modulating Htt aggregation, toxicity, and protein-protein interactions has been the subject of intense study in the HD field for the past few years. Unlike the Htt polyQ or polyP domains, this small N17 domain is highly modifiable and may provide an avenue for developing novel therapeutics for HD. The goal of my dissertation is to address the following important questions to better understand the biological function of Htt and the role of its N17 domain: 1) What are the full-length Htt protein-protein interactions and protein networks in the mammalian brain? How do these interactions change in different brain regions (affected *vs* unaffected)? How do these interactions change over the course of disease (pre-symptomatic *vs* post-symptomatic? What new biology is revealed from the Htt protein networks in the brain? 2) How does mimicking Ser13 and Ser16 phosphorylation effect Htt toxicity *in vivo*? 3) How does deletion of the N17 domain effect mHtt aggregation and toxicity *in vivo*? 4) What are the Ser13 and Ser16 phosphorylation-dependent and N17-dependent Htt protein-protein interactions in the mammalian brain? Is any new Htt N17-mediated biology revealed?

In Chapter 2, I describe a novel spatiotemporal proteomic and network biology approach used to profile full-length Htt protein interactions from wildtype and BACHD mouse brain. This chapter is a reprint of the article: Shirasaki, D.I.*, Greiner, E.R.*, Al-Ramahi, I., Gray, M., Boontheung, P., Botas, J., Coppola, G., Horvath, S., Loo, J.A., Yang, X.W. (2012) Network Organization of the Huntingtin Proteomic Interactome in Mammalian Brain. *Neuron* (in review).
* The authors contributed equally to this manuscript.

Chapter 3 is divided into two parts, in which I describe the biochemical characterization of transgenic mouse models of HD with mutations made to the Htt N17 domain. In the first part of Chapter 3, I describe the Htt Ser13 and Ser13 phosphomimetic (SD) and phosphoresistant (SA) mouse models of HD. This chapter is a reprint of the manuscript: Gu, X., Greiner, E.R., Mishra, R., Kodali, R., Osmand, A., Finkbeiner, S., Steffan, J.S., Thompson, L.M., Wetzel, R.,

Yang, X.W. (2009) Serines 13 and 16 are Critical Determinants of Full-Length Human Mutant Huntingtin Induced Disease Pathogenesis in HD Mice. *Neuron* 64, 828-840. In the second part of Chapter 3, I characterize the novel BACHD-ΔN17 and BACWT-ΔN17 mouse models of HD. I also describe the purification and solubilization of mHtt nuclear aggregates, and my use of mass spectrometry/proteomic approaches to probe for aggregate-interacting proteins in the aged BACHD-ΔN17 mouse brain.

In Chapter 4, I perform a spatiotemporal proteomic profiling and network analysis of the full-length Htt interactomes from the SD, SA, and BACHD-ΔN17 mouse models and provide validation of a few N17-specific interactions by co-IP/IB using BACHD and BACHD-ΔN17 mice.

Finally, in Chapter 5, I discuss the major findings from my dissertation and provide future directions for the field.

CHAPTER 2

Network Organization of the Full-length Huntingtin Interactome in Mammalian Brain

This chapter is the version of the manuscript that was accepted to Neuron for publication: Shirasaki, D.I.*, Greiner, E.R.*, Al-Ramahi, I., Gray, M., Boontheung, P., Botas, J., Coppola, G., Horvath, S., Loo, J.A., Yang, X.W. (2012) Network Organization of the Huntingtin Proteomic Interactome in Mammalian Brain. *Neuron* (in press).

* The authors contributed equally to this manuscript.

My contribution to this manuscript as co-first author was to write and prepare all of the figures, tables, and supplementary material for the manuscript. Dr. Dyna Shirasaki pioneered this spatiotemporal proteomic study, while Dr. Giovanni Coppola and Dr. Steve Horvath performed the WGCNA network organization of the full-length Htt interactome. My specific research efforts focused on validating Red Module Htt interactors by co-IP/IB, performing the BSA spike-in peptide correlation experiment, and analyzing and interpreting the Htt interactome and WGCNA network results.

2.1. Abstract

We used affinity-purification mass spectrometry (AP-MS) to profile proteins complexed with Huntingtin (Htt) in the cortex, striatum, and cerebellum of 2- and 12-month old Huntington's disease (HD) and wildtype (WT) mice. The *in vivo* Htt interactome consists of 747 candidate proteins and is significantly enriched with known Htt interactors. To gain a systems-level view of the Htt interactome, we analyzed the entire proteomic dataset using Weighted Gene Correlation Network Analysis (WGCNA). WGCNA analyses unveiled a verifiable rank of Htt-correlated proteins and a robust network of Htt-interacting protein modules, with each module highlighting distinct aspects of Htt biology. Importantly, the module containing Htt is highly enriched with proteins involved in 14-3-3 signaling, microtubule-based transport, and proteostasis. Several top candidate proteins in this module were validated as novel Htt interactors and genetic modifiers in an HD fly model, including Vps35, Ywhae (14-3-3ε), Hsp90ab1 and Tcp1. Together, our study provides a spatiotemporal compendium of full-length Htt-interacting proteins in the mammalian brain, and presents a conceptually novel and simple approach to building an *in vivo* protein complex network from multi-dimensional proteomic interactome datasets.

2.2. Introduction

Huntington's disease (HD) is one of the most common dominantly inherited neurodegenerative disorders clinically characterized by a triad of movement disorder, cognitive dysfunction, and psychiatric impairment (Bates and Harper, 2002). HD neuropathology is characterized by selective and massive degeneration of the striatal medium spiny neurons (MSNs), and to a lesser extent, the deep layer cortical pyramidal neurons (Vonsattel and Difiglia, 1998). The disease is caused by a CAG repeat expansion resulting in an elongated polyglutamine (polyQ) stretch near the N-terminus of Huntingtin (Htt) (The Huntington's Disease Collaborative Research Group, 1993). HD is one of nine polyQ disorders with shared molecular

genetic features such as an inverse relationship between the expanded repeat length and the age of disease onset, and evidence for toxic gain-of-function as a result of the polyQ expansion (Orr and Zoghbi, 2007). However, each of the different polyQ disorders appears to target a distinct subset of neurons leading to disease-specific symptoms; hence, it is postulated that molecular determinants beyond the polyQ repeat itself may be critical to disease pathogenesis.

Protein interacting cis-domains (Lim et al., 2008) and post-translational modifications (PTMs) (Emamian et al., 2003; Gu et al., 2009) can contribute to disease pathogenesis *in vivo*. Thus, studying the proteins that interact with domains other than the polyQ region may provide important clues to disease mechanisms. In the case of HD, several hundred putative Htt interactors have been discovered using *ex vivo* methods such as yeast two-hybrid (Y2H) or *in vitro* affinity pull-down assays, utilizing only small, N-terminal fragments of Htt (Goehler et al., 2004; Kaltenbach et al., 2007). Such studies have provided insight into Htt's normal function as a scaffolding protein involved in vesicular and axonal transport and nuclear transcription (Caviston and Holzbaur, 2009). The caveats of the prior Htt interactome studies include the exclusive use of small Htt N-terminal fragments as baits and the isolation of interactors *ex vivo*. Hence, it is not known which proteins can complex with full-length Htt (fl-Htt) *in vivo* within distinct brain regions and at different ages. Such information may shed light on age-dependent, selective neuropathogenesis in HD.

Immunoaffinity purification of native protein complexes followed by identification of its individual components using mass spectrometry (MS) has emerged as a powerful tool for deciphering *in vivo* neuronal signaling interactomes (Fernández et al., 2009; Husi et al., 2000) and disease-related interactomes (Major et al., 2007). Although a "shotgun" neuroproteomic approach is useful in creating a list of native interacting protein candidates from relevant mammalian tissues, formidable challenges exist in the unbiased bioinformatic analyses of such

complex proteomic datasets to identify high-confidence interactors and to build accurate, endogenous protein interaction networks (Liao et al., 2009).

In this study, we performed a spatiotemporal *in vivo* proteomic interactome study of fl-Htt using dissected brain regions from a mouse model for HD and wildtype controls. The BACHD mouse model used in the study expresses full-length human mutant Htt (mHtt) with 97Q under the control of human Htt genomic regulatory elements on a BAC transgene (Gray et al., 2008). BACHD mice exhibit multiple disease-like phenotypes over the course of 12 months, including progressive motor, cognitive and psychiatric-like deficits and selective cortical and striatal atrophy (Gray et al., 2008; Menalled et al., 2009). Our multidimensional AP-MS study uncovered a total of 747 candidate proteins complexed with fl-Htt in the mammalian brain. Moreover, we applied WGCNA to analyze the entire fl-Htt interactome dataset to define a verifiable rank of Htt-interacting proteins, and to uncover the organization of *in vivo* fl-Htt-interacting protein networks in the mammalian brain.

2.3. Results

2.3.1. Building an *In Vivo* Spatiotemporal Full-length Htt Interactome in BACHD and Wildtype Mouse Brains

To define the *in vivo* protein interactome for fl-Htt in BACHD and WT mouse brains, we performed immunoprecipitation (IP) of full-length mutant and WT Htt from BACHD and control mouse brains and identified the co-purified proteins by mass spectrometry (Fernández et al., 2009). Since previous studies suggest that the majority of Htt interactors bind to Htt N-terminal fragments, with very few binding to the C-terminal region (Kaltenbach et al., 2007), we reasoned that IP with a Htt antibody against the C-terminal region of the protein should preserve the vast majority of *in vivo* Htt protein interactions. We identified a monoclonal antibody (clone

HDB4E10) capable of preferentially pulling-down human Htt in BACHD brains, with lesser affinity for immunoprecipitating murine Htt in both BACHD and WT mice (Figure 2.1A). Considering the lack of suitable Htt antibodies that can immunoprecipitate only polyQ-expanded or WT Htt with equal efficiency, our AP-MS strategy of using HDB4E10 should be considered as a survey of *in vivo* Htt-complexed proteins regardless of Htt polyQ length. This is a reasonable strategy since full-length human mHtt can fully substitute the essential function of murine Htt in mice (Gray et al., 2008), and hence both forms should share the majority of *in vivo* interacting proteins.

Human and/or murine fl-Htt complexes were immunoaffinity purified from the cortex, striatum, and cerebellum of BACHD and WT mice at 2- or 12-months of age using HDB4E10 (Figure 2.1B). As a negative control, a mock IP for each condition (defined by specific brain region, age and genotype) was performed in the absence of the Htt antibody. Therefore, a total of 30 independent IP experiments were performed, and approximately 765 trypsin-digested gel slices were subjected to LC-MS/MS analysis (Figure 2.1C). Using the MASCOT (Matrix Science) sequence database-searching tool, we identified a total of 747 high-scoring, putative Htt-interacting proteins from BACHD and WT mouse brains (Supplemental Table 2.1). Consistent with the claim that we are surveying fl-Htt-interacting proteins, we identified Htt peptides spanning the entire sequence of Htt in both BACHD and WT samples (Figure 2.1D and Supplemental Table 2.2). As confirmation that HDB4E10 more efficiently immunoprecipitates human Htt than murine Htt, we observed more Htt peptides and more extensive sequence coverage of fl-Htt in BACHD mice compared to WT mice.

2.3.2. The *In Vivo* fl-Htt Interactome Is Enriched With Known Htt Interactors and Proteins Involved in Pathways Relevant to HD

We next performed several standard bioinformatic analyses to determine the validity of our approach in isolating Htt interactors *in vivo*, and to define potential biological pathways that Htt may be engaged in at various ages within different brain regions. We compared our list of 747 candidates with previously reported Htt interactors. Among a curated list of 877 proteins previously identified as putative *ex vivo* Htt interactors, most of which were obtained from Y2H experiments (Goehler et al., 2004; Kaltenbach et al., 2007)HDbase.org), we found 139 proteins also present in our *in vivo* Htt interactome (Figures 2.1E and Supplemental Table 2.3). This represents a highly significant enrichment ($P = 7.00 \times 10^{-50}$; hypergeometric test). The disease specificity of our interactome is supported by the comparison of our dataset with that of another polyQ disease protein, Ataxin 1 (Lim et al., 2006). Despite that one-third of our samples originated from the cerebellum, the same tissue source as the Ataxin 1 interactome study, only 38 proteins were present in both datasets with only modest overall enrichment ($P = 0.0005$; Figure 2.1E and Supplemental Table 2.3). Thus, our *in vivo* fl-Htt interactome appears to be specific to Htt, and provides a valuable list of Htt-interacting proteins, both *in vivo* and *ex vivo*, for further investigation to determine their roles in novel Htt biology and HD pathogenesis.

Gene Ontology (GO) analysis of our *in vivo* fl-Htt interactome dataset (Supplemental Table 2.4) showed significant overrepresentation of proteins involved in ‘Intracellular Transport’, ‘Synaptic Transmission’, and ‘Protein Folding’ (all previously implicated in HD pathogenesis), as well as proteins involved in pathways related to the ‘Generation of Precursor Metabolites and Energy’, ‘Cytoplasmic Membrane-Bound Organelles’, and ‘Nucleotide Binding’. This supports Htt’s involvement in multiple biological functions within several subcellular compartments in the brain (Li and Li, 2006).

We next probed the biological and disease pathways enriched in our *in vivo* fl-Htt interactome using Ingenuity Pathway Analyses (IPA, Ingenuity Systems®, www.ingenuity.com), a large curated database of published information on mammalian biology and disease (Figure 2.1F; Supplemental Table 2.5). As independent validation for the relevancy of our interactome to HD biology, the 'Huntington's disease signaling' pathway was significantly enriched. Importantly, other top IPA signaling pathways enriched in our fl-Htt interactome include 'Protein Kinase A Signaling' and 'CREB Signaling in Neurons', which are pathways previously implicated in HD pathogenesis and therapy (Kleiman et al., 2011; Sugars et al., 2004).

Our rationale for examining samples from three different brain regions at two different time points was to reveal dynamic *in vivo* differences between fl-Htt interactomes, which could possibly provide insight into selective, age-dependent disease processes. To this end, we identified candidate fl-Htt interactors exclusively from brain regions or ages relevant to HD (Figure 2.2, Supplemental Table 2.6), providing an interesting subset of proteins to further investigate their putative roles in selective neuronal vulnerability in HD. While the majority of proteins in our interactome are shared between all three brains regions (34.9%) and both age time points (57.3%), dynamic differences between proteins identified in specific brain regions (Cerebellum, 15.1%; Cortex, 23.1%; and Striatum 5.5%) and age time points (2m, 20.9%; and 12m, 22.0%) exist. The proteins that appear reproducibly (at least 2 peptides in two IP conditions) and selectively complex with Htt at 12m, or in the striatum or cortex of our AP-MS dataset, are putative candidates for mediating age-dependent selective pathogenesis in HD, while those in complex with Htt at 2m or in the cerebellum may be neuroprotective (Figure 2.2C-D).

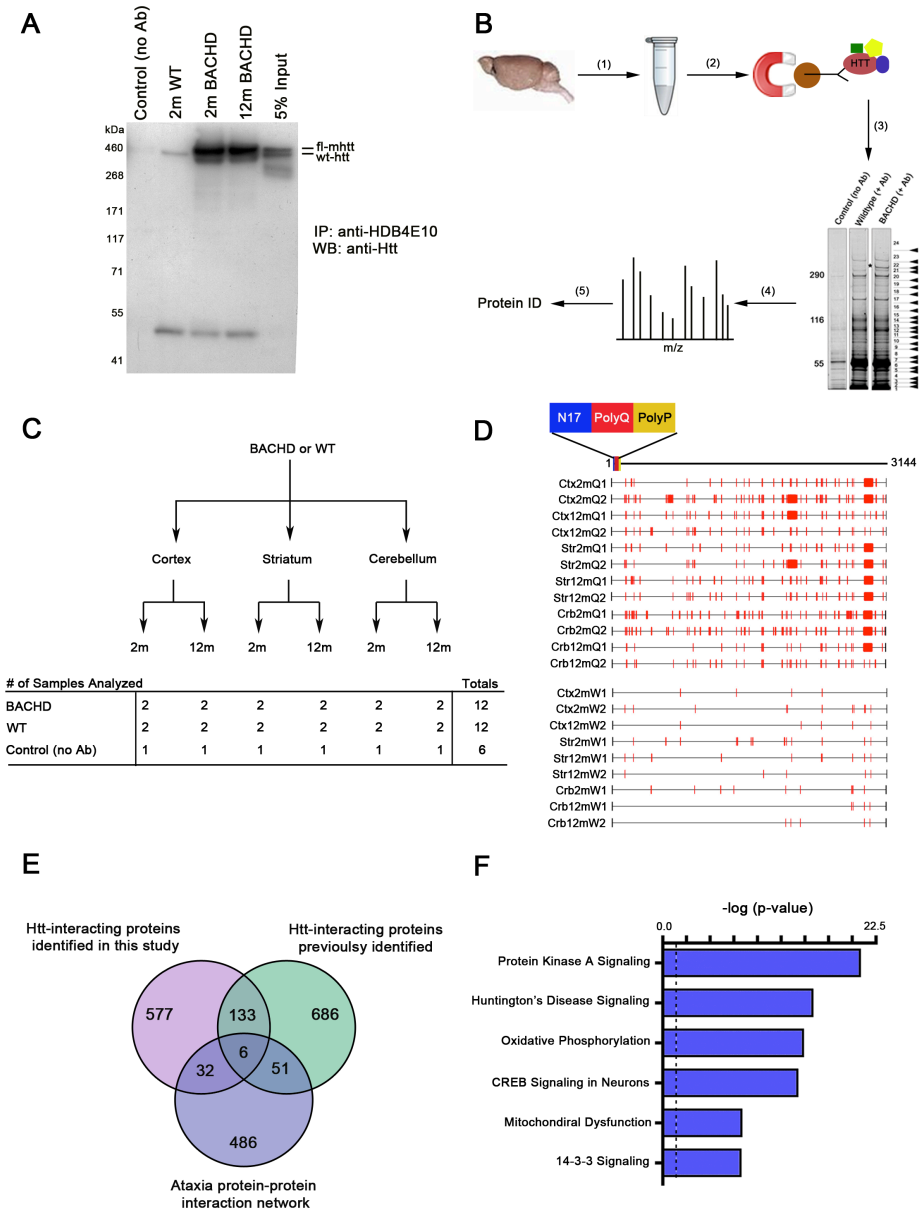
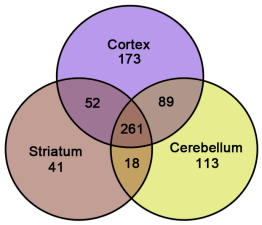


Figure 2.1. Generation and characterization of a full-length Htt interactome from wildtype and BACHD mouse brains. (A) Anti-Htt co-immunoprecipitation using a C-terminal Htt antibody (aa 1844-2131, clone HDB4E10) followed by immunoblot analysis (MAB2166) confirms full-length Htt is pulled-down in both 2-month WT and 2- and 12-month BACHD soluble cortical extracts. A negative control (no Htt antibody) and 5% input loading control were also performed. **(B)** The affinity purification followed by mass spectrometry (AP-MS) proteomic approach used to identify endogenous fl-Htt protein interactors: (1**(C)** Experimental overview of the spatiotemporal proteomic approach we used to profile full-length Htt protein-protein interactions from 30 independent IP experiments. **(D)** A schematic representation of the Htt tryptic peptides identified along the full-length Htt primary sequence (aa 1-3144). BACHD IP conditions labeled with Q and WT IP conditions labeled W. **(E)** Venn diagram comparison of Htt-interacting proteins identified in this study, literature-curated Htt-interacting proteins, and the published ataxia protein network. (**F**) Representative canonical pathway comparison of the Htt interactome using Ingenuity Pathway Analysis (IPA, www.ingenuity.com), plotted as a value of p-value significance. The black dotted line indicates canonical pathway genome-wide p-value significance ($p < 0.05$).

A



B



C

Brain Region		
Striatum	**Cortex**	**Cerebellum**
Kcnab1	Dhx9	Acot11
Pde1b	Grin1	Ahcy
	Grin2b	Atp1b2
	Lancl2	Atp2a3
	Map4k4	Calb1
	Mark2	Dld
	Myl6	Gbas
	Myl9	Gnat1
	Napg	Grid2
	Ncl	Homer3
	Pex5l	Hspb8
	Ppfia3	Kctd12
	Ptk2	Ldhc
	Rpl7	Mfn2
	Sirpa	Ncoa6
	Snrpa	Ndrg2
	Tpp2	Ndufv1
	Trim3	Nos1
		Rps6ka1
		Sash1
		Sdhb
		Setbp1
		Slc1a6
		Uqcrc1

D

Age	
2m	**12m**
Arhgef2	Acadl
Atp2a3	Ahcy
Bin1	C1qa
Cdk5	Cend1
Dhx9	Dock8
Gnaq	Ehd1
Hsp110	Ehd3
Ldhc	Epb41l3
Nars	Gbas
Numbl	Grik5
Pclo	Huwe1
Pde1b	Mfn2
Psmc4	Mvp
Ranbp5	Myl6
Tardbp	Myl9
Tuba1b	Napg
	Ndrg2
	Ndufv1
	Nos1
	Pacsin2
	Rab4b
	Rpl10a
	Rps10
	Rps6
	Rps6ka1
	Sash1
	Sdhb
	Sept6
	Sfrs4
	Sptb
	Srgap3
	Uqcrc1

Figure 2.2. Brain regional and age-specific protein interactions revealed in Htt interactome. (A-B) Venn diagram comparison of the age (2- and 12-month) and brain region (cortex, striatum, and cerebellum) specific Htt protein interactions identified in this study. **(C-D)** A list of high confidence age and brain regional Htt protein interactions (protein identified in > 2 IP conditions, > 3 total peptides identified, no peptides identified in no antibody IP control).

2.3.3. Semi-Quantitative Measures of Protein Abundance Allow Ranking of Candidate Interactors Based on Correlation With Fl-Htt

Although initial bioinformatics analyses indicated that our fl-Htt interactome was relevant to HD, we still needed to determine how to best prioritize the interacting proteins for biological validation. For this reason, we sought to explore whether the semi-quantitative MS information embedded within our dataset could be utilized to provide a system-level view of the interactome and enable a rationale prioritization of candidate interactors for functional studies. We performed a protein spiking experiment by adding increasing concentrations of bovine serum albumin (BSA) to our BACHD 2-month cortical extracts prior to LC-MS/MS (Supplemental

Figure 2.1). Similar to a prior study (Liu et al., 2004), under our experimental condition, the unique peptide counts for BSA were significantly correlated with the known BSA concentration in different samples ($R^2 = 0.822$). To use such semi-quantitative information to uncover any novel relationships between candidate fl-Htt interactors and Htt, we took advantage of the observation that Htt peptide counts were consistently higher in BACHD samples than in WT control (or blank control) samples across all 30 IP experiments. This is because there is approximately a two-fold increased level of fl-Htt in BACHD compared to WT control brains (Gray et al., 2008), and the selectivity of HDB4E10 for human Htt over murine Htt (Figure 2.3A). We reasoned that the ubiquitously expressed proteins that complex with fl-Htt should also have relative peptide abundances across our dataset similar to that of Htt (*i.e.,* high in BACHD, low in WT, and none in the blank). We calculated pairwise correlations between fl-Htt and the 747 putative interacting proteins, using as input the unique tryptic peptide counts identified for each protein amongst the 30 sample conditions (Supplemental Tables 2.7 and 2.8). The proteins significantly correlated with Htt in our dataset (163, $P < 0.05$, Supplemental Table 2.8), and the top 10 most correlated proteins consisted of well-characterized direct Htt interactors, including Cct8, Cntn1, F8a1 (Hap40), Hsp90ab1, Ndufs3, and Ywhae (14-3-3ε) (Figure 2.3B; (Kaltenbach et al., 2007). Importantly, F8a1/Hap40, a known fl-Htt-interacting protein previously implicated in HD pathogenesis (Peters and Ross, 2001), was identified as being the most significantly correlated with Htt, despite having 3 or fewer peptides in a given sample (Supplemental Tables 2.7 and 2.8).

To further increase our confidence in the relevancy of our Htt-correlation ranking to HD biology, we divided the entire 747 Htt interactors into 6 bins of about 125 proteins, each based on ranking, and annotated each bin using IPA 'Huntington's Disease Signaling Pathway.' Interestingly, the results showed a significant correlation between the fl-Htt correlation ranking and the IPA annotation of known Htt biology, with the top two bins being the most significantly

enriched with 'Huntington's Disease Signaling' proteins, while the bottom bins were only marginally or not significantly enriched at all (Figure 2.3C and Supplemental Table 2.9). As a control, the top bins of Htt-correlated proteins are not significantly enriched with an Alzheimer's Disease related IPA pathway (Figure 2.3C). This analysis provides independent support of the biological relevance of the Htt correlation ranking of the *in vivo* fl-Htt interactome.

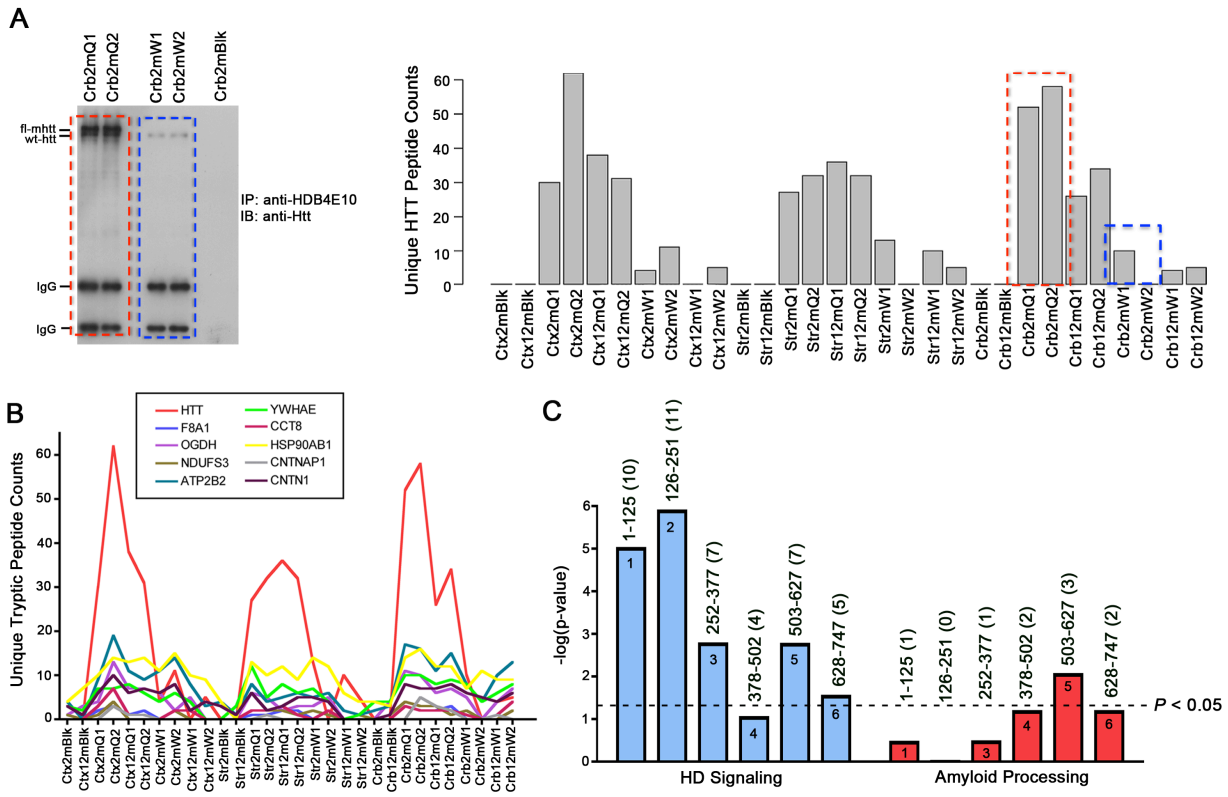


Figure 2.3. Unique peptide counts as a measure of relative protein abundance reveals proteins most correlated with Htt. (A) Western blot analysis using anti-Htt (mAb2166) (left) of the anti-Htt immunoprecipitation (clone HDB4E10) of 2-month BACHD cerebellum biological duplicates (Crb2mQ1 and Crb2mQ2, red dashed box), 2-month WT cerebellum biological duplicates (Crb2mW1 and Crb2mW2, blue dashed box), and 2-month BACHD cerebellum no antibody control (Crb2mBlk) and the bar graph of unique tryptic Htt peptide counts identified across 30 experimental IP conditions (right) illustrate the variance in the amount of Htt that is pulled-down across the different age, brain region, and genotype samples. **(B)** Unique Htt peptide counts of the top nine proteins most correlated with Htt across the 30 sample conditions. **(C)** Htt correlation bins 1-6 (each consisting of 125 proteins, where bin 1 contains the proteins most correlated with Htt and bin 6 contains the proteins least correlated with Htt) were submitted to IPA canonical pathway analysis and the HD signaling and amyloid processing pathways were plotted as p-value significance (where the black dotted line indicates $p < 0.05$). The number in parenthesis indicates the number of proteins identified in each category.

2.3.4. Weighted Gene Correlation Network Analyses (WGCNA) Organizes the *In Vivo* fl-Htt Interactome into Network Modules

The construction of interacting protein networks based exclusively on AP-MS datasets has been largely limited to simple organisms (*e.g.*, yeast). The use of AP-MS proteomic interactome information derived from complex biological systems to directly construct protein networks has been a challenge, but an important direction for the field (Vidal et al., 2011). WGCNA (Zhang and Horvath, 2005) was designed to provide a global analysis of microarray data across tissues, species, or disease conditions, and to build global gene networks based on co-expression relationships in order to identify gene modules that are tightly correlated across entire datasets (Millet et al., 2008; Oldham et al., 2008). However, to date, this method has never been applied to proteomics data.

Because the semi-quantitative data provided by AP-MS provides a good proxy for relative protein abundance, we applied WGCNA to our proteomic dataset. We call this adapted application of the method to protein analysis, WeiGhted Correlation Network Analyses, (still abbreviated as WGCNA). Briefly, after selecting proteins present in at least three samples (n = 412), the pairwise correlation coefficients between one protein and every other detected protein were computed, weighted using a power function (Langfelder and Horvath, 2008; Zhang and Horvath, 2005), and used to determine the topological overlap, a measure of connection strength or 'neighborhood sharing' in the network. A pair of nodes in a network is said to have high topological overlap if they are both strongly connected to the same group of nodes. In WGCNA networks, genes with high topological overlap have been found to have an increased chance of being part of the same tissue, cell type, or biological pathway. Our analyses of the fl-Htt interactome produced 8 clusters of highly correlated proteins, or modules, with each including 22-145 proteins (Figure 2.4A, Supplemental Table 2.10). Based on the convention of

WGCNA (*ibid*), the modules were named with different colors (Red, Yellow, Blue, Cyan, Pink, Green, Navy, Brown and Grey).

To investigate the biological underpinning of the WGCNA modules, we addressed whether each module could have differential correlation strength with the central protein in our interactome, fl-Htt. We computed a Module Eigenprotein (MP) for each module, which is defined as the most representative protein member (*i.e.,* a weighted summary) among all proteins in the module. We then calculated each MP correlation with fl-Htt (Figure 2.4B and Supplemental Table 2.11). The relationship between module membership (MM, defined as the correlation between each protein in the network and MP) and fl-Htt levels was determined (Supplemental Figure 2.2A-H). Both measures pointed to one module (Red) as the most correlated to fl-Htt across samples, with five other modules (Yellow, Blue, Cyan, Pink, and Green) also highly significantly correlated with fl-Htt. Importantly, the Red Module (comprised of 62 proteins, where 19 were previously known Htt interactors) includes Htt itself, thus giving further support that the proteins assigned to this module may have important biological relationships with Htt (Supplemental Table 2.12).

To further validate the Htt-correlated modules, we input the proteins in each module into IPA and analyzed for enrichment for 'HD Signaling Pathway' proteins. The Red, Blue, Cyan, Yellow, Green, Pink, and Navy Modules were significantly enriched with proteins in this pathway (Figure 2.4C; Supplemental Table 2.13). The Brown Module was not significantly correlated with Htt, and is also not significantly enriched with IPA HD Signaling proteins (Figure 2.4C; Supplemental Table 2.13). Together, our analyses support the biological relevance to Htt of multiple WGCNA modules derived from our fl-Htt interactome.

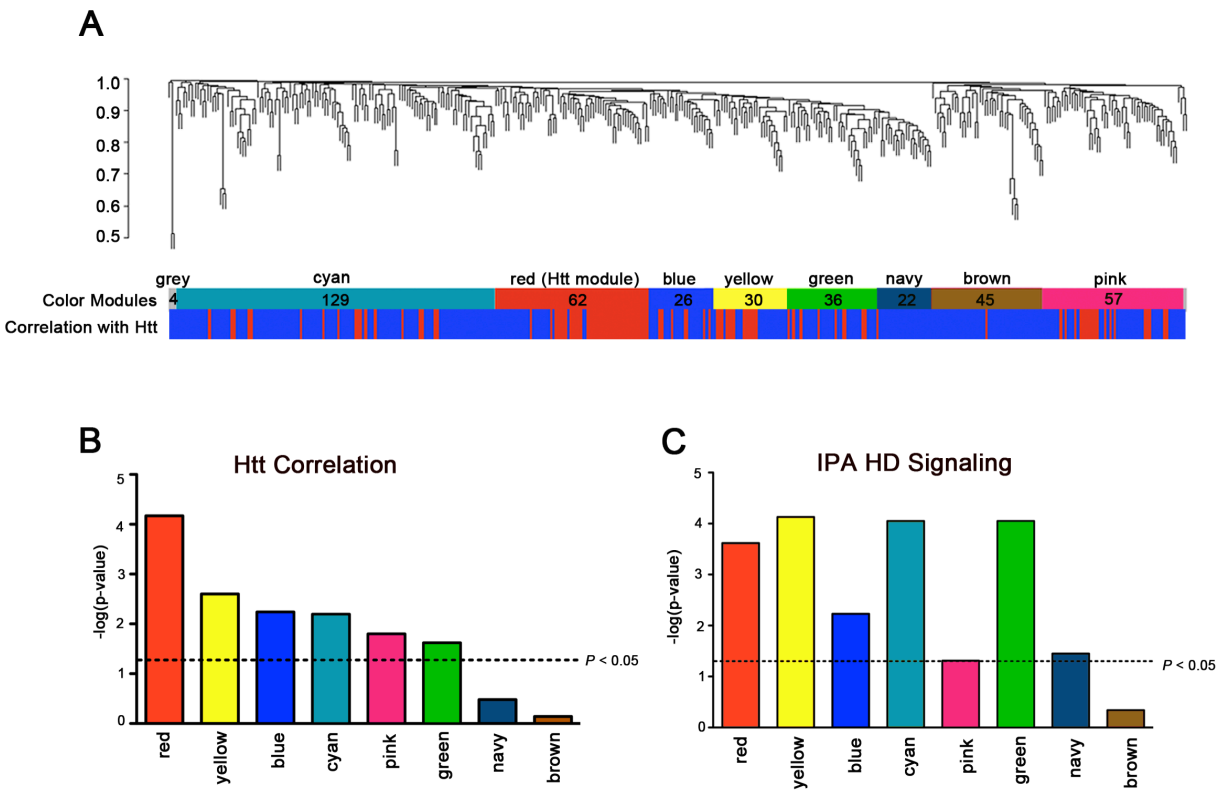


Figure 2.4. Weighted Gene Correlation Network Analysis (WGCNA) of fl-Htt interactome. (A) Cluster dendrogram generated by hierarchical clustering of proteins on the basis of topological overlap. Modules of correlated proteins were assigned colors and names (Cyan, Red, Blue, Yellow, Green, Navy, Brown, and Pink respectively) and are indicated by the horizontal bar beneath the dengrogram, where all unassigned proteins were placed in the grey module (labeled Color Modules). The number in the color modules represents the number of proteins assigned to each module. Pairwise correlations were calculated for each protein to the Htt protein, and the p-value significance is colored below in the horizontal bar where a significant ($p < 0.05$, red) or non-significant correlation ($p > 0.05$, blue) with Htt protein levels is indicated. **(B)** Barplot depicting the –log10 p-values of the pairwise correlations between each module's eigenprotein (see text) and Htt. Dotted black line: significance level at $p = 0.05$. **(C)** Scatterplots depicting the correlation between module membership and fl-Htt expression levels. Pairwise correlation levels and p-values were calculated for each module and are indicated above each plot.

2.3.5. Enrichment of Htt Interactome Modules and Meta-Networks in Specific Sample Conditions

We hypothesized that one of the underlying biological relationships driving the formation of different modules could be the differential enrichment of proteins within distinct AP-MS sample conditions (*e.g.,* brain region, age, or genotype). To test this, we correlated the MPs for the six WGCNA modules to the 30 experimental conditions (Figure 2.5A-F). We found that Red Module is enriched in the cortical and cerebellar samples; the Blue, Yellow and Green Modules are enriched in the cortical samples; and Pink Module is enriched in the cerebellar samples. Interestingly, the Cyan Module appears to be an age-dependent module, with proteins consistently enriched in 12-month but not 2-month cortical samples in both BACHD and WT mice (Figure 2.5F).

Finally, the unbiased process of constructing WGCNA network modules also yields a higher-order meta-network called “module eigenprotein network”, which can be calculated based on pairwise correlation relationships of all possible pairs of MPs (Figure 2.5G). The two main branches of the network appear to represent either modules that are enriched with proteins in cortical samples (Red, Cyan, Blue, Green, and Yellow) or those enriched in the cerebellar samples (Pink). These analyses suggest that the hierarchical organization of the fl-Htt interactome modules and their meta-networks may reflect the tightly correlated group of proteins that preferentially complex with Htt in distinct sample conditions (brain regions and age).

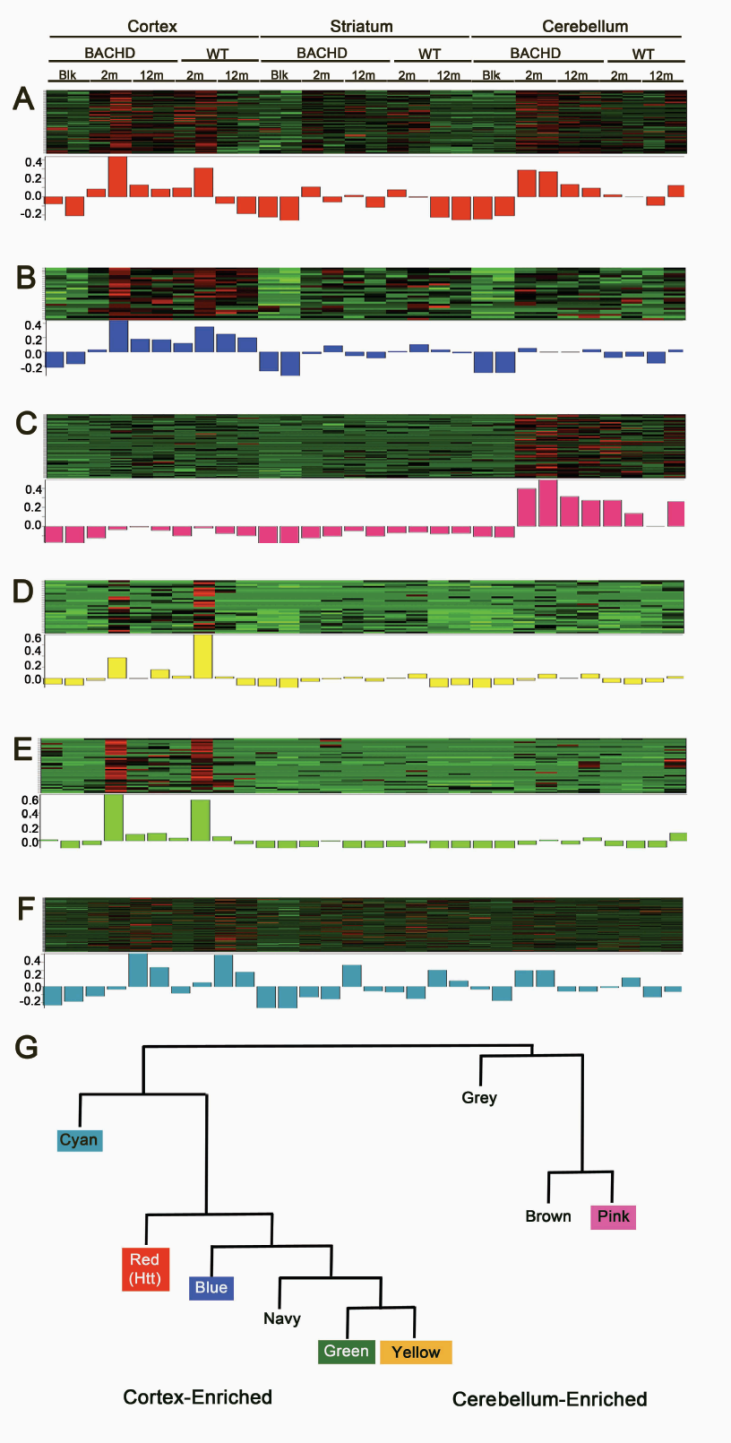


Figure 2.5. Top Htt-correlated modules reveal spatiotemporal protein relationships. (A-F) The heat map correlation profiles (rows) across samples (columns) for proteins in the following color modules are shown: A) Red B) Blue C) Pink D) Yellow E) Green F) Cyan where green indicates areas of low correlation profiles and red indicates areas of high correlation profiles. **(G)** Module eigenprotein network reveals cortical-enriched and cerebellum-enriched modules in Htt interactome.

2.3.6. WGCNA Modules Are Related With Distinct Aspects of Htt Biology

A key motivation for constructing an unbiased fl-Htt interactome network is to decipher different aspects of Htt molecular function in the intact mammalian brain. We analyzed the six Htt-correlated WGCNA modules using Gene Ontology and IPA (Supplemental Tables 2.13 and 2.14). HD-relevance and novel molecular characteristics of each module can be assessed based on their top module hub proteins, which are defined as the proteins with the highest correlation with each MP (Figure 2.6; ranked by Kwithin in Supplemental Table 2.10).

The Red Module, which is the most Htt-correlated module and contains Htt itself, is significantly enriched with hub proteins involved in proteostasis, 14-3-3 signaling, microtubule-based intracellular transport, and mitochondrial function (Figure 2.6A). Chaperones are key proteins involved in maintaining a healthy proteome (proteostasis) by preventing protein misfolding, a pathway directly implicated in the pathogenesis of neurodegenerative disorders including HD (Balch et al., 2008). Several chaperones in the Red Module (Tcp1, Hsp90s) have been shown to physically interact with Htt or modify mHtt toxicity in cell and invertebrate models of HD (Table 2.1). The roles of the others remain to be explored.

The second molecular feature of the Red Module is the presence of six 14-3-3 family proteins (Ywhab, Ywhae, Ywhag, Ywhah, Ywhaq, Ywhaz), with Ywhae as a top hub gene (Figure 6A). Impressively, '14-3-3-mediated signaling' in the Red Module is the most significantly enriched IPA Canonical Pathway for all modules in the fl-Htt interactome network (Supplemental Table 2.13). The 14-3-3 pathway has been implicated in the pathogenesis of a variety of neurodegenerative disorders (Chen et al., 2003), and four 14-3-3 members have been shown to physically or genetically interact with Htt N-terminal fragments (Kaltenbach et al., 2007; Omi et al., 2008) (Supplemental Table S3). Since 14-3-3 proteins are phospho-serine/phospho-threonine binding proteins (Morrison, 2009), and Htt phosphorylation at several serine residues has been shown to modify HD pathogenesis (Gu et al., 2009; Humbert et al.,

2002; Thompson et al., 2009), it could be a promising direction to investigate whether 14-3-3 proteins in the Red Module could directly interact with relevant phospho-Htt species to affect the disease process.

The third molecular pathway enriched in the Red Module is 'Intracellular Protein Transport' (Stx1a, Vcp, Ran, Syngr1, Stx1b, 14-3-3s) consistent with the convergent evidence supporting the role of Htt function in the microtubule-based transport process (Caviston and Holzbaur, 2009) and the disruption of such function in HD (Gauthier et al., 2004).

Although the Red Module appears to be enriched with proteins from divergent molecular processes, several lines of evidence suggest these proteins indeed have close biological connectivity. First, 26 out of the 61 Red Module proteins are included in the same IPA network, which is constructed based on the archived IPA Knowledge Base derived from published studies. This network has the highest IPA network score among all of the networks constructed from Htt interactome modules (Supplemental Table 2.13), suggesting that the proteins in Red Module already have a close functional link based on existing knowledge. Second, the Red Module has a marked enrichment for proteins implicated in other neurological and genetic disorders. Using another IPA core analysis (IPA Function), the Red Module has dramatically higher enrichment for proteins in the categories of Neurological Disorders and Genetic Disorders compared to the other modules (Supplemental Figure 2.3A-B), which cannot be accounted for by enrichment of the HD Signaling Pathway alone (Figure 2.4C). Furthermore, 16 Red Module proteins (Supplemental Figure 2.3C-D) are mutated in neurological disorders ranging from Frontotemporal dementia (Vcp) to Parkinson's disease (Vps35). Finally, among the top 50 Red Module proteins based on module memberships, there are 19 proteins that are known to interact with Htt that can modify mHtt toxicity in cell or invertebrate models of HD (Table 2.1), and several genes are also known therapeutic targets for HD (*e.g.,* creatine targeting Ckb; and 17-AAG targeting Hsp90s) (Dorsey and Shoulson, 2012; Herbst and

Wanker, 2007). In summary, the Red Module contains proteins that are highly correlated with Htt (including Htt itself), and is enriched in a highly connected group of proteins involved in proteostasis, 14-3-3 signaling, microtubule-based transport and mitochondria function.

The second most Htt-correlated module is the Blue Module, with its member proteins enriched in the cortex and playing roles in presynaptic function. The most significant GO terms enriched in Blue Module are 'Coated Membrane' and 'Neurotransmitter Transport' (Supplemental Table 2.14). The top IPA Canonical Signaling Pathways enriched in Blue Module are 'GABA Receptor Signaling', 'Clathrin-Mediated Endocytosis' and 'HD Signaling'. The hub proteins in Blue Module (Ap2a2, Dnm1, and Syt1) are members of a Htt protein network previously established based on *ex vivo* interactions with mHtt fragments and are validated as genetic modifiers in an HD fly model (Kaltenbach et al., 2007). Together, this evidence supports the notion that Blue Module contains cortex-enriched Htt interactors that preferentially function in pre-synaptic terminals, and hence may influence corticostriatal neurotransmission which is known to be affected in HD (Raymond et al., 2011).

The Pink Module is a cerebellum-enriched module with HD-relevant hub proteins functioning in calcium signaling (Itpr1 and Itpr2), mitochondria function (Ndufa9, Ndufs2 and Uqcrc2), and glutamate receptor function (Grid2 and Slc1a3). Not surprisingly, several hub proteins are either selectively expressed (Grid2 and Slc1a3) or highly enriched in the cerebellum (Itpr1, Syt2 and Gpd1; see Allen Brain Atlas). Consistent with the idea that cerebellar-enriched Htt interactors may confer beneficial neuroprotective function, one interesting Pink Module protein, Ucqrc2, was recently shown to be one of nine core modulators of the proteostasis network (*e.g.,* mHtt polyQ fragment and endogenous metastable proteins) in a genomewide *C. elegans* screen (Silva et al., 2011). Since our interactome also identified more Ucqrc2 peptides in brain tissues (cerebellum) and at ages (2m) relatively unaffected in HD mice

(Supplemental Table 2.7), this evidence strongly encourages further investigation in the role of Ucqrc2 and its interaction with Htt in HD selective pathogenesis.

The Yellow Module is driven by top hub proteins involved in excitatory post-synaptic function (Supplemental Table 2.14). Two of the top hub proteins (Grin2b/NR2b and Dlg4/PSD95) have been implicated in pathogenesis in HD mice (Fan et al., 2009; Zeron et al., 2002). Another interesting member is beta-catenin (Ctnnb1), a known modifier of mHtt-induced toxicity in HD fly and cell models (Godin et al., 2010). Ctnnb1 is also a key member of the Wnt signaling pathway, which has been implicated in multiple neurodegenerative disorders (Wexler et al., 2011) and is being explored for neuroprotective therapies (Todelo et al., 2008). Thus, further study of Yellow Module hub proteins may yield new therapeutic targets for mitigating synaptic dysfunction in HD.

The Green Module is highly enriched with proteins involved in actin cytoskeleton organization (Figure 2.6E). The annotation of this module is consistent with the emerging role of Htt as a direct actin binding protein (Angeli et al., 2010), with an evolutionarily-ancient function in regulating the actin-binding protein, myosin, in chemotaxis and cytokinesia (Yu Wang et al., 2011). Green Module hub proteins, including Cdk5 (Anne et al., 2007), Rph3A (Smith et al., 2007), Rock2 (Shao et al., 2008a), and Gja1/Connexin-43 (Vis et al., 1998), have previously been implicated in HD. Therefore, this module provides a novel set of actin binding candidates impetus to study in the context of normal Htt function and HD pathogenesis.

Finally, the Cyan Module is the only age-dependent module and is also highly enriched with proteins residing in mitochondria, or functioning in inflammation, G-protein signaling and as modifiers of mHtt aggregation. Several of these proteins (Usp9x, Rock1, and Sirt2) appear to modify mHtt aggregation or toxicity in cellular models and are known drug targets (Kaltenbach et al., 2007) (Shao et al., 2008a) (Luthi-Carter et al., 2010; Pallos et al., 2008). The role of Cyan Module proteins in influencing mHtt aggregation gained further support after a recent

genomewide RNA interference screen for modifiers of mHtt aggregation identified a number of similar genes, including Aldoa, Csnk2a1, Hspa9, Pfkm, and Rab1a in *Drosophila* cells (Zhang et al, 2010) Thus, the Cyan Module is enriched with Htt-interacting proteins complexed with Htt in an age-dependent manner, which may help to elucidate the poorly understood role of aging in the pathogenesis of HD.

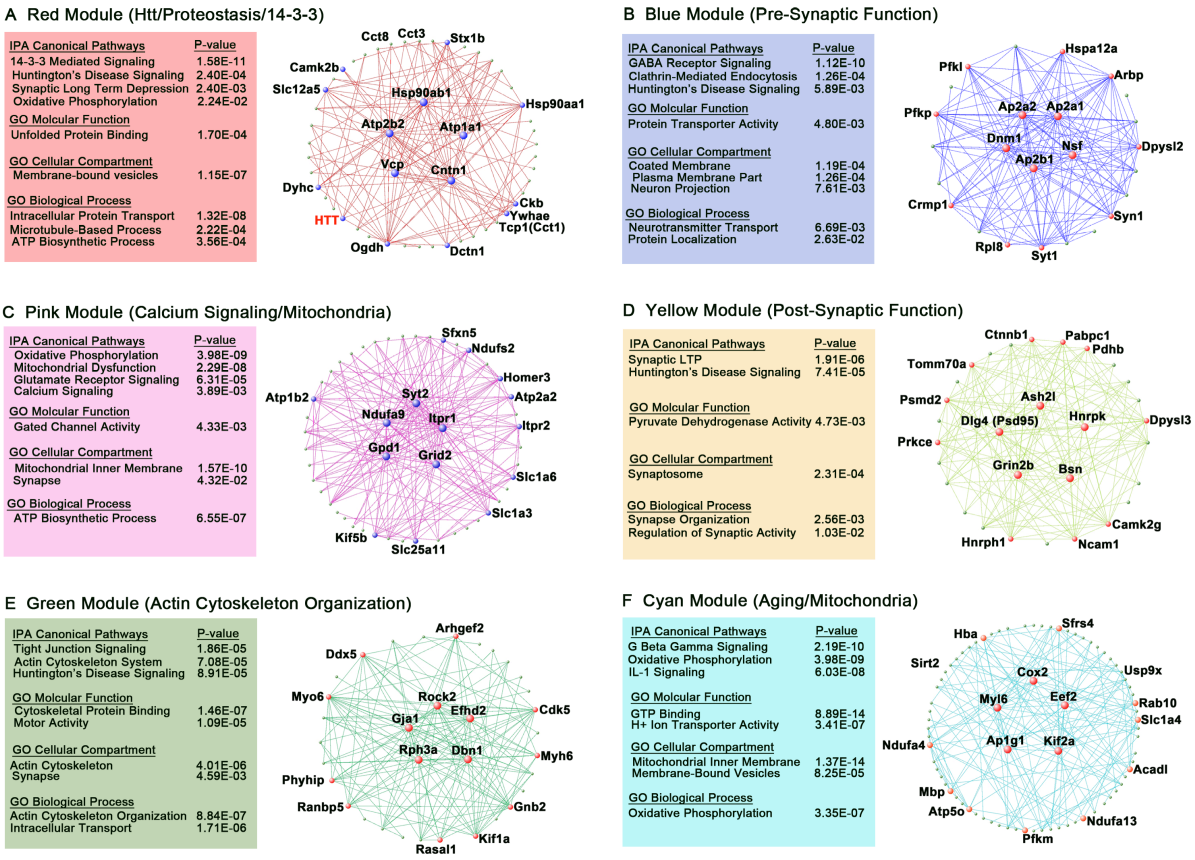


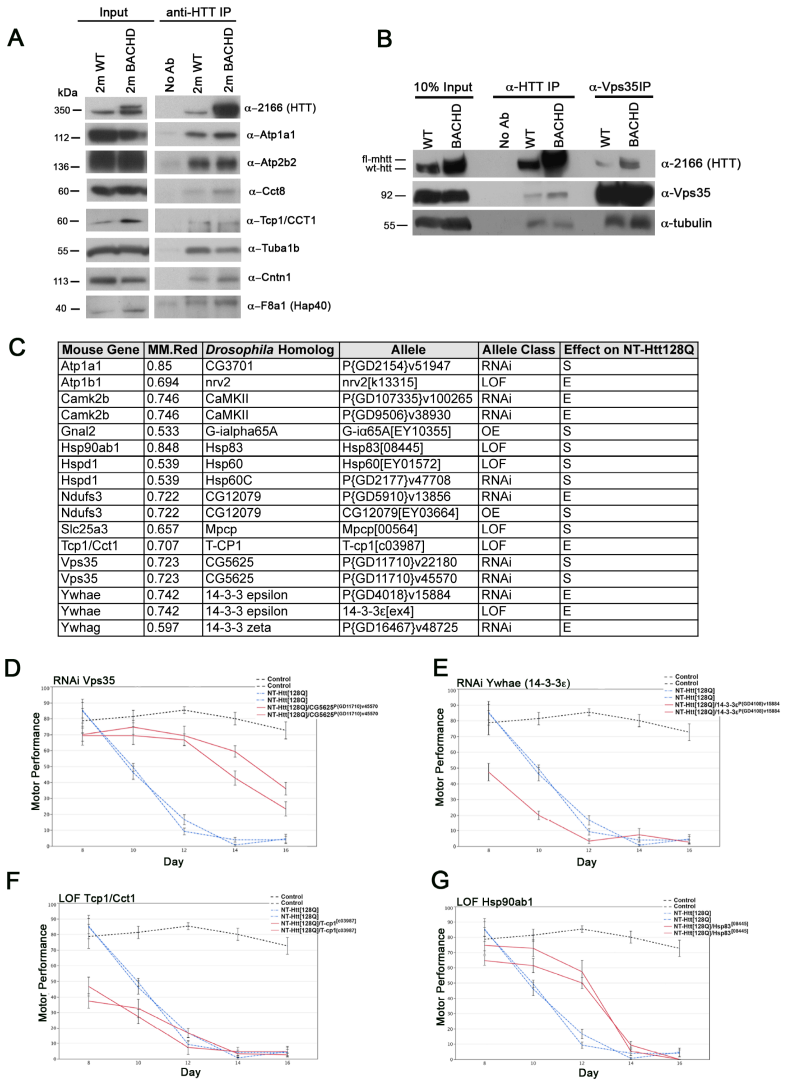
Figure 2.6. Functional annotation of top Htt-correlated modules. (A-F) The Visant plots, IPA, and GO terms most enriched in the top Htt-correlated modules are shown for: A) Red B) Blue C) Pink D) Yellow E) Green and F) Cyan Modules. Visant plots are shown representing the top 150 protein connections in each color module. The enlarged labeled nodes represent the top 15 proteins with the largest module connectivity values (kwithin) for each module, and the nodes in the middle of each Visant plot are the "hub genes" for each module.

2.3.7. Experimental Validation of Red Module Proteins as Huntingtin Interactors and Genetic Modifiers of Functional Deficit in a Fly Model of HD

We next sought to validate those proteins not previously implicated in HD, but with a high Red Module connectivity (hub proteins) as novel Htt physical interactors and/or genetic modifiers (Table 2.1). We performed an anti-Htt co-IP from BACHD and WT mouse brains followed by Western blot analysis for the specific candidate proteins to confirm interaction (Figure 2.7A). We confirmed six novel proteins (Atp1a1, Atp2b2, Cct8, Cct1, Tuba1b, Cntn1) and one positive control Red Module protein (Hap40/F8A1) as co-immunoprecipitating with Htt. Furthermore, Vps35, a protein in the retromer complex that functions in the retrieval of certain membrane proteins from the endosome to the plasma membrane (Attar and Cullen, 2010), was found in both the IP of Htt in both the BACHD and WT mouse brain extracts (Figure 2.7B). Moreover, Htt is also present in the reciprocal co-IP of Vps35 from these brain extracts (Figure 2.7B). Thus, the top Red Module proteins are indeed complexed with Htt in the mouse brain.

To test the hypothesis that Red Module proteins are also modifiers of mHtt toxicity *in vivo*, we performed a genetic modifier study using an established *Drosophila* model of HD expressing human Htt (amino acids 1-336) with an expanded polyQ repeat of 128 glutamines (NT-Htt[128Q]) (Kaltenbach et al., 2007). Directed expression of NT-Htt[128Q] to all neurons of the CNS using the elav-GAL4 driver results in a robust and progressive motor deficit that can be quantified in a climbing assay. We used this behavioral assay to test 32 Red Module genes for which there were available mutants in the corresponding *Drosophila* ortholog genes, and we were able to validate 12 Red Module hub proteins as novel modifiers of neuronal dysfunction (Figure 2.7C-G; Supplemental Figure 2.4A-J). Among the genetic enhancers of the HD motor deficits are Atp1b1, Camk2b, Ndufs3, Tcp1/Cct1, Ywhae, and Ywhag. The genetic suppressors are Atp1a1, Gnai2, Hsp90ab1, Hspd1, Ndufs3, Vps35, and Slc25a3. Interestingly, Ndufs3 is both a suppressor when over-expressed, and an enhancer by partial loss of function

demonstrating dosage sensitive modulation of mHtt-induced motor deficits. In summary, our validation studies confirmed six Red Module proteins as novel Htt-complexed proteins *in vivo* and 12 Red Module proteins as novel genetic modifiers in HD fly. By integrating our validation studies with the existing HD literature, we found a total of 25 out of the top 50 Red Module proteins (based on MMred) to physically or genetically capable of interacting with Htt in various HD model systems (Table 2.1), lending further support that the Red Module is a central Htt *in vivo* protein network, mediating critical aspects of normal Htt function and HD pathogenesis in the brain.



Mouse Gene	MM.Red	*Drosophila* Homolog	Allele	Allele Class	Effect on NT-Htt128Q
Atp1a1	0.85	CG3701	P{GD2154}v51947	RNAi	S
Atp1b1	0.694	nrv2	nrv2[k13315]	LOF	E
Camk2b	0.746	CaMKII	P{GD107335}v100265	RNAi	E
Camk2b	0.746	CaMKII	P{GD9506}v38930	RNAi	E
Gnal2	0.533	G-ialpha65A	G-iα65A[EY10355]	OE	S
Hsp90ab1	0.848	Hsp83	Hsp83[08445]	LOF	S
Hspd1	0.539	Hsp60	Hsp60[EY01572]	LOF	S
Hspd1	0.539	Hsp60C	P{GD2177}v47708	RNAi	S
Ndufs3	0.722	CG12079	P{GD5910}v13856	RNAi	E
Ndufs3	0.722	CG12079	CG12079[EY03664]	OE	S
Slc25a3	0.657	Mpcp	Mpcp[00564]	LOF	S
Tcp1/Cct1	0.707	T-CP1	T-cp1[c03987]	LOF	E
Vps35	0.723	CG5625	P{GD11710}v22180	RNAi	S
Vps35	0.723	CG5625	P{GD11710}v45570	RNAi	S
Ywhae	0.742	14-3-3 epsilon	P{GD4018}v15884	RNAi	E
Ywhae	0.742	14-3-3 epsilon	14-3-3ε[ex4]	LOF	E
Ywhag	0.597	14-3-3 zeta	P{GD16467}v48725	RNAi	E

Figure 2.7. Validation of Red Module proteins in Htt interactome uncovers Htt-interacting proteins in WT and BACHD mice and novel genetic modifiers of disease in a fly model of HD. (A) Co-immunoprecipitation of top MM.Red proteins from 2-month WT and BACHD mouse brains. Htt was immunoprecipitated with anti-Htt (clone HDB4E10) and probed with mouse monoclonal antibody MAB2166. The 10% input for each protein (left panels) and resulting immunoprecipitations are shown (right panels). A no Htt antibody negative control was performed in parallel to confirm specific protein interaction. F8a1 (Hap40) served as the positive control for Htt protein interaction. **(B)** Reciprocal co-immunoprecipitation of Htt and Vps35 in 2-month WT and BACHD mouse brains. Anti-alpha tubulin was used as a loading control. **(C)** Table summarizing the effects caused by modulating the levels of the indicated Red Module proteins on NT-Htt[128Q]-induced motor performance in a HD *Drosophila* model. **(D-G)** Charts represent motor performance as a function of age. Each chart includes controls (elav-GAL4) and animals expressing NT-Htt[128Q] either alone or together with a loss of function allele targeting the *Drosophila* homolog of the indicated gene (red continuous lines). Control flies show robust motor performance for the duration of the experiment (black dashed line). Animals expressing NT-Htt[128Q] in the nervous system using elav-GAL4 show a progressive decline in their motor performance (blue discontinuous lines). D and G show the suppressor effect of decreasing the levels of the *Drosophila* homologs of Vps35 and Hsp90ab1. E and F show the enhancer effect of decreasing the levels of the *Drosophila* homologs of Ywhae and Tcp1/Cct1. Error bars represent S.E.M. Two experimental replicates are shown for the NT-Htt128Q and the NT-Htt128Q/modifier animals except for G.

Table 2.1. Summary of Top 50 Red Module Membership Proteins

Protein	Module	Htt Correlation	MM.Red	IPA Function	IPA Subcellular Distribution	Interactors	Genetic Modifiers	IPA Drugs
Cntn1	red	1.000	0.911	Cell adhesion	Membrane	Known		
Atp2b2	red	1.000	0.907	ATP biosynthesis	Membrane	This study		
Vcp	red	0.999	0.866	DNA repair	Cytoplasm		f, w	
Atp1a1	red	0.999	0.850	ATP biosynthesis	Membrane	This study	f [This study]	Digoxin, Omeprazole
Hsp90ab1	red	1.000	0.848	Molecular chaperone	Cytoplasm		f [This study]	17-AAG
Hsp90aa1	red	0.999	0.804	Molecular chaperone	Cytoplasm		f	17-AAG
Ckb	red	0.999	0.802	Creatine metabolism	Cytoplasm			Creatine
Slc12a5	red	0.999	0.802	Transporter	Membrane			
Ogdh	red	1.000	0.795	Glycolysis	Cytoplasm			
Dync1h1	red	0.999	0.774	Microtubule movement	Cytoplasm	Known	f, w, m	
Stx1b	red	0.999	0.771	Neurotransmitter transport	Membrane			
Dctn1	red	0.999	0.765	Dynein retrograde movement	Cytoplasm			
Ncam1	yellow	0.999	0.748	Glycolysis	Membrane			BB-10901
Camk2b	red	0.999	0.746	Kinase	Cytoplasm		f [This study]	
Ywhae	red	0.999	0.742	Signal transduction	Cytoplasm	Known	f, f [This study]	
Cct8	red	0.999	0.733	Molecular chaperone	Cytoplasm	Known		
Tubb3	red	0.998	0.727	Microtubule movement	Cytoplasm			Colchicine, Epothiolone B
Tubb4	red	0.998	0.726	Microtubule movement	Cytoplasm			Colchicine, Epothiolone B
Vps35	green	0.999	0.723	Transporter	Cytoplasm	This study	f [This study]	
Ndufs3	red	0.999	0.722	Electron transport	Cytoplasm	Known	f [This study]	
HTT	red	1.000	0.710	Signaling, transport, etc.	Cytoplasm			
Tcp1	red	0.997	0.707	Molecular chaperone	Cytoplasm	Known	c, f, f [This study]	
Slc3a2	red	0.998	0.707	Transporter	Membrane			
Atp1b1	yellow	0.997	0.694	ATP biosynthesis	Membrane	Known	f [This study]	
Ddx5	green	0.998	0.682	mRNA processing	Nucleus			
Tuba1b	red	0.998	0.676	Microtubule cytoskeleton	Cytoplasm	This study		
Pdhb	yellow	0.998	0.670	Glycolysis	Cytoplasm			
Atp2a2	pink	0.997	0.666	ATP biosynthesis	Membrane			
Pc	red	0.997	0.664	Gluconeogenesis	Cytoplasm			
Nefm	yellow	0.996	0.663	Microtubule cytoskeleton	Cytoplasm			
Sept3	red	0.998	0.662	Cytokinesis	Cytoplasm			
Slc25a3	red	0.998	0.657	Transporter	Cytoplasm	Known	f [This study]	
Slc1a3	pink	0.998	0.657	Transporter	Membrane			Riluzole
Ywhaz	red	0.997	0.651	Signal transduction	Cytoplasm	Known	c, f	
Rplp0	blue	0.998	0.650	Protein synthesis	Cytoplasm		w	
Nfasc	yellow	0.998	0.650	Cell adhesion	Membrane			
Tomm70a	yellow	0.996	0.648	Transporter	Cytoplasm			
Nsf	blue	0.998	0.646	Vesicle-mediated transport	Cytoplasm		w	
Kif1a	green	0.997	0.643	Molecular movement	Cytoplasm			
Syngr1	red	0.997	0.643	Synaptic plasticity	Membrane			
Rad23b	red	0.998	0.632	Nucleotide-excision repair	Nucleus			
Ap1b1	green	0.997	0.630	Protein transport	Cytoplasm		c, w	
Cdk5	green	0.998	0.629	Kinase	Nucleus			Flavopiridol
Hspa8	green	0.997	0.626	Molecular chaperone	Cytoplasm		c, f, w	
Ipo5	green	0.997	0.621	GTPase inhibitor activity	Nucleus		f, w	
Kif5c	pink	0.998	0.621	Molecular movement	Cytoplasm			
Atp1a4	red	0.992	0.621	ATP biosynthesis	Membrane			Digoxin, Omeprazole
Ppp2ca	yellow	0.997	0.613	Phosphatase	Cytoplasm			
Gnao1	cyan	0.996	0.608	Signal transduction	Membrane	Known		
Stxbp1	cyan	0.997	0.607	Exocytosis	Cytoplasm	Known	f	

Protein function, subcellular distribution, and drug annotation was based on Ingenuity Pathway Analysis (IPA). Protein interactors validated by co-IP/IB and fly genetic modifiers identified from 'This Study' are indicated. Previously identified Htt interactors are labeled as 'Known', and previously identified genetic modifiers (cells, c; fly, f, worm, w, and mouse, m) are indicated above. See Supplemental Material for complete list of references.

2.4. Discussion

We have used a spatiotemporal AP-MS approach to obtain the first compendium of *in vivo* full-length Htt-interacting proteins in the mammalian brain, with the identification of 747 candidate proteins that complex with fl-Htt *in vivo*, creating one of the largest *in vivo* proteomic interactome datasets to date and directly validating more than 100 previously identified *ex vivo* interactors shown to associate with small N-terminal Htt fragments. We have also provided information on the context (age or brain regions) in which these proteins associate with fl-Htt. Moreover, we were able unbiasedly rank the interacting proteins, based on their correlation strength with Htt, and to construct a WGCNA network that describes this interactome. Proteins in several WGCNA network modules are highly correlated with Htt itself, and appear to reflect distinct biological contexts in their interactions with Htt. Finally, we were able to validate dozens of Red Module proteins (the module containing Htt itself) as *in vivo* physical interactors or genetic modifiers in an HD fly model. In summary, our study provides the first comprehensive survey of proteins complexed with fl-Htt in distinct brain regions at different ages, and demonstrates a conceptually novel but simple approach to building unbiased *in vivo* interactomes based on AP-MS data from tissues as complex as the mammalian brain.

This study highlights core HD-relevant molecules and pathways via integration of our spatiotemporal fl-Htt interactome with previously generated large-scale genomic, genetic, and proteomic datasets obtained using *ex vivo*, single cell and invertebrate models of HD. We show that 139 previously identified *ex vivo* Htt interactors (*e.g.,* Y2H) also complex with fl-Htt in the mammalian brain (Goehler et al., 2004; Kaltenbach et al., 2007; Oldham et al., 2008). Moreover, comparison of our interactome with datasets derived from genetic modifier screens in *Drosophila* and *C. elegans* models of HD may also help identify proteins that can interact with mHtt in the mammalian brain and possibly modify its toxicity, and could be prioritized for further validation in mammalian models of HD. For example, comparison of our dataset with data

obtained from genetic screens in yeast, *C. elegans,* and fly models of HD (Nollen et al., 2004; Silva et al., 2011; Wang et al., 2009; Zhang et al., 2010) reveal several Red Module (CCTs, Hsp90s, 14-3-3s, and Vcp; Table 1) and Pink Module (Uqcrc2) proteins in common, which could possibly represent evolutionarily conserved modifiers of mHtt-induced toxicity. Therefore, their disease-modifying role should be fully explored in HD mammalian models.

A key motivation for this work was to obtain an unbiased global view of complex biological or disease processes related to fl-Htt protein in the intact brain, and to formulate novel, testable hypotheses. The first crucial insight obtained from our WGCNA analyses is that distinct Htt-correlated modules represent proteins preferentially complexed with Htt in specific sample conditions that reflect key biological processes: cortical Htt IP samples (Red, Blue, Yellow and Green Modules), cerebellar Htt IP samples (Pink Module), and 12-month but not 2-month cortical samples (Cyan Module). The second important insight is that each of the six significant modules provides critical aspects of known Htt and HD biology. All are significantly enriched with HD signaling in IPA (Figure 2.4C). Knowing the relevance of each module with respect to Htt can seed novel hypotheses based on important hubs identified within that module and/or molecular or pathogenic processes defined by the module (*e.g.,* Cntn1 and Vcp in Red Module mediating mHtt toxicity; Rad23b in Red Module implicating specific DNA repair and ubiquitin/proteasome pathway in Htt biology; Sirt2, Cox2 and Usp9x in the Cyan Module in age-dependent pathogenesis; and Itpr1 and Grid2 in cerebellar neuroprotection in HD). Testing such hypotheses will constitute a crucial next step towards not only unraveling the complex biology of Htt in healthy and diseased brain, but also validating the biological significance of this approach to organize *in vivo* interactome data from complex mammalian tissue (such as the brain).

One potentially exciting area of data integration would be to combine proteomic interactome data with large-scale genetic modifier/gene expression profiling studies from HD patients. The increasing capacity of DNA sequencing provides an unprecedented opportunity for

such large-scale studies using patient samples, and our fl-Htt brain interactome may provide converging information on candidates that may have both a genetic and proteomic link to Htt. Thus, our study lends strong support to a systems biology strategy of vertically integrating large genetic, genomic, and interactome datasets (Geschwind and Konopka,2009) derived from HD models of different organismal complexity to unravel the conserved mechanism related to Htt biology and HD pathogenesis.

Our study supports the view that the majority of Htt-interacting proteins are relatively stable across brain tissue and age (Figure 2.2A-B), while a portion of the Htt interactome is quite dynamic. The latter group of proteins, particularly those that consistently complex with mHtt in a brain-regional-specific or age-specific manner (Figure 2.2C-D), could be interesting candidates to study for their contribution to selective neuronal or regional vulnerability and age-dependent pathogenesis in HD. Our studies also raised the intriguing possibility that age-dependent changes in the normal brain proteome (*e.g.* Sirt2) may alter Htt interactions, which could in turn contribute to the presently unexplained role of aging in disease pathogenesis (Maxwell et al., 2011).

A major advance in this study is the use of a systems biology approach to construct *in vivo* protein interaction networks exclusively using interactome datasets generated from complex tissue, such as the mammalian brain. We applied, for the first time, WGCNA to analyze all the peptide count information for an entire group of Htt complexed proteins in our spatiotemporal AP-MS dataset. WGCNA provides an unbiased systems level organization of gene expression modules in both normal and diseased brains (Voineagu et al., 2011) and has been demonstrated to be among the most powerful methods for global network construction (Allen et al., 2012). Several lines of evidence support the validity and value of WGCNA analyses of our *in vivo* Htt interactome dataset. We were able to show that the pairwise correlation measure leads to a meaningful ranking of Htt related proteins with respect to the external

annotated knowledge of HD related proteins (HD Signaling in IPA; Figure 2.3C). WGCNA identified six significant Htt-correlated modules with distinct tissue- or age-specific over-representation, and significant enrichment of distinct biological function previously implicated in Htt biology (Figure 2.6), effectively providing an *in silico* dissection of the molecular processes related to fl-Htt biology.

Several experimental factors were instrumental to the construction of WGCNA networks based on our AP-MS dataset. First, the relative level of bait protein (fl-Htt) brought down by IP is markedly, but reproducibly, variable across all samples. Such variation is due to our experimental design of using samples from distinct brain regions, ages, genotypes, and no-antibody controls, and also from the use of an anti-Htt antibody that preferentially binds to human over murine Htt. The quantitative difference in the amount of Htt precipitated in each sample results in a similar quantitative variation for those proteins that were tightly associated with Htt (*i.e,* highly correlated with Htt), while background proteins (false positives) in the sample varied to a lesser extent. Hence, rather than being weakened by experimental variance, WGCNA was able to extract the quantitative correlation relationships among the proteins identified in our study. The second important factor for WGCNA analyses was the large-scale and multi-dimensional nature (*e.g.,* brain region, age, and genotype) of our study. We estimated that one would need at least 24 independent AP-MS experiments (at least one biological replicates per sample condition), with systematic changes in the sample conditions to create differential pull-down of the bait protein and its complexes in order to construct a robust WGCNA protein interaction network. One caveat of the current study is our use of MS unique tryptic peptide counts as a semi-quantitative readout of relative protein abundance. Such limitation could have been resolved by using stable isotope labeling in intact animals for a quantitative AP-MS study (Krüger et al., 2008).

Finally, our analysis provides a central molecular network, the Red Module, which is likely to contain proteins crucial to Htt biology and may constitute novel molecular targets to study for HD pathogenesis and therapeutics. The Red Module has Htt as its member, and is highly enriched with Htt interactors and genetic modifiers (Table 2.1). We were able to validate 6 Red Module proteins as novel *in vivo* Htt interactors by co-IP (Figure 2.7) and 12 as novel modifiers of Htt-induced neuronal dysfunction in a fly model (Figure 2.7; Supplemental Figure 2.4A-J). Moreover, Red Module proteins are targets for small molecules that are in HD clinical trials (*i.e.,* creatine targeting Ckb; (Hersch et al., 2006), or show effectiveness in preclinical studies in HD or other polyglutamine disorders in mice (Masuda et al., 2008; Waza et al., 2005). Considering several other proteins in this module can also be targeted by small molecules (Table 2.1), it would be interesting to explore whether pharmacological targeting of these proteins could be therapeutic in HD preclinical models.

In conclusion, we have constructed the first compendium of *in vivo* fl-Htt complexed proteins and provided systems level analyses of the fl-Htt-interacting protein network, thereby providing a valuable resource for further exploration of the biological function of Htt in the brain and identification of novel targets critical to HD pathogenesis and therapy. Moreover, we have demonstrated an innovative approach utilizing WGCNA to analyze multidimensional AP-MS datasets to produce *in vivo* protein complex networks consisting of potential bait proteins, and validate key candidates *in vivo* in fly. This powerful application of systems biology to proteomics can be readily applied to decipher *in vivo* protein networks for other complex biological processes or disease systems, in tissues as complex as the mammalian brain.

2.5. Experimental Methods

Mouse Breeding, Maintenance, and Genotyping

BACHD mice were bred, maintained in the FvB/NJ background, and genotyped as previously described (Gray et al., 2008). BACHD mice were maintained under standard conditions consistent with National Institutes of Health guidelines and approved by the University of California, Los Angeles, Institutional Animal Care and Use Committees.

Brain Tissue Lysate Preparation and Anti-Htt Immunoprecipitation

Protein was prepared as previously described (Gu et al., 2009). Briefly, BACHD and WT mouse brains were dissected in ice-cold 100 mM PBS and homogenized in modified RIPA buffer supplemented with Complete Protease Inhibitor Mixture tablets (Roche) using 10 strokes from a Potter-Elvehjem homogenizer followed by centrifugation at 4°C for 15 min at 16,000*g*. The resultant supernatant is the soluble fraction and protein concentrations were determined using the Bio-Rad Protein Assay (Bio-Rad). Brain lysates (2.5-mg) were subjected to immunoprecipitation with anti-huntingtin clone HDB4E10 (MCA2050, AbD Serotec, 1:500) using Protein G Dynabeads (Invitrogen). Immunoprecipitated proteins (500-ug) were washed, eluted with NuPAGE LDS loading buffer and subjected to Western blot analysis.

In-gel Trypsin Digestion

Immunoprecipitated protein samples were separated on NuPAGE 3-8% Tris-Acetate gels (Invitrogen). Gels were stained using GelCode Blue stain reagent (Pierce) according to the manufacturer's protocol, destained in ddH_2O, and then cut into approximately 24-27 gel slices. The gel slices were washed 3x in alternating solutions of a 50:50 mix of 100mM $NaHCO_3$ buffer/CH_3CN and 100% CH_3CN. Disulfide bonds were reduced by incubation in 10mM dithiothreitol (DTT) at 60°C for 1 hour. Free sulfhydryl bonds were blocked by incubating in

50mM iodoactamide at 45°C for 45 minutes in the dark, followed by washing 3x in alternating solutions of 100mM $NaHCO_3$ and CH_3CN. The slices were dried, and then incubated in a 20-ng/μL solution of porcine trypsin (Promega) for 45 minutes at 4°C, followed by incubation at 37°C for 4 to 6 hours. Afterwards, the supernatant was transferred into a fresh collection tube. The gels were incubated for 10 minutes in a solution of 50% CH_3CN/1% trifluoroacetic acid (TFA), in which the supernatant was removed and combined with the previously removed supernatants. This step was repeated a total of 3 times. The supernatant samples containing the peptides were then spun to dryness and prepared for LC-MS/MS analysis by resuspension in 10-μL of 0.1% formic acid**.**

Mass Spectrometry Analysis

Peptide sequencing was accomplished by nanoLC-MS/MS with a QqTOF-MS (QSTAR Pulsar XL, Applied Biosystems) equipped with nanoelectrospray interface (Protana, Odense, Denmark) and LC Packings (Sunnyvale, CA) nano-LC system. The nano-LC was equipped with homemade precolumn (150 mm x 5 mm) and analytical column (75 mm x 150 mm) packed with Jupiter Proteo C12 resin (particle size 4 mm, Phenomenex, Torrance, CA). The dried peptides were resuspended in 1% formic acid (FA) solution. Six mL of sample solution was loaded to the precolumn for each LC-MS/MS run. The precolumn was washed with the loading solvent (0.1% FA) for 4 min before the sample was injected onto the LC column. The eluants used for the LC were 0.1% FA (solvent A) and 95% ACN containing 0.1% FA (solvent B). The flow rate was 200 nL/min, and the following gradient was used: 3% B to 35% B in 72 min, 35% B to 80% B in 18 min, and maintained at 80% B for 9 min. The column was finally equilibrated with 3% B for 15 min prior to the next run. Electrospray ionization was performed using a 30 mm (i.d.) nano-bore stainless steel online emitter (Proxeon, Odense, Denmark) and a voltage set at 1900 V. Sequences were searched against Swiss-Prot mouse and mammalian genomes using

MASCOT software versions 2.1.0 and 2.1.04 (Matrix Science, London, UK). Peptides were required to have a rank =1 and a score >18.

Peptide Count Correlation of BSA Spiked into BACHD Lysate

Bovine serum albumin (BSA, BP1605-100, Fisher) was spiked into a 2-month BACHD cortex soluble lysate at the following percentages (400-ug total protein): 25%, 2.5%, 0.250%, and 0.125%. The spiked lysates (40-ug) were resolved on a NuPAGE 3-8% Tris-Acetate gel (Invitrogen), stained with GelCode Blue Stain reagent (Pierce), the BSA gel bands (at approximately 66 kDa) were excised from the gel, and the gel bands were subjected to trypsin digestion. Peptide sequencing was accomplished by nanoACQUITY UPLC coupled with the Xevo QTof MS (Waters). The nanoACQUITY UPLC was equipped with 180μm x 20mm Symmetry 5μm C18 trap column (Waters) and a C18 BEH130 (particle size 1.7μm, 75μm x 100mm) analytical column (Waters). The dried peptides were resuspended in 5% formic acid (FA) solution. Triplicate injections of 2mL of sample solution were loaded to the trap column for each LC-MS/MS run. The eluants used for the LC were 0.1% FA in H_2O (solvent A) and 95% ACN containing 0.1% FA (solvent B). The flow rate was 300 nL/min, and the following gradient was used: 1% B to 40% B in 30 min. The column was finally equilibrated with 3% B for 15 min prior to the next run. DDA LC-MS/MS acquisition was performed with lockmass corrected data using [Glu^1]-fibrinopeptide B (785.84 Da) [1-pmol/μL] delivered at 0.3-μL/min and sampled every 60 seconds. MS survey scans of 1.0 second per function over 350-2000 Da were obtained, and MS/MS data was acquired when intensity of an individual ion (charge state 2^+, 3^+, or 4^+) rises above 50 counts/sec at a scan rate of 1.0 s and a collision energy ramp from 15 to 35 eV. Acquisition was returned to MS mode when the TIC rises > 10,000 counts/sec or after 2 sec elapsed. Data was processed using the ProteinLynx Global Server version 2.4 (RC7) and queried against the Swiss-Prot mouse database (with the addition of BSA, human huntingtin,

and keratin sequences). Linear regression correlation plot was rendered using Prism software (version 4).

Weighted Gene Correlation Network Analysis and Module Detection

To determine a weighted correlation network, we first calculated a correlation matrix for all pair-wise correlations of identified proteins across all samples. The resulting correlation matrix was transformed into a signed weighted adjacency matrix as follow is $a_{ij} = ((\text{cor}(x_i, x_j)+1)/2)^{\beta}$ where the power beta represents a soft threshold. Note that negative correlations lead to an adjacency of zero while high positive correlations lead to non-negligible adjacencies. By raising the correlation to a power $\beta \geq 1$ (soft thresholding), the weighted correlation network construction emphasizes large correlations at the expense of low correlations. We used the default soft threshold value of $\beta=15$ which also leads to approximate scale-free topology of the resulting network. To organize proteins into modules, we used the topological overlap matrix (TOM), which is a robust measure of interconnectedness for each pair of proteins in relation to all other proteins identified in the network (Ravasz et al., 2002; Yip and Horvath, 2007). We performed a series of permutations to the network using the criterion that proteins had to be identified in at least 1, 2, or 3 out of the 30 sample conditions. It was determined that proteins present in 3 independent sample conditions resulted in a network enriched with proteins with high topological overlap. Therefore, the list of 750 proteins was reduced to 412 proteins. A dynamic tree-cutting algorithm was used to “cut” 9 branches (modules) off the cluster dendrogram (Langfelder et al., 2008). Proteins that were not assigned to modules were assigned to the color grey.

Connectivity and Defining Module Membership Values

Here we focus on connectivity measures that are useful within the WGCNA context. Whole network connectivity $k(i)$ (also known as degree) is the sum of the connection strengths (adjacencies) between a particular protein x_i and all other proteins in the network. However, we have found that intramodular connectivity MM is often a more meaningful measure of connectivity in module based analyses since it quantifies module membership (Horvath and Dong, 2008; Zhang and Horvath, 2005).

The module membership $MM^q(i)$=Cor(x_i, MP^q)is defined as the correlation between the i-th protein expression profile x_i and the q-th module eigenprotein, MP^q. One can show that the module eigenprotein-based connectivity measure is highly correlated with intramodular connectivity (Horvath and Dong, 2008), but the module membership measure has several advantages including that its definition can be easily extended to proteins outside the original module and that it allows one to use a correlation test to assess the statistical significance (p-value) of module membership. WGCNA also outputs the corresponding correlation test p-value for module membership (denoted by PvalueMMblue).

I

Immunoprecipitation and Immunoblot Analysis of Htt-interacting Proteins

We validated full-length huntingtin protein-protein interactions by anti-Htt immunoprecipitation (as described above), followed by immunoblot analysis with the antibodies listed below.

Antibody	Host/Clonality	Primary	Secondary	Catalog #	Vendor
HTT	Mouse, monoclonal	1:3000	1:3000	MAB2166	Millipore
ATP1A1	Mouse, monoclonal	1:10,000	1:10,000	NB300-146	Novus Biologicals
ATP2B2	Mouse, monoclonal	1:500	1:5000	610932	BD Transduction Labs
VPS35	Rabbit, polyclonal	1:1000	1:3000	Ab76329	Abcam
CCT8	Rabbit, polyclonal	1:1000	1:10,000	12263-1-AP	ProteinTech Group, Inc.
CCT1	Goat, polyclonal	1:200	1:3000	sc-13869	Santa Cruz Biotechnology
TUBA1B	Mouse, monoclonal	1:10,000	1:20,000	T 6074	Sigma
F8A1	Rabbit, polyclonal	1:500	1:3000	ab1139	Abcam
CNTN1	Mouse, monoclonal	1:100	1:3000	75-038	UC Davis NeuroMab Facility

Drosophila Motor Performance Assay

Using a population of 15 age-matched (+/- 4 hours) virgin female flies, we estimate the % of animals able to climb past a line set at 9cm in 15sec. These tests are repeated 10 consecutive times for each replicate per experimental day. The experiment is carried out in duplicate (2 populations of 15 animals) in flies that were 8, 10, 12, 14, and 16 days old. Tests are always performed in the same time of the day and in the same place, to avoid circadian rhythm and environmental variability. The average number of flies climbing per day is averaged and plotted independently for each replicate.

Fisher's Exact Hypergeometric Test

Significance of overlap between 2 gene lists was performed using the hypergeometric test (), and assuming the total number of possible proteins being 20,000 ().

Overlap with Y2H:

Set1: 747
Set2: 877
Overlap: 139
Total number of genes: 20000

Representation factor: 4.2
p < 7.243e-50

Overlap with ataxia

Set1: 747
Set2: 575
Overlap: 38
Total number of genes: 20000

Representation factor: 1.8
p < 5.381e-04

CHAPTER 3

Biochemical Characterization of BAC Transgenic Mouse Models of HD with Htt N17 Mutations

Part I:

Biochemical Characterization of the SD and SA Mouse Models

This first part of Chapter 3 is a reprint of the article:

Gu, X., Greiner, E.R., Mishra, R., Kodali, R., Osmand, A., Finkbeiner, S., Steffan, J.S., Thompson, L.M., Wetzel, R., Yang, X.W. (2009) Serines 13 and 16 are Critical Determinants of Full-Length Human Mutant Huntingtin Induced Disease Pathogenesis in HD Mice. *Neuron* 64, 828-840.

My contribution to this manuscript as second author was performing all of the biochemical analysis on the SD and SA mice. More specifically, I quantified full-length mutant huntingtin levels in the SD and SA mice using the polyQ antibodies 1C2 and 4H7H7, verified that Ser13 and Ser16 residues can be phosphorylated in the BACHD mouse model, determined that full-length mutant huntingtin protein levels do not change over time in young (1m) versus old (12m) SD and SA cortical lysates, confirmed the genetic rescue of the SD and SA transgene by Western blot analysis, and analyzed full-length mutant huntingtin protein levels in various subcellular fractions in SD and SA cortical tissues.

Neuron
Article

Serines 13 and 16 Are Critical Determinants of Full-Length Human Mutant Huntingtin Induced Disease Pathogenesis in HD Mice

Xiaofeng Gu,[1,2,3] Erin R. Greiner,[1,4] Rakesh Mishra,[5] Ravindra Kodali,[5] Alex Osmand,[6] Steven Finkbeiner,[7] Joan S. Steffan,[8] Leslie Michels Thompson,[8,9,10] Ronald Wetzel,[5] and X. William Yang[1,2,3,*]
[1]Center for Neurobehavioral Genetics, The Jane and Terry Semel Institute for Neuroscience and Human Behavior
[2]Department of Psychiatry and Biobehavioral Sciences
[3]Brain Research Institute
David Geffen School of Medicine at University of California, Los Angeles, Los Angeles, CA 90095, USA
[4]Department of Chemistry and Biochemistry, University of California, Los Angeles, Los Angeles, CA 90095, USA
[5]Department of Structural Biology and Pittsburgh Institute for Neurodegenerative Diseases, University of Pittsburgh School of Medicine, Pittsburgh, PA 15260, USA
[6]Department of Medicine, University of Tennessee Graduate School of Medicine, Knoxville, TN 37920, USA
[7]Gladstone Institute of Neurological Disease, Taube-Koret Center for Huntington's Disease Research, Departments of Neurology and Physiology, University of California, San Francisco, San Francisco, CA 94158, USA
[8]Department of Psychiatry and Human Behavior
[9]Department of Neurobiology and Behavior
[10]Department of Biological Chemistry
University of California, Irvine, Irvine, CA 92697, USA
*Correspondence: xwyang@mednet.ucla.edu
DOI 10.1016/j.neuron.2009.11.020

SUMMARY

The N-terminal 17 amino acids of huntingtin (NT17) can be phosphorylated on serines 13 and 16; however, the significance of these modifications in Huntington's disease pathogenesis remains unknown. In this study, we developed BAC transgenic mice expressing full-length mutant huntingtin (fl-mhtt) with serines 13 and 16 mutated to either aspartate (phosphomimetic or SD) or alanine (phosphoresistant or SA). Both mutant proteins preserve the essential function of huntingtin in rescuing knockout mouse phenotypes. However, fl-mhtt-induced disease pathogenesis, including motor and psychiatric-like behavioral deficits, mhtt aggregation, and selective neurodegeneration are abolished in SD but preserved in SA mice. Moreover, modification of these serines in expanded repeat huntingtin peptides modulates aggregation and amyloid fibril formation in vitro. Together, our findings demonstrate that serines 13 and 16 are critical determinants of fl-mhtt-induced disease pathogenesis in vivo, supporting the targeting of huntingtin NT17 domain and its modifications in HD therapy.

INTRODUCTION

Huntington's disease (HD) is an autosomal-dominant and progressive neurodegenerative disorder characterized by movement disorders, cognitive impairment, and psychiatric symptoms (Harper, 1996). HD is caused by a polyglutamine (polyQ) repeat expansion near the N terminus of huntingtin (Htt), a very large 350 kDa protein (The Huntington's Disease Collaborative Research Group, 1993). Huntingtin is thought to function as a scaffolding protein that mediates a variety of protein-protein interactions involved in vesicular trafficking, signaling, and transcription (MacDonald, 2003; Li and Li, 2006). HD neuropathology is characterized by the selective loss of predominantly medium-sized spiny neurons (MSNs) in the striatum and to a lesser extent the pyramidal neurons in the deep layers of the cortex (Vonsattel and DiFiglia, 1998). Another pathological hallmark of HD is the accumulation of nuclear and cytoplasmic protein aggregates containing mhtt N-terminal polyQ fragments in the cortex and striatum (DiFiglia et al., 1997; Gutekunst et al., 1999). Currently, it remains unclear how mhtt can cause progressive neuronal dysfunction and selective neurodegeneration in the brain (Orr and Zoghbi, 2007; Li and Li, 2006). Unraveling the underlying pathogenic mechanisms may provide important clues to the development of effective treatments for this lethal neurodegenerative disorder.

Although protein misfolding due to polyQ expansion appears to be a shared pathogenic mechanism in all polyQ disorders (Orr and Zoghbi, 2007; Williams and Paulson, 2008; Bates, 2003; Ross and Poirier, 2004), the critical molecular pathway through which misfolded polyQ proteins elicit disease-specific clinical and pathological outcomes remain unresolved. Recent studies reveal a critical role for the specific protein context beyond the expanded polyQ domain in modifying disease pathogenesis (Gatchel and Zoghbi, 2005; Orr and Zoghbi, 2007; Katsuno et al., 2002). In HD, covalent posttranslational modifications of mhtt have been implicated in disease pathogenesis (Schilling et al., 2006; Steffan et al., 2004; Jeong et al., 2009;

Humbert et al., 2002; Anne et al., 2007; Yanai et al., 2006). However, in all but one case (i.e., the caspase-6 cleavage site; Graham et al., 2006), the pathogenic significance of htt *cis*-domain modifications in vivo has been assessed using mhtt N-terminal fragment models. Therefore, it remains to be addressed how these modifications may influence disease pathogenesis in the context of fl-mhtt in a mammalian model of HD.

Emerging data suggest that the N-terminal 1–17 amino acids of htt (NT17 domain) immediately preceding the polyQ domain may constitute a critical functional domain for htt function and HD pathogenesis (Steffan et al., 2004; Cornett et al., 2005; Rockabrand et al., 2007; Atwal et al., 2007; Aiken et al., 2009). The NT17 domain is highly conserved evolutionarily and can mediate htt binding to peripheral membranous structures (Atwal et al., 2007; Rockabrand et al., 2007). The NT17 domain can function as a cytoplasmic retention signal and deletions or certain point mutations in this domain result in nuclear accumulation of htt in cultured cells (Rockabrand et al., 2007; Cornett et al., 2005; Steffan et al., 2004; Atwal et al., 2007). The NT17 domain can also be covalently modified by ubiquitylation and SUMOylation, which appear to have opposing effects on the toxicity of mhtt fragments in a transgenic *Drosophila* model (Steffan et al., 2004). Recent biochemical analyses reveal that interaction of the NT17 domain with the adjacent polyQ domain can accelerate mhtt exon 1 peptide aggregation via a novel and complex pathway (Thakur et al., 2009). This converging evidence suggests that the NT17 domain and its modifications may play important roles in the physical and biological properties of wild-type htt, and in the toxicity of fl-mhtt and its toxic fragments.

In neurodegenerative diseases, phosphorylation of disease proteins such as tau (Ballatore et al., 2007), SCA1 (Emamian et al., 2003), and α-synuclein (Fujiwara et al., 2002) has been shown to play important roles in disease pathogenesis. Recent studies reveal that serines 13 and 16 (S13 and S16) in htt NT17 domain can be phosphorylated in cultured mammalian cells (Aiken et al., 2009; Thompson et al., 2009). To address the importance of these modifications in disease pathogenesis elicited by fl-mhtt in a mammalian model of HD, we have introduced either phosphomimetic (SD) or phosphoresistant (SA) mutations into fl-mhtt. Dramatically, SD but not SA fl-mhtt can prevent progressive neuronal dysfunction, mhtt aggregation, and late-onset neurodegenerative pathology in vivo. Moreover, an in vitro aggregation assay reveals that the SD mutations significantly compromise the fibrillization of mhtt-exon 1 peptides, whereas SA mutations do not. Thus, we provide strong evidence that S13 and S16 in htt NT17 domain play a critical role in modulating polyQ-induced misfolding and/or aggregation in vitro and fl-mhtt-induced disease pathogenesis in vivo.

RESULTS

Generation and Biochemical Characterization of BAC Transgenic Mice with Mutations at S13 and S16 of Full-Length Mutant Huntingtin

To evaluate the pathogenic relevance of S13 and S16 phosphorylation in mammalian models of HD, we re-engineered the S13 and S16 residues of our previous BACHD construct (fl-mhtt-[97Q]; Gray et al., 2008) to aspartate (SD), a mutation commonly used to mimic serine phosphorylation. We also mutated the two serine residues to alanine (SA), which renders the mhtt NT17 domain incapable of being phosphorylated at these sites (Figure 1A). The structural integrity of the engineered SD and SA BACs were confirmed with pulse field gel electrophoresis (Figure S1A) and the purified DNA was microinjected into FvB/N one-cell embryos to generate transgenic founders (Figures S1B and S1C). Five founders for the BACHD-SD construct and two founders for the BACHD-SA mutant were obtained, and initial expression analyses of the F1 mice from these lines identified two lines with SD mutations (lines B and C) and one line with SA mutations expressing fl-mhtt protein at suitable levels (see below). The mutant htt exon 1 region was PCR amplified and sequenced to confirm the appropriate mutations at S13 and S16, and a polyQ repeat length of 97 (Figures S1D and S1E; Table 1). These mouse lines were expanded by breeding with FvB/NJ wild-type mice, the same inbred mouse background used in the previous phenotypic characterization of BACHD mice (Gray et al., 2008; Spampanato et al., 2008; Menalled et al., 2009).

We next used S13- and S16-phosphospecific htt antibodies to confirm the specificity of the S13 and S16 mutations at the protein level in SD and SA mice. The binding of these antibodies should be prevented following either SD or SA mutation in fl-mhtt, and only unmodified, phosphorylated htt will be recognized by phosphospecific antibodies. Consistent with this prediction, we were able to immunoprecipitate fl-mhtt from BACHD brains using S13- and S16-phosphospecific htt antibodies, but not the NT17-mutated fl-mhtt from SD and SA brains (Figure S2). Thus, we were able to show that the phosphorylated species of fl-mhtt can be detected in BACHD brains and confirm the molecular specificity of the S13 and S16 mutations in the context of fl-mhtt-[97Q] protein isolated from SD and SA brains.

We next assessed the fl-mhtt-[97Q] protein levels in BACHD, BACHD-L, BACHD-SD, and BACHD-SA mice. BACHD-L mice express fl-mhtt-[97Q] at about one-third the level of the BACHD mice but still demonstrate evidence of disease pathogenesis (Gray et al., 2008; Table 1). We performed quantitative western blot analysis to ensure that fl-mhtt-[97Q] protein levels in SD and SA mice were at or above the fl-mhtt-[97Q] level in BACHD-L mice and therefore would be expected to elicit at least some disease pathogenesis. We quantified the relative expression of fl-mhtt-[97Q] using two anti-polyQ monoclonal antibodies: 1C2 (Figure 1B) and 4H7H7 (Figure S3A). The mouse monoclonal 4H7H7 antibody can recognize mhtt N-terminal fragment (1–480 amino acid) with 68Q but not the same htt fragment with 17Q (Figure S3B). 4H7H7 can also recognize on western blots two other expanded polyQ proteins, mutant ataxin-1 and ataxin-3, but not their corresponding wild-type proteins with nonpathogenic polyQ repeats (Figures S3C and S3D). In our series of BACHD models, both 4H7H7 and 1C2 can specifically recognize human mhtt but not endogenous murine wild-type htt (Figures 1B and S3A). Since these different BACHD mouse lines all have the same length polyQ repeat, western blot quantification of fl-mhtt with the anti-polyQ antibody 1C2 can accurately determine the relative expression level of soluble, steady-state fl-mhtt (Figure 1C and Table 1). We determined the relative levels of fl-mhtt-[97Q] in brain extracts

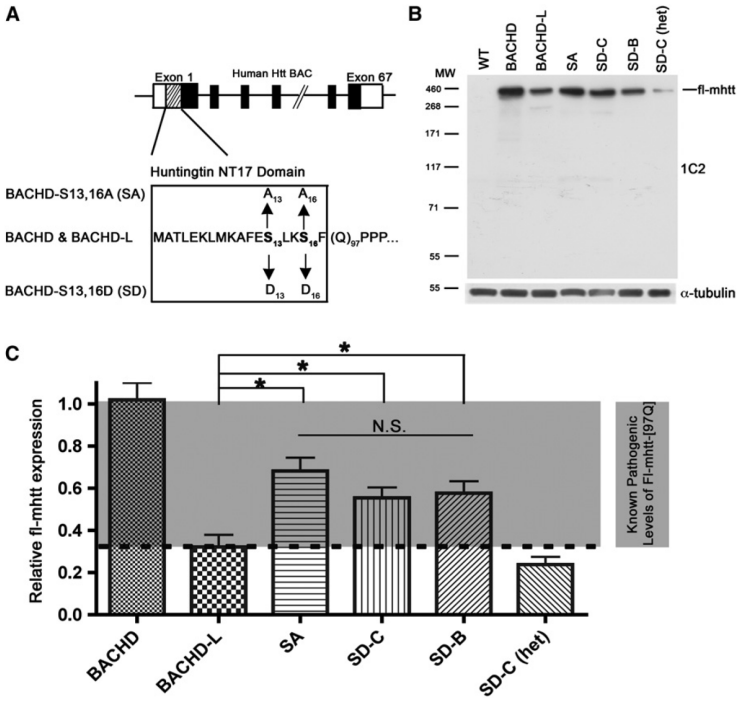


Figure 1. Generation and Biochemical Characterization of the Phosphomimetic (SD) and Phosphoresistant (SA) BACHD Transgenic Mice

(A) A schematic representation of the S13,16A and S13,16D mutations within the NT17 domain in the BACHD construct (Gray et al., 2008).

(B) A representative western blot of cortical protein extracts made from 1-month-old BACHD, BACHD-L, SA, SD-B, SD-C, and SD-C heterozygous (het) mice. The blot was probed with polyQ-specific 1C2 antibody followed by anti-tubulin antibody for loading controls.

(C) Quantification of the fl-mhtt expression levels in various HD transgenic mouse lines. Densitometry values of individual bands are based on three 1C2 western blots using independent cortical extracts. The input in each lane is normalized using the anti-α-tubulin control. The results of three independent experiments are expressed as means ± SEM. One-way ANOVA analysis reveals that there are significant differences between the fl-mhtt expression levels in BACHD, BACHD-L, SA, SD-C, SD-B, and SD-C (het) mice ($F(4,11) = 22.090$, $p < 0.001$). The post hoc test (LSD) indicates that the BACHD-L fl-mhtt expression level is significantly lower than the fl-mhtt expression level in the BACHD ($p < 0.001$), SA ($p = 0.001$), SD-C ($p = 0.017$), and SD-B ($p = 0.01$) mice, but does not differ from the SD-C (het) mice ($p = 0.34$).

Error bars indicate mean ± SEM.

from BACHD and BACHD-L heterozygotes, SA heterozygotes, SD-B line homozygotes, and SD-C line homozygotes and heterozygotes [SD-C (het)] (n = 3 per genotype). Using one-way ANOVA with post hoc analysis, we determined that there are no significant differences in fl-mhtt expression levels between the SA, SD-B, and SD-C mice, whereas all of these lines express fl-mhtt-[97Q] protein at significantly higher levels than the BACHD-L line but at lower levels than the BACHD line, suggesting that the SA, SD-B, and SD-C mice express sufficient levels of fl-mhtt-[97Q] to elicit a disease phenotype.

To assess whether the SD or SA mutations affect the subcellular distribution and/or the steady-state level of fl-mhtt, we performed a series of western blot analyses. First, subcellular fractionation of cytosolic, nuclear, microsomal, and mitochondrial fractions of the BACHD, SA, and SD-C mice at 2 months of age (n = 3 per genotype) was performed and followed by western analysis using the 1C2 antibody. At our level of detection in the mouse brain extracts, we do not observe any major shifts of the subcellular localization of fl-mhtt or its detectable fragments in SD or SA mutant mice compared to BACHD mice (Figure S4). Next, we sought to determine the steady-state levels of soluble fl-mhtt protein during the aging process to assess whether there is any notable shift in fl-mhtt protein levels or increase in the production of soluble mhtt fragments over time. In each of the three mutant HD mouse lines we have examined, the levels of soluble fl-mhtt are comparable between 2 and 12 months (Figure S5). Moreover, in SD and SA mice, we do not detect any aberrant increase of soluble mhtt polyQ fragments at 12 months, suggesting that age-dependent differences in the abundance of soluble full-length and fragmented mhtt cannot account for any phenotypic changes.

In summary, our biochemical analyses demonstrate that SA, SD-B, and SD-C mice express fl-mhtt-[97Q] at levels well above the range expected to elicit disease pathogenesis in vivo. Furthermore, we cannot detect marked differences in S13 and S16 modified fl-mhtt and its polyQ fragments in their subcellular localization or their steady-state, soluble levels over time.

Full-Length Mutant Huntingtin with S13 and S16 Mutations Preserves Normal Htt Function during Development and in Adult Cortical Neurons

We next asked whether S13 and S16 mutated fl-mhtt could still exhibit the essential functions of htt in vivo. We evaluated whether *cis*-modified htt can rescue the phenotypes of htt knockout mice, including embryonic lethality in the complete null mutant mice (Zeitlin et al., 1995; White et al., 1997) and late-onset cortical neuron degeneration in the forebrain-specific deletion of the htt gene (Dragatsis et al., 2000). We previously demonstrated that fl-mhtt-[97Q] in BACHD mice can rescue the embryonic lethality of htt knockout mice, confirming that fl-mhtt retains the essential developmental function of htt (Gray et al., 2008). To assess whether fl-mhtt-[97Q] with SD or SA mutations retain the function of htt, we crossed SA, SD-B, and SD-C heterozygous alleles onto the htt knockout background and scored for the number of the rescued mice born (Gray et al., 2008). In all three lines, the rescued mice were born in

Table 1. Phenotypic Summary of Different BAC Transgenic Mouse Models of HD

BAC Lines	PolyQ Repeat	Fl-mhtt Protein (% BACHD)	Motor Dysfunction: Rotarod 2 mo	Motor Dysfunction: Rotarod 6 mo	Motor Dysfunction: Rotarod 12 mo	Psychiatric-like Deficits: Anxiety 12 mo	Psychiatric-like Deficits: Depressive-like 12 mo	Selective Neuropathology 12 mo	mhtt Aggregates 12 mo
BACHD	97	100%	+	+	+	+	+	+	+
BACHD-L	97	32%	+	+	n.d.	n.d	n.d.	n.d	+
SA	97	70%	+	+	+	+	+	+	+
SD-B	97	54%	-	-	-	-	-	-	-
SD-C	97	57%	-	-	-	-	-	-	-
SD-C (het)	97	23%	-	-	-	-	-	-	-

a Mendelian ratio (Figure 2A). Overall, we have obtained at least seven rescued mice per genotype, and these rescued mice express only fl-mhtt-[97Q] with S13 and S16 mutations, but not endogenous wild-type murine htt (Figures 2B and 2C). Since these rescued mice do not show obvious deterioration with age, we could assess whether S13 and S16 mutated fl-mhtt could also rescue the robust late-onset cortical neurodegeneration phenotype between 6 and 12 months of age in the forebrain-specific htt knockout mice (Dragatsis et al., 2000). We performed neuropathological evaluation of the brain sections from 12-month-old SD-B rescue mice and WT control littermates (n = 3 per genotype). As shown in Figures 2D–2G, we did not detect any evidence for neurodegeneration in the cortex of SD-B rescue mice (Figures 2F and 2G), including the piriform cortex near the external capsule where the conditional knockout of htt produced the most notable neurodegeneration (ibid). Together, these studies demonstrate that fl-mhtt with SD or SA mutations retains the essential developmental and neuroprotective function of murine htt.

Phosphomimetic Mutations at S13 and S16 Abolish Motor and Psychiatric-like Deficits Induced by the Expression of Full-Length Mutant Huntingtin

BACHD mice exhibit both motor deficits and enhanced psychiatric-like deficits (Gray et al., 2008; Menalled et al., 2009), which can be used to address whether S13 and S16 site mutations affect the neuronal dysfunction elicited by fl-mhtt in vivo. To assess motor dysfunction, we applied a two-way mixed factorial design to repeatedly examine the rotarod performance in a cohort of SA, SD-B, and SD-C mice at 2, 6, and 12 months of age. Similar to BACHD and BACHD-L mice (Gray et al., 2008; Table 1), we found that SA mice also exhibit significant rotarod deficits starting at 2 months of age ($p < 0.0001$, independent sample Student's t test), which progressively worsen at 6 and 12 months of age ($p = 0.0001$ for 6 month age, $p < 0.0001$ for 12 month age, Figure 3A). Repeated-measure two-way ANOVA further revealed a significant genotype effect ($F_{(1,30)} = 29.301$, $p < 0.0001$). There is also a significant interaction between genotype and age ($F_{(1,30)} = 4.965$, $p = 0.034$). To further evaluate effects of age on motor performance within each genotype, we used one-way ANOVA to analyze the age contribution to rotarod performance in separate genotypes. We did not find any significant overall age effect in wild-type mice ($F(2,45) = 0.089$, $p = 0.915$), but did find a significant main effect of age in SA mice, ($F(2, 45) = 3.390$, $p = 0.043$), which suggests a progressive impairment of rotarod performance. Contrary to the findings in SA mice, two independent lines of SD mice (SD-C and SD-B homozygotes) did not exhibit any rotarod deficits compared to their respective WT littermate controls at 2, 6, and 12 months (Figures 3B and 3C). Repeated-measure two-way ANOVA did not detect a significant genotype effect (for SD-B: $F_{(1, 17)} = 0.695$, $p = 0.416$; for SD-C: $F_{(1,22)} = 0.373$, $p = 0.548$). Moreover, there is no significant interaction between genotype and age (for SD-B: $F_{(1, 17)} = 1.345$, $p = 0.262$; for SD-C: $F_{(1, 22)} = 0.006$, $p = 0.938$).

We then compared rotarod performance of SD and SA mice to the BACHD-L line. BACHD-L mice have significant rotarod impairment at 6 months of age (Figure 3D). We also compared the 6-month rotarod performance of the WT control mice from different HD mouse lines using one-way ANOVA analysis and found no significant differences among the four groups' WT controls ($F_{(3, 38)} = 1.292$, $p = 0.285$ and $p > 0.05$ in pairwise comparisons, Figure S6). Thus, rotarod performance changes in these lines cannot be attributed to any differences in the WT controls. We then compared the pooled WT controls with SD-B and SD-C mice in their 6-month rotarod performance (Figure 3D), which did not reveal any significant differences between the genotypes (WT = 42, SD-B = 10, SD-C = 12, one-way ANOVA with Fisher's LSD post hoc test, $p > 0.05$). On the other hand, both BACHD-L mice and the SA mice exhibited significant motor impairment compared to WT, SD-B and SD-C mice (BACHD-L = 12, SA = 8, one-way ANOVA with Fisher's LSD post hoc test, BACHD-L versus SD-B, $p = 0.032$; BACHD-L versus SD-C, $p = 0.025$; SA versus SD-B, $p < 0.0001$; SA versus SD-C, $p < 0.0001$; SA versus BACHD-L, $p = 0.029$). Together, these studies demonstrate that SA mutations still retain the toxicity of fl-mhtt and can elicit motor deficits, while SD mutations abolish this disease phenotype in the BACHD model system.

Although psychiatric symptoms are particularly difficult to model in animals, several tests have been developed to assess psychiatric-like behaviors that have at least some predictive validity in patients (Crawley, 2008). BACHD mice were found to exhibit a higher level of anxiety as measured by two different tasks, the light-dark box and elevated plus maze (Menalled et al., 2009). To assess whether SD or SA mutations in fl-mhtt can modulate these anxiety-like behavioral deficits, we tested 12-month-old SD-B, SD-C, and SA mice and their respective

A

	Total Number of Offspring	Expected Number of Rescued Mice	Actual Number of Rescued Mice
SD-B line	60	9	11
SD-C line	45	6	8
SA line	56	8	7

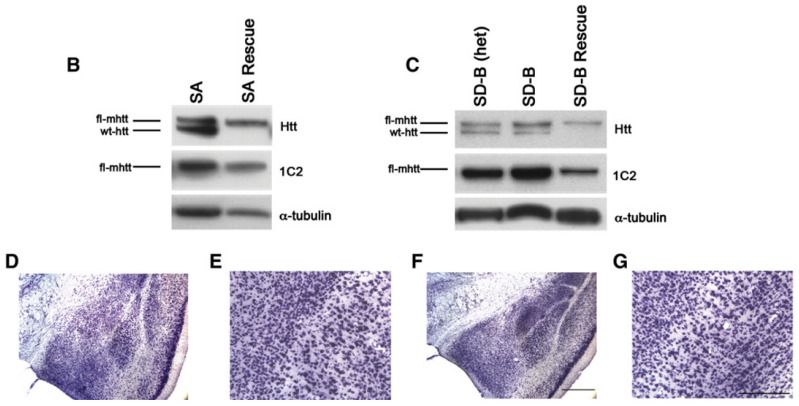


Figure 2. Mutant Huntingtin with S13 and S16 Mutations Preserve Normal Htt Function during Development and in Adult Cortical Neurons

(A) Heterozygous SD-B, SD-C, and SA transgenes were bred in two successive generations with murine *Hdh* heterozygous knockout mice (Zeitlin et al., 1995) to generate the rescue mice (i.e., fl-mhtt transgene rescue the embryonic lethality of htt null mice). Since the homozygous *Hdh* null mice are embryonic lethal (ibid), the expected ratio of rescue mice among the live mice born is 1 out of 7. The rescue mice for SD-B, SD-C, and SA were born with such Mendelian ratio.

(B and C) Western blot analyses with mAb2166 (Htt) and 1C2 to confirm that the rescue mice only express fl-mhtt and lack endogenous murine htt.

(D–G) SD fl-mhtt retains the essential adult neuronal function of htt in vivo. Nissl-stained coronal brain sections of 12-month-old SD-B rescue mice (F and G) and WT littermates (D and E) at two different magnifications. No evidence of late-onset cortical neurodegeneration, as previously reported in the forebrain-specific htt null mice (Dragatsis et al., 2000), was detected in these rescue mice.

Scale bars: (F) 500 μm, (G) 50 μm.

WT controls. Similar to BACHD, SA mice still exhibit a significant anxiety phenotype compared to the controls ($p = 0.0002$, independent sample Student's t test), while the SD-B and SD-C mice no longer exhibit the anxiety-like behavior compared to their respective controls (SD-B versus WT $p = 0.8991$; SD-C versus WT, $p = 0.7606$, independent sample Student's t test; Figure 3E). Thus, consistent with the motor test, the SD but not SA mutations also appear to abolish the psychiatric-like behavioral deficit observed in BACHD mice.

Full-Length Huntingtin with Phosphomimetic S13 and S16 Mutations Can Prevent the Onset of Neurodegenerative Pathology In Vivo

BACHD brains at 12 months of age recapitulate aspects of selective neurodegenerative pathology in HD, particularly the selective atrophy of the cortex and striatum with relative preservation of the cerebellum (Gray et al., 2008). We next addressed whether the SA and SD mutations in fl-mhtt could differentially impact the pathogenesis of selective neurodegeneration in vivo. Similar to BACHD mice, significant forebrain weight loss was detected in SA mice compared to their WT littermate controls (Figure 4A, $p = 0.0064$, Student's t test). However, both SD-B and SD-C mice do not exhibit the forebrain atrophy phenotype compared to their respective WT controls (SD-B versus WT, $p = 0.1975$; and SD-C versus WT, $p = 0.7155$, Student's t test). In all three genotypes, no significant cerebellar atrophy was detected (Figure 4B).

To more quantitatively evaluate both the cortical and striatal atrophy in SA and SD mice, we applied the unbiased stereology method to measure both the cortical and striatal volumes in 12-month-old SA and SD-B mice. Similar to the BACHD mice (Gray et al., 2008), we found that SA mice exhibit 17% reduction of both the striatal and cortical volumes compared with their WT littermates (Figures 4C and 4D; number of mice: WT = 4, SA = 5; striatal volume: WT = 15.97 ± 0.8301 mm^3; SA = 13.25 ± 0.6435 mm^3; $p = 0.0336$, Student's t test; cortical volume: WT = 50.91 ± 1.332 mm^3; SA = 42.49 ± 1.318 mm^3; $p = 0.003$, Student's t test). On the contrary, SD-B mice do not exhibit any striatal or cortical volume loss compared to their WT controls (number of mice: WT = 4; SD-B = 5; striatal volume: WT = 16.00 ± 0.5836 mm^3; SD-B = 16.13 ± 0.4873 mm^3; $p = 0.8635$, Student's t test; cortical volume: WT = 50.88 ± 0.7701 mm^3; SD-B = 50.67 ± 1.357 mm^3; $p = 0.9025$, Student's t test; Figures 4C and 4D).

Together, these data reveal that the SA and SD mutations have opposing effects on the neurodegeneration phenotypes elicited by fl-mhtt, with the SA fl-mhtt remaining neuropathogenic whereas the SD fl-mhtt no longer induce the selective neurodegenerative pathology in vivo.

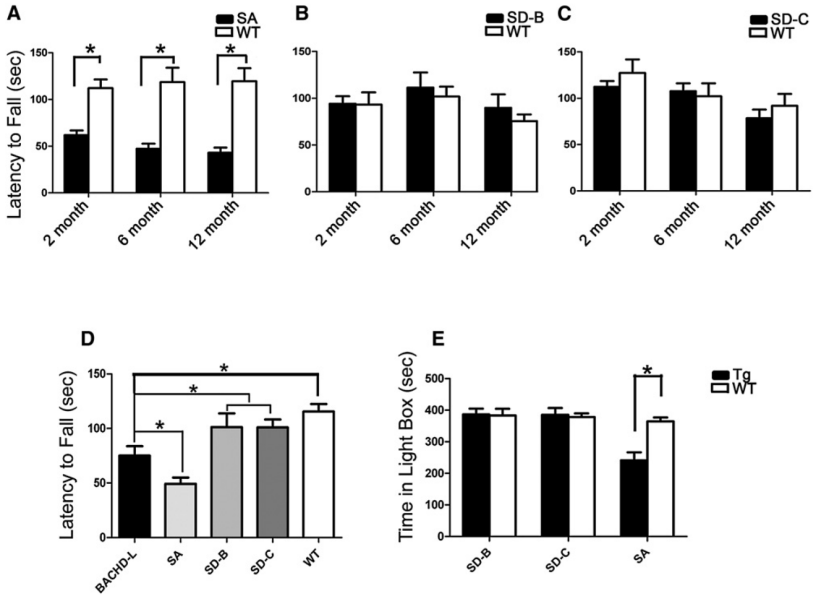


Figure 3. The SA but Not the SD Mice Demonstrate Motor and Psychiatric-like Behavioral Deficits

A mixed model two-way ANOVA design was used to examine the rotarod performance in a cohort of SA, SD-B, and SD-C mice at 2, 6, and 12 months of age.

(A) SA mice exhibit significant rotarod deficits starting at 2 months of age and persisting at 6 and 12 month ages (*$p < 0.0001$, Student's t test).

(B and C) Two independent lines of SD mice (SD-C and SD-B homozygotes) did not exhibit any rotarod deficits compared to their respective WT littermate controls at 2, 6, and 12 months.

(D) Comparison of 6-month-old BACHD-L, SA, SD-B, and SD-C lines rotarod performance. SD-B and SD-C mice did not show any significant impairment in their 6 month rotarod performance compared to wild-type controls. On the other hand, both BACHD-L mice and SA mice exhibited significant impairment compared to WT, SD-B, and SD-C mice (one-way ANOVA with Fisher's LSD post hoc test, $p < 0.05$; for details, see main text).

(E) The SA mice ($p = 0.0002$, Student's t test) but not SD mice demonstrate significantly enhanced anxiety in light/dark box exploration test.

Error bars indicate mean ± SEM.

Phosphomimetic S13 and S16 Mutations Prevent the Accumulation of Mutant Huntingtin Aggregates In Vivo

The ability of mhtt N-terminal fragments to form cytoplasmic aggregates and nuclear inclusions was first discovered in a HD mouse model (Davies et al., 1997), and such aggregates are seen in BACHD mice (Gray et al., 2008). We tested whether the monoclonal antibody 4H7H7 could detect mhtt aggregates containing the expanded polyQ fragments in situ. Using antigen retrieval followed by immunohistochemistry (Osmand et al., 2006), 4H7H7 can selectively detect at least a subset of mhtt aggregates in the HD patient cortices, but not age-matched control cortices (Figure S7; see Supplemental Results). Moreover, we showed that the same 4H7H7 immunostaining procedure allows for sensitive detection of mhtt neuropil and nuclear aggregates in the cortex and striatum of four different HD mouse models (Figure S8) (Davies et al., 1997; Gu et al., 2005; Slow et al., 2003; Menalled et al., 2003).

In BACHD mice at 12 months of age, the 4H7H7 antibody can readily detect mhtt aggregates in cortical and striatal sections following the antigen-retrieval protocol, while the WT controls do not have such staining (Figure 5). We can readily detect mhtt aggregates in the cortex and striatum of 12-month-old SA mice, albeit at a somewhat lower level than in BACHD mice, consistent with the lower expression of fl-mhtt in SA mice compared to BACHD (Figure 5). The formation of these aggregates in SA mice appears to be progressive, as they were not detected at 2 months of age, and only sparsely detected at 6 months (Figure S9; data not shown). These results are consistent with the progressive accumulation of mhtt aggregation in the brains of HD mice and HD patients (Bates, 2003). Interestingly, we did not detect 4H7H7-immunoreactive mhtt aggregates in brain sections from 12-month-old SD mice (SD-B and SD-C) (Figure 5).

Taken together, the in vivo results suggest that the SD mutation prevents the onset of behavioral deficits and neuropathology normally arising from polyQ repeat expansion in the context of full-length human mhtt in HD mice, including motor and psychiatric-like behavioral deficits, selective neurodegenerative pathology, and mhtt aggregation.

Phosphomimetic mHtt Exon1 Peptides Retard Aggregation In Vitro

Since the SD or SA mutations appear to have differential effects on disease pathogenesis, we hypothesize that they may confer

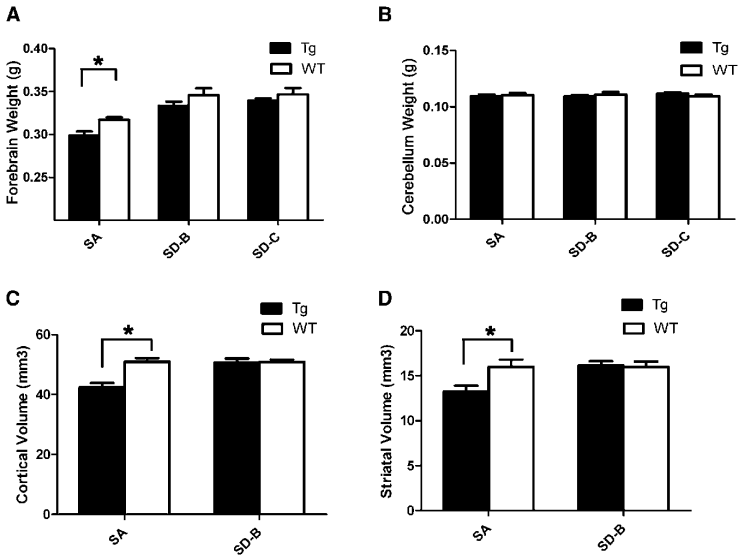


Figure 4. The SA but Not the SD Mice Elicit Selective Neurodegeneration at 12 Month Age

(A) Significant forebrain weight loss was detected in 12-month-old SA mice compared to their WT littermate controls ($p = 0.0064$, Student's t test) but not in SD-B or SD-C mice compared to their respective controls.

(B) In all three genotypes, SA, SD-B, and SD-C, no significant cerebellar atrophy was detected ($p > 0.05$, Student's t test).

(C) Unbiased stereology reveals significant cortical volume loss in SA mice compared with WT littermates ($p = 0.0030$, Student's t test) but not SD-B mice ($p = 0.9025$, Student's t test).

(D) Unbiased stereology reveals significant striatal volume loss in SA mice compared with their WT littermates ($p = 0.0336$, Student's t test). SD-B mice do not exhibit significant striatal volume loss compared to their WT controls ($p = 0.8635$, Student's t test).

Error bars indicate mean ± SEM.

distinct biophysical properties that alter the folding, association, and/or aggregation properties of mhtt. In an in vitro study of htt exon-1-related peptides, the NT17 sequence engages in a reciprocal crosstalk with expanded polyQ sequences to radically alter the aggregation pathway while greatly enhancing aggregation rate and producing an array of prefibrillar intermediates and mature amyloid fibrils (Thakur et al., 2009). In this study, reduction of net hydrophobicity via multiple mutations within NT17 clearly suppressed the aggregation rate (Thakur et al., 2009). Based on this result, we expected that the SA mutation (increased hydrophobicity) in NT17 might enhance aggregation, while the SD mutation (decreased hydrophobicity) might decrease aggregation.

We used synthetic exon-1 peptides containing the WT, SD, and SA NT17 domains to test these predictions. For synthetic feasibility and convenience in the kinetics, we studied peptides containing a Q37 repeat, a polyQ length at the threshold for HD disease risk. Using an HPLC sedimentation assay, we found that the SA double mutant of the exon-1 peptide aggregates more rapidly than the same peptide with the WT NT17 sequence, while the SD double mutant peptide aggregates more slowly (Figure 6A; $p < 0.005$ for both, Student's t test). More qualitative differences are seen when the aggregation products are analyzed by electron microscopy (EM). We harvested aggregates at 96 hr, when aggregation was essentially complete. The aggregates of the SA double mutant exon-1 peptide (Figure 6C) are morphologically indistinguishable from the aggregates of the WT peptide (Figure 6B), both being highly homogeneous preparations of long, straight, relatively thick fibrils. In contrast, the aggregates from the SD double mutant exon-1 peptide are quite heterogeneous, consisting of an assortment of short, protofibril-like aggregates and bundles of very thin filaments (Figures 6D–6H). Based on the EM data, the SD aggregates appear to be a mixture of stabilized exon-1 aggregation intermediates, and products of an alternative aggregation pathway (A.K. Thakur, M. Jayaraman, R. Kodali, R. Mishra, and R. Wetzel, unpublished data).

We next asked whether a single phosphomimetic mutation at S13 or S16 can recapitulate the effects of SD double mutations on mhtt exon-1 peptide aggregation. Interestingly, the S16D single mutant can mimic the reduced aggregation rate of the SD double mutant in the HPLC sedimentation assay, while the S13D mutant aggregates at a comparable rate to the WT peptide (Figure S10). However, when we examined the morphologies of the completed aggregation product at 96 hr, both S13D and S16D single mutant peptides resulted in mixtures of mature amyloid fibrils similar to those from WT NT17 and short protofibril-like aggregates similar to those from SD double mutants (Figure S10). Since the SD double mutant exhibits negligible mature fibrils, it appears that both the S13D and S16D mutations contribute, in a cumulative fashion, to altering the exon-1 aggregation pathway.

While more work is required to understand the mechanism of the SD mutations' effects on the aggregation, structure, and physical properties of the htt aggregation products, our in vitro results suggest that SD mutations somehow modulate the misfolding and aggregation of mhtt fragment induced by polyQ expansion. The SD mutations appear to act by either redirecting aggregation down a different assembly pathway or by retarding the normal assembly pathway, in either case resulting in reduced aggregation kinetics and altered aggregate morphologies.

DISCUSSION

Our study provides direct in vivo mammalian genetic evidence to support a critical role for htt S13 and S16 residues in preventing fl-mhtt-induced disease pathogenesis in HD mouse models. Both phosphomimetic mutations (SD) and phosphoresistant mutations (SA) can rescue phenotypes of htt null mice. The

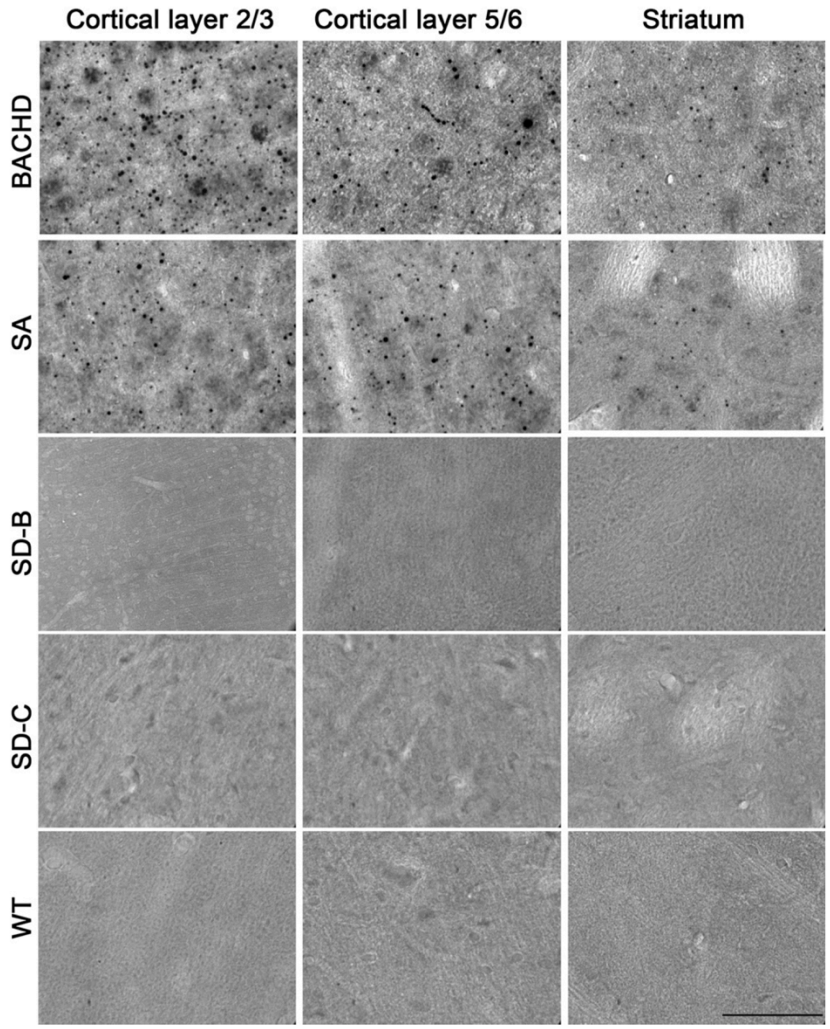


Figure 5. SD Mutations but Not SA Mutations Prevent the Accumulation of mhtt polyQ Aggregate in the Brain

Mutant huntingtin aggregates in HD patient brains and existing HD mouse brains can be readily detected by immunostaining with 4H7H7, a monoclonal antibody that selectively recognizes the expanded polyQ epitope (see Figures S3, S6, and S7 and Supplemental Results). Using the same antibody, we can readily detect mhtt aggregates accumulated in the cortical layers 2–3, layers 5–6, and striata of 12-month-old BACHD and SA mice but not WT littermate controls brains. Such stainings are absent in the 2-month-old SA mice (Figure S8). However, in the 12-month-old SD-B and SD-C brains, 4H7H7-stained mhtt aggregates are absent in all brain regions, including cortical layers 2–3, layers 5–6, and striata.

Scale bar, 50 μm.

most important finding of this study is that SD but not SA mutations in the context of fl-mhtt can prevent behavioral deficits, selective neurodegeneration, and accumulation of mhtt aggregates in the BAC transgenic mouse models of HD (Table 1). In vitro kinetic studies with purified mhtt exon-1 peptides reveal that modifications of serines 13 and 16 alter the course and kinetics of aggregation, with SD reducing fibrillization while accumulating alternative aggregate products, and SA maintaining the normal aggregation patterns of the expanded repeat length (Thakur et al., 2009). These results suggest that modification of the two serine residues is capable of altering the structural properties of this domain. Taken together, the results demonstrate that subtle molecular changes of only two amino acids in the NT17 domain in the context of the large full-length human mutant htt protein can dramatically reduce the pathogenic potential of the mutant protein in vivo. Hence, our results provide strong support for the hypothesis that S13 and S16 in the htt NT17 domain may act as a molecular switch to regulate disease

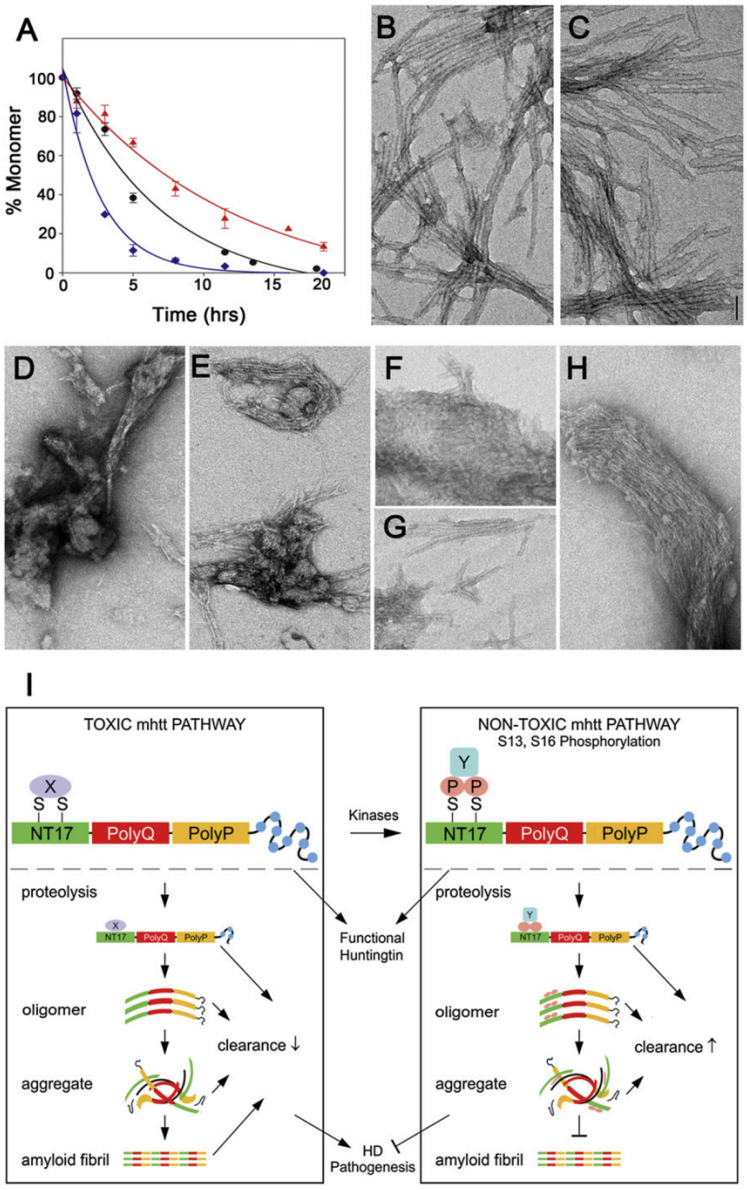


Figure 6. In Vitro Aggregation of Exon-1 Peptides and a Schematic Model on Serines 13 and 16 as a Critical Molecular Switch of HD Pathogenesis

(A) HPLC-based sedimentation assays indicate differences in the aggregation of WT:10.8 μM (●, R^2 = 0.9832, SE = 6.7), SA:10.9 μM (◆, R^2 = 0.9843, SE = 6.3), and SD:10 μM (▲, R^2 = 0.9863, SE = 3.2) $NT17Q_{37}P_{10}K_2$ peptides. The experiments were done in duplicate (for WT) and triplicate (SA and SD mutants), and the data were fit using Sigma Plot 10.0 software to a single-exponential three-parameter decay function. Error bars indicate mean ± SEM.

(B–H) Electron microscope images on aggregates harvested after 96 hr aggregation time. WT (B) and SA mutant (C) peptide aggregates are morphologically equivalent. SD mutant peptide aggregates (D–H) include none of these mature amyloids but rather are composed of a mixture of alternative morphologies associated with aborted and/or alternative aggregation pathways.

(I) A schematic model of how serines 13 and 16 act as a molecular switch to dichotomize fl-mhtt-induced disease pathogenesis. Depending on the molecular state of S13 and S16, fl-mhtt may be involved in two distinct molecular pathways. In the toxic mhtt pathway, when S13 and S16 are not phosphorylated, a state mimicked by SA mutations, fl-mhtt may mediate its toxicity via interaction with yet undefined protein X, or it may be cleaved into toxic mhtt polyQ fragments that may misfold and form toxic monomers, oligomers, aggregates, and mature amyloid fibrils. Moreover, these mhtt species may be difficult to be cleared by the lysosome or proteosome (Thompson et al., 2009). Overall, the unphosphorylated or SA form of fl-mhtt can elicit HD pathogenesis in vivo. In contrast, phosphorylation of S13 and S16, modeled by SD mutations, may induce biophysical changes to alter its polyQ-induced protein misfolding and/or protein-protein interactions (e.g., interacting with protein Y instead of protein X) and slow the kinetics of htt aggregation and impair the formation of mature amyloid fibrils, thereby enhancing the clearance of mhtt species. Overall, our study provides the proof-of-principle that molecular targeting of S13 and S16 (i.e., SD mutations) may convert fl-mhtt into a functional but nontoxic form in vivo and hence represents an attractive novel target for HD therapy.

pathogenesis elicited by fl-mhtt, and that targeting such a critical molecular pathogenic mechanism may have a dramatic therapeutic impact.

Significance of S13 and S16 Residues in HD Pathogenesis In Vivo

A critical challenge in HD research is to identify which subset of molecular mechanisms could have a significant role in determining disease pathogenesis and in developing therapeutics (Orr and Zoghbi, 2007; Beal and Ferrante, 2004; Li and Li, 2006). One fruitful approach to study polyQ disease pathogenesis is to assess how the distinct protein context of the polyQ repeat (i.e., other domains or covalent modifications) may be involved in controlling disease pathogenesis (Orr and Zoghbi, 2007). In HD, multiple htt protein domains and covalent htt modifications have been implicated in disease pathogenesis (e.g., Steffan et al., 2004; Duennwald et al., 2006; Jeong et al., 2009). However, only the caspase cleavage sites have been

tested thus far for pathogenic significance in the context of fl-mhtt in transgenic mice (Graham et al., 2006). The in vivo significance of the modification of S13 and S16 in the context of fl-mhtt-induced disease pathogenesis in a mammalian model of HD is directly addressed by this study.

An important goal in studying HD pathogenesis is to identify critical molecular pathogenic mechanisms that can prevent the early-onset neuronal dysfunction and late-onset neurodegeneration induced by mhtt (Gusella and MacDonald, 2000). Our study clearly demonstrates that the S13 and S16 sites may act as a molecular switch to prevent these pathogenic events. We determined that SD mice do not display early neuronal dysfunction as demonstrated by motor and psychiatric-like behavioral deficits, which are readily detectable in mice with SA mutations or with unmodified fl-mhtt (Gray et al., 2008; Menalled et al., 2009). In addition, we were able to demonstrate that SD, but not SA mutants can rescue late-onset neurodegeneration as assayed by selective forebrain weight loss and cortical and striatal atrophy. Our study suggests that NT17 domain and its modifications are critical regulators of very early pathogenic events that initiate the cascade of downstream pathogenic events.

S13 and S16 Modification May Regulate Mutant Huntingtin Misfolding and Aggregation

Protein misfolding leading to amyloid fibril formation is a widely investigated molecular pathogenic mechanism for a large group of age-dependent neurodegenerative disorders (Ross and Poirier, 2004; Williams and Paulson, 2008; Bossy-Wetzel et al., 2004). A key mechanistic finding of this study is the effect of S13 and S16 mutations on mhtt misfolding and aggregation. Accumulation of nuclear and cytoplasmic aggregates is a pathological hallmark of HD (DiFiglia et al., 1997; Gutekunst et al., 1999). Prior studies have demonstrated that mutations in the NT17 domain may affect the aggregation and/or nuclear accumulation of mhtt N-terminal fragments in transfected cells (Rockabrand et al., 2007; Atwal et al., 2007). We have found that modification of the NT17 Ser residues can dramatically alter the course of aggregation. In particular, the SD double mutant slows the aggregation rate and prevents the normal course of the aggregation reaction. In contrast, the SA double mutant aggregates more rapidly than the WT NT17 peptide to generate products with morphology indistinguishable from that of the WT. Moreover, the single S13D or S16D mutants appear to offer partial protection against formation of mature amyloid fibrils, suggesting that a cumulative effect of Ser to Asp mutations underlies the ability of the SD double mutant to counteract the propensities of mhtt exon-1 peptides for misfolding and aggregation in vitro. These results are consistent with previous in vitro results showing that mutations within the NT17 domain that reduce hydrophobicity reduce aggregation rates (Thakur et al., 2009).

Importantly, the aggregation behavior of these exon-1 model peptides correlates well with the differential mhtt aggregate accumulation in the SD and SA brains in vivo, suggesting that the SD mutations may also have a significant impact on the structure and physical properties of fl-mhtt or its fragments in vivo. We have found that 12-month-old SA mutants, which have phenotypes similar to BACHD mice, exhibit mhtt aggregates in the cortex and striatum, while 12-month-old SD mutants exhibit no detectible aggregates (Figure 5). Consistent with the in vitro aggregation results (Figure 6), the lack of detectible aggregates in the SD mice may be due to a slow and incomplete aggregation process or prolonged lifetimes of aggregation intermediates. These aggregation intermediates might be less readily detected by the 4H7H7 antibody or may be more easily cleared in affected neurons compared to mature amyloid fibrils from SA and WT mhtt. The latter possibility is supported by the findings that SD but not SA mutations in the context of mhtt exon-1 fragments or fl-mhtt can enhance its clearance via lysosome or proteosome in cultured mammalian cells (Thompson et al., 2009). In summary, our study provides convergent in vitro and in vivo evidence that SD but not SA mutations alter the biophysical properties of NT17 domain, counteracting the molecular consequences of mhtt polyQ expansion such as protein misfolding and aggregation.

Molecular Pathways Implicated in S13 and S16 Phosphorylation in Huntingtin

Our study suggests that the phosphorylation status of the two serine residues in the NT17 domain can influence the pathogenic consequences of expression of fl-mhtt protein in the mammalian brain (Figure 6I). This is consistent with the converging evidence supporting the important role of NT17 domain and its modifications in mhtt-induced neuronal toxicity in cellular and invertebrate models of HD (Steffan et al., 2004; Rockabrand et al., 2007; Atwal et al., 2007; Subramaniam et al., 2009; Thompson et al., 2009). Our result highlights the importance of elucidating the molecular pathways, particularly the kinases and phosphatases, which modulate these phosphorylation events in the HD brain. Also, it will be important to uncover the downstream molecular cascades resulting from S13 and S16 phosphorylation that mediate the suppression of fl-mhtt-induced disease pathogenesis (Figure 6I).

Currently, very little is known about the potential partners that can interact with htt via the NT17 domain. However, two recent studies may shed some light onto this issue. In both a yeast and mammalian cell line model (Omi et al., 2008; Wang et al., 2009), the htt NT17 domain is shown to bind to 14-3-3 proteins, which are known to bind to phosphorylated proteins. Since the NT17 domain has two serine and one threonine residue, we speculate that 14-3-3 proteins may be able to bind to S13 or S16 upon its phosphorylation and such binding may modulate mhtt toxicity in vivo. This hypothetical model for HD is reminiscent of SCA1 pathogenesis in which 14-3-3 proteins can modulate polyQ expanded ataxin-1 mediated disease via binding to phosphorylated serine 776 (Chen et al., 2003). Thus, future molecular studies should focus on establishing the signaling pathways that lead to alteration of htt S13 and S16 phosphorylation and in identifying phosphorylation-dependent protein-protein interaction that may be responsible for the suppression of fl-mhtt toxicities in vivo.

Therapeutic Implications of Huntingtin S13 and S16 Phosphorylation

Our study suggests that targeting the mhtt NT17 domain may be therapeutic for HD, particularly prior to the onset of disease. Consistent with this, a single-chain Fv intrabody against htt

NT17 domain reduced neurotoxicity and aggregation of mhtt N-terminal fragments in vivo (Wolfgang et al., 2005; Southwell et al., 2008). Another important finding of our study is that S13 and S16 phosphomimetic mutations do not elicit disease pathogenesis but do maintain normal htt function in embryonic development and the adult brain (Figures 2 and 6I). This result suggests an exciting therapeutic possibility of converting a toxic form of fl-mhtt into a functional but nontoxic form. Molecular analyses of the differences between SD mhtt and other forms of mhtt may help to design high-throughput screening assays for identification of compounds that modify fl-mhtt elicited disease pathogenesis.

In conclusion, we have demonstrated the significance of S13 and S16 residues in disease pathogenesis elicited by HD transgenic mouse models. Our findings suggest that specific S13 and S16 modifications in fl-mhtt may act as a molecular switch to suppress HD pathogenesis in the mammalian brain, thus providing an important avenue for the development of new therapeutics for this currently incurable neurodegenerative brain disorder.

EXPERIMENTAL PROCEDURES

Generation of BAC Transgenic Mice

We used site-directed mutagenesis to modify the shuttle vector plasmid, pLD53-SCAB-HDexon1-97Q (Gray et al., 2008). Serines 13 and 16 were mutated to either aspartic acid (SD) or alanine (SA) using QuikChange Multi Site-Directed Mutagenesis Kit (Stratagene). The following oligonucleotide primers were used to introduce the SD mutation (5′-AAG CTG ATG AAG GCC TTC GAG GAC CTC AAA GAC TTC CAA CAG CAG CAA CAG CAA C-3′) or SA mutation (5′-AAG CTG ATG AAG GCC TTC GAG GCC CTC AAA GCC TTC CAA CAG CAG CAA CAG CAA C-3′). PCR products from mutagenesis reactions were used to transfect Pir2 competent cells (Invitrogen). Correct RecA-based shuttle vector plasmids were used to engineer a human htt BAC (Gray et al., 2008) to introduce the SD and SA mutations (Yang et al., 1997; Gong et al., 2002; Yang and Gong, 2005). The final modified BAC were confirmed by DNA sequencing to contain the SD or SA mutations and to have 97 mixed CAA-CAG codons encoding the expanded polyQ repeat (see Supplemental Experimental Procedures). The modified BAC DNA was prepared according to our published protocols and microinjected into FvB fertilized oocytes at the UCLA Transgenic Core. BACHD, BACHD-L, SD, and SA mice were maintained in the FvB/NJ background and bred and maintained under standard conditions consistent with National Institutes of Health guidelines and approved by the UCLA Institutional Animal Care and Use Committees.

Preparation of Brain Extracts and Western Blotting

We used our published protocols for the preparation of brain protein extracts and western blot analyses (Gray et al., 2008; see Supplemental Experimental Procedures). Immunoblots were probed with anti-Htt 2166 (Abcam, mAb2166, 1:3000), 1C2 (Millipore, MAB1574, 1:3000), S13-P, and S16-P phosphor-specific antibodies (1:1000; Thompson et al., 2009), and α-tubulin (Sigma, 1:10,000).

Genetic Rescue of Murine Huntingtin Null Phenotypes by SD and SA BAC Transgenes

The genetic rescue of murine htt knockout phenotypes during embryonic development is similar to our published study (Gray et al., 2008). Briefly, heterozygous BACHD-SD and BACHD-SA transgene alleles were bred with murine *Hdh* heterozygous mice (Zeitlin et al., 1995) to generate double heterozygous mice. These double heterozygous mice were then crossed to *Hdh* heterozygotes to create homozygous *Hdh* mice either with or without the BAC transgenes, and the number of mice with these genotypes were scored among the offspring born. The rescue mice were defined as mice without two endogenous *Hdh* alleles but with the heterozygous BACHD-SD or BACHD-SA transgenes. No mice with both *Hdh* null alleles but without any BACHD-SD or SA transgenes were among the live littermates in our study (Zeitlin et al., 1995).

To assess the ability of BACHD-SD transgene in rescuing the adult neurodegeneration phenotype of *Hdh* forebrain-specific knockout mice, three BACHD-SD rescue mice and WT littermate controls were sacrificed at 12 months of age. Coronal brain sections were prepared and used to examine for marked cortical neurodegeneration as described before (Dragatsis et al., 2000).

Behavioral Tests of Mutant HD Mice

Mice were tested for motor impairment using our established rotarod test (Gray et al., 2008). We tested the following group of mice at 2, 6, and 12 months: SA mice (WT = 12, Tg = 13), SD-B (WT = 10, Tg = 13), SD-C (WT = 10, Tg = 13), and BACHD-L (WT = 17; Tg = 20). For each genotype, we used approximately equal number of males and females. The mice were trained on an Ugo Basile 7650 accelerating rotarod (0 to 40 RPM in 5 min) for three trials per day for 2 days at 2 months of age. The same cohort of mice was tested for three trials per day for 3 consecutive days at 2, 6, and 12 months of age. All rotarod tests were performed during the light phase of the light cycle.

Anxiety-like behavior was assessed in the light/dark box exploration test (File, 1997). The light/dark exploration box is made of plexiglass with a clear (light) side (27 × 27 × 30 cm) and a smaller, fully opaque (dark) side (18 × 27 × 30 cm) separated by a partition with a small opening. The dark side is completely closed to light. The lighted side is illuminated with a 60 W light bulb or light with an illuminance of about 400 lux. Light/dark exploration was performed during the early phase of the light/dark cycle. Mice were placed in testing room at least 1 hr before testing. The mice are tested for 10 min in the light/dark box and assessed for movements from one side to another. The same cohort of SD and SA mice and respective wild-type controls from the above rotarod tests were tested at 12 months of age in this light/dark exploration test.

Antigen Retrieval and Immunohistochemical Staining of polyQ Mutant Htt Aggregates with Monoclonal 4H7H7 Antibody

Mice were perfused transcardially with 4% paraformaldehyde in 0.1 M PBS. After 6 hr post-fix at 4°C, brains were cryoprotected with 30% sucrose in 0.1 M PBS at 4°C, and frozen coronal brain sections (40 μm) were cut on a cryostat. The antigen-retrieval procedure is described in more detail elsewhere (Osmand et al., 2006). Briefly, the brain sections were antigen treated with formic acid and followed by 1% sodium borohydride. Biotinylated monoclonal antibody 4H7H7 was then used at a concentration of 50 ng/ml and incubated with the brain sections overnight at 4°C. Subsequently, the immunostaining signal was amplified with Tyramide Signal Amplification kit (Perkin Elmer) and detected with SD-AG chromogen (Vector Lab.).

Brain Weight and Stereological Brain Volume Measurements

The quantitative analyses of brain weights and stereological measurements of cortical and striatal volumes using the optical fractionator method using Stereo Investigator software (MicroBrightField) were identical to our published protocols for BACHD mice (Gray et al., 2008).

Analysis of In Vitro Htt-exon 1 Peptide Aggregate Formation

Chemically synthesized peptides were obtained from the Keck Biotechnology Center at the Yale University (http://keck.med.yale.edu/ssps/), purified by reverse phase HPLC, and the purity determined and identities confirmed by mass spectrometry using an Agilent 1100 Electrospray MSD. The structures of the peptides used were NT17-$Q_{37}P_{10}K_2$, in which the sequence of wild-type NT17 is MATLEKLMKAFESLKSW and the underscored Ser residues are the ones replaced by Ala or Asp in the SA, SD, and single S13D and S16D mutants. Phe_{17} was replaced by Trp in these peptides to be used as a fluorescent probe; we have observed no effects on aggregation or other properties in Phe17→Trp mutants (Thakur et al., 2009). Purified peptides were lyophilized and freshly disaggregated before use as described (O'Nuallain et al., 2006), then dissolved in phosphate-buffered saline and incubated

at 37°C. The aggregation propensity of each peptide was determined by measuring the amount of monomer remaining in solution at different times using the sedimentation assay (O'Nuallain et al., 2006). Electron micrographs of the aggregates were obtained by directly analyzing aliquots of the reaction mixture collected at different times. For each determination, 5 μl of the sample was placed on a freshly glow-discharged Formvar carbon-coated grid and adsorbed for 2 min, after which the grid was washed with deionized water before staining the protein with 2 μl of 1% (w/v) uranyl acetate and removing excess stain by blotting. Grids were imaged on a Tecnai T12 microscope (FEI) operating at 120 kV and 30,000× magnification and equipped with an UltraScan 1000 CCD camera (Gatan) with postcolumn magnification of 1.4×.

Statistical Analysis

Statistical analyses of the behavioral phenotypes and neuropathological phentoypes of BACHD-SD and SA mice and BACHD-L mice were similar to our published protocols (Gray et al., 2008). All data are shown as the mean ± standard error of the mean (SEM). For rotarod analysis, SPSS 14.0 statistics software (Chicago, IL) was used. The significance level was set at 0.05. A general linear model ANOVA with repeated-measures was performed to assess the main effects of age, genotype, and their interaction. In some data sets, one-way ANOVA was used to analyze the time effect on rotarod performance of BACHD mice and wild-type mice from 2, 6, and 12 months of age. Fisher's LSD post hoc analysis was performed for pairwise comparisons among ages. For neuropathology and stereology studies, all comparisons between BACHD and wild-type mice are shown as mean ± SEM. Comparisons were made with an independent sample Student's t test with a significance level of 0.05. For electrophysiological studies, data in the text and figures are presented as mean ± SEM. Differences between groups were assessed with Student's t tests or appropriate designed ANOVAs. The significance level was set at 0.05.

SUPPLEMENTAL DATA

Supplemental Data include ten figures, Supplemental Results, and Supplemental Experimental Procedures and can be found with this article online at http://www.cell.com/neuron/supplemental/S0896-6273(09)00936-2.

ACKNOWLEDGMENTS

We would like to thank Nancy Wexler, Carl Johnson, and the Hereditary Disease Foundation (HDF) for their tremendous support of this project. HD research in X.W.Y. lab at UCLA is supported by a contract from HDF, and by grants from NINDS/NIH (R01NS049501; 3R01NS049501-05S1) and CHDI Foundation. R.W. was supported by a research grant from the Huntington Society of Canada and the Huntington's Disease Society of America (HDSA), and by NIH RO1 grant AG019322. The work of J.S.S. and L.M.T. was supported by HDF, the Fox Family Foundation (J.S.S.), the CHDI Foundation, the HDSA, and NIH awards NS52789 and NS045283 (L.M.T.). S.F. was supported by 2R01NS39074, 2R01NS45491, 2P01AG022074, CHDI, and the Taube-Koret Center for HD Research. A.P.O. was supported by HDF. We also would like to thank Scott Zeitlin for the *Hdh* Knockout mice; M.A. Hickey, M.F. Chesselet, and M.S. Levine for providing R6/2 and CAG140 brain sections, R. Truant for sharing unpublished studies, and members of the Yang Lab, particularly X.H. Lu, M. Gray, J.P. Cantle, Y. Cui, and T.K. Murphy for discussions and critical reading of the manuscript.

Accepted: November 11, 2009
Published: December 23, 2009

REFERENCES

Aiken, C.T., Steffan, J.S., Guerrero, C.M., Khashwji, H., Lukacsovich, T., Simmons, D., Purcell, J.M., Menhaji, K., Zhu, Y.Z., Green, K., et al. (2009). Phosphorylation of threonine-3: Implications for huntingtin aggregation and neurotoxicity. J. Biol. Chem. *284*, 29427–29436.

Anne, S.L., Saudou, F., and Humbert, S. (2007). Phosphorylation of huntingtin by cyclin-dependent kinase 5 is induced by DNA damage and regulates wild-type and mutant huntingtin toxicity in neurons. J. Neurosci. *27*, 7318–7328.

Atwal, R.S., Xia, J., Pinchev, D., Taylor, J., Epand, R.M., and Truant, R. (2007). Huntingtin has a membrane association signal that can modulate huntingtin aggregation, nuclear entry and toxicity. Hum. Mol. Genet. *16*, 2600–2615.

Ballatore, C., Lee, V.M., and Trojanowski, J.Q. (2007). Tau-mediated neurodegeneration in Alzheimer's disease and related disorders. Nat. Rev. Neurosci. *8*, 663–672.

Bates, G. (2003). Huntingtin aggregation and toxicity in Huntington's disease. Lancet *361*, 1642–1644.

Beal, M.F., and Ferrante, R.J. (2004). Experimental therapeutics in transgenic mouse models of Huntington's disease. Nat. Rev. Neurosci. *5*, 373–384.

Bossy-Wetzel, E., Schwarzenbacher, R., and Lipton, S.A. (2004). Molecular pathways to neurodegeneration. Nat. Med. *10* (*Suppl*), S2–S9.

Chen, H.K., Fernandez-Funez, P., Acevedo, S.F., Lam, Y.C., Kaytor, M.D., Fernandez, M.H., Aitken, A., Skoulakis, E.M., Orr, H.T., Botas, J., and Zoghbi, H.Y. (2003). Interaction of Akt-phosphorylated ataxin-1 with 14-3-3 mediates neurodegeneration in spinocerebellar ataxia type 1. Cell *113*, 457–468.

Cornett, J., Cao, F., Wang, C.E., Ross, C.A., Bates, G.P., Li, S.H., and Li, X.J. (2005). Polyglutamine expansion of huntingtin impairs its nuclear export. Nat. Genet. *37*, 198–204.

Crawley, J.N. (2008). Behavioral phenotyping strategies for mutant mice. Neuron *57*, 809–818.

Davies, S.W., Turmaine, M., Cozens, B.A., DiFiglia, M., Sharp, A.H., Ross, C.A., Scherzinger, E., Wanker, E.E., Mangiarini, L., and Bates, G.P. (1997). Formation of neuronal intranuclear inclusions underlies the neurological dysfunction in mice transgenic for the HD mutation. Cell *90*, 537–548.

DiFiglia, M., Sapp, E., Chase, K.O., Davies, S.W., Bates, G.P., Vonsattel, J.P., and Aronin, N. (1997). Aggregation of huntingtin in neuronal intranuclear inclusions and dystrophic neurites in brain. Science *277*, 1990–1993.

Dragatsis, I., Levine, M.S., and Zeitlin, S. (2000). Inactivation of Hdh in the brain and testis results in progressive neurodegeneration and sterility in mice. Nat. Genet. *26*, 300–306.

Duennwald, M.L., Jagadish, S., Muchowski, P.J., and Lindquist, S. (2006). Flanking sequences profoundly alter polyglutamine toxicity in yeast. Proc. Natl. Acad. Sci. USA *103*, 11045–11050.

Emamian, E.S., Kaytor, M.D., Duvick, L.A., Zu, T., Tousey, S.K., Zoghbi, H.Y., Clark, H.B., and Orr, H.T. (2003). Serine 776 of ataxin-1 is critical for polyglutamine-induced disease in SCA1 transgenic mice. Neuron *38*, 375–387.

File, S.E. (1997). Animal tests of anxiety. Current Protocols in Neuroscience *8*, 3.1–3.15.

Fujiwara, H., Hasegawa, M., Dohmae, N., Kawashima, A., Masliah, E., Goldberg, M.S., Shen, J., Takio, K., and Iwatsubo, T. (2002). alpha-Synuclein is phosphorylated in synucleinopathy lesions. Nat. Cell Biol. *4*, 160–164.

Gatchel, J.R., and Zoghbi, H.Y. (2005). Diseases of unstable repeat expansion: mechanisms and common principles. Nat. Rev. Genet. *6*, 743–755.

Gong, S., Yang, X.W., Li, C., and Heintz, N. (2002). Highly efficient modification of bacterial artificial chromosomes (BACs) using novel shuttle vectors containing the R6Kgamma origin of replication. Genome Res. *12*, 1992–1998.

Graham, R.K., Deng, Y., Slow, E.J., Haigh, B., Bissada, N., Lu, G., Pearson, J., Shehadeh, J., Bertram, L., Murphy, Z., et al. (2006). Cleavage at the caspase-6 site is required for neuronal dysfunction and degeneration due to mutant huntingtin. Cell *125*, 1179–1191.

Gray, M., Shirasaki, D.I., Cepeda, C., André, V.M., Wilburn, B., Lu, X.H., Tao, J., Yamazaki, I., Li, S.H., Sun, Y.E., et al. (2008). Full-length human mutant huntingtin with a stable polyglutamine repeat can elicit progressive and selective neuropathogenesis in BACHD mice. J. Neurosci. *28*, 6182–6195.

Gu, X., Li, C., Wei, W., Lo, V., Gong, S., Li, S.H., Iwasato, T., Itohara, S., Li, X.J., Mody, I., et al. (2005). Pathological cell-cell interactions elicited by a neuropathogenic form of mutant Huntingtin contribute to cortical pathogenesis in HD mice. Neuron *46*, 433–444.

Gusella, J.F., and MacDonald, M.E. (2000). Molecular genetics: unmasking polyglutamine triggers in neurodegenerative disease. Nat. Rev. Neurosci. *1*, 109–115.

Gutekunst, C.A., Li, S.H., Yi, H., Mulroy, J.S., Kuemmerle, S., Jones, R., Rye, D., Ferrante, R.J., Hersch, S.M., and Li, X.J. (1999). Nuclear and neuropil aggregates in Huntington's disease: relationship to neuropathology. J. Neurosci. *19*, 2522–2534.

Harper, P.S. (1996). New genes for old diseases: the molecular basis of myotonic dystrophy and Huntington's disease. The Lumleian Lecture 1995. J. R. Coll. Physicians Lond. *30*, 221–231.

Humbert, S., Bryson, E.A., Cordelières, F.P., Connors, N.C., Datta, S.R., Finkbeiner, S., Greenberg, M.E., and Saudou, F. (2002). The IGF-1/Akt pathway is neuroprotective in Huntington's disease and involves Huntingtin phosphorylation by Akt. Dev. Cell *2*, 831–837.

The Huntington's Disease Collaborative Research Group. (1993). A novel gene containing a trinucleotide repeat that is expanded and unstable on Huntington's disease chromosomes. Cell *72*, 971–983.

Jeong, H., Then, F., Melia, T.J., Jr., Mazzulli, J.R., Cui, L., Savas, J.N., Voisine, C., Paganetti, P., Tanese, N., Hart, A.C., et al. (2009). Acetylation targets mutant huntingtin to autophagosomes for degradation. Cell *137*, 60–72.

Katsuno, M., Adachi, H., Kume, A., Li, M., Nakagomi, Y., Niwa, H., Sang, C., Kobayashi, Y., Doyu, M., and Sobue, G. (2002). Testosterone reduction prevents phenotypic expression in a transgenic mouse model of spinal and bulbar muscular atrophy. Neuron *35*, 843–854.

Li, S., and Li, X.J. (2006). Multiple pathways contribute to the pathogenesis of Huntington disease. Mol. Neurodegener. *1*, 19.

MacDonald, M.E. (2003). Huntingtin: alive and well and working in middle management. Sci. STKE *2003*, pe48.

Menalled, L.B., Sison, J.D., Dragatsis, I., Zeitlin, S., and Chesselet, M.F. (2003). Time course of early motor and neuropathological anomalies in a knock-in mouse model of Huntington's disease with 140 CAG repeats. J. Comp. Neurol. *465*, 11–26.

Menalled, L., El-Khodor, B., Patry, M., and Suarez-Farinas, M. (2009). Systematic behavioral evaluation of Huntington's disease transgenic and knock-in mouse models. Neurobiol. Dis. *35*, 319–336.

O'Nuallain, B., Thakur, A.K., Williams, A.D., Bhattacharyya, A.M., Chen, S., Thiagarajan, G., and Wetzel, R. (2006). Kinetics and thermodynamics of amyloid assembly using a high-performance liquid chromatography-based sedimentation assay. Methods Enzymol. *413*, 34–74.

Omi, K., Hachiya, N.S., Tanaka, M., Tokunaga, K., and Kaneko, K. (2008). 14-3-3zeta is indispensable for aggregate formation of polyglutamine-expanded huntingtin protein. Neurosci. Lett. *431*, 45–50.

Orr, H.T., and Zoghbi, H.Y. (2007). Trinucleotide repeat disorders. Annu. Rev. Neurosci. *30*, 575–621.

Osmand, A.P., Berthelier, V., and Wetzel, R. (2006). Imaging polyglutamine deposits in brain tissue. Methods Enzymol. *412*, 106–122.

Rockabrand, E., Slepko, N., Pantalone, A., Nukala, V.N., Kazantsev, A., Marsh, J.L., Sullivan, P.G., Steffan, J.S., Sensi, S.L., and Thompson, L.M. (2007). The first 17 amino acids of Huntingtin modulate its sub-cellular localization, aggregation and effects on calcium homeostasis. Hum. Mol. Genet. *16*, 61–77.

Ross, C.A., and Poirier, M.A. (2004). Protein aggregation and neurodegenerative disease. Nat. Med. *10* (*Suppl*), S10–S17.

Schilling, B., Gafni, J., Torcassi, C., Cong, X., Row, R.H., LaFevre-Bernt, M.A., Cusack, M.P., Ratovitski, T., Hirschhorn, R., Ross, C.A., et al. (2006). Huntingtin phosphorylation sites mapped by mass spectrometry. Modulation of cleavage and toxicity. J. Biol. Chem. *281*, 23686–23697.

Slow, E.J., van Raamsdonk, J., Rogers, D., Coleman, S.H., Graham, R.K., Deng, Y., Oh, R., Bissada, N., Hossain, S.M., Yang, Y.Z., et al. (2003). Selective striatal neuronal loss in a YAC128 mouse model of Huntington disease. Hum. Mol. Genet. *12*, 1555–1567.

Southwell, A.L., Khoshnan, A., Dunn, D.E., Bugg, C.W., Lo, D.C., and Patterson, P.H. (2008). Intrabodies binding the proline-rich domains of mutant huntingtin increase its turnover and reduce neurotoxicity. J. Neurosci. *28*, 9013–9020.

Spampanato, J., Gu, X., Yang, X.W., and Mody, I. (2008). Progressive synaptic pathology of motor cortical neurons in a BAC transgenic mouse model of Huntington's disease. Neuroscience *157*, 606–620.

Steffan, J.S., Agrawal, N., Pallos, J., Rockabrand, E., Trotman, L.C., Slepko, N., Illes, K., Lukacsovich, T., Zhu, Y.Z., Cattaneo, E., et al. (2004). SUMO modification of Huntingtin and Huntington's disease pathology. Science *304*, 100–104.

Subramaniam, S., Sixt, K.M., Barrow, R., and Snyder, S.H. (2009). Rhes, a striatal specific protein, mediates mutant-huntingtin cytotoxicity. Science *324*, 1327–1330.

Thakur, A.K., Jayaraman, M., Mishra, R., Thakur, M., Chellgren, V.M., Byeon, I.J., Anjum, D.H., Kodali, R., Creamer, T.P., Conway, J.F., et al. (2009). Polyglutamine disruption of the huntingtin exon 1 N terminus triggers a complex aggregation mechanism. Nat. Struct. Mol. Biol. *16*, 380–389.

Thompson, L.M., Aiken, C.T., Kaltenbach, L.S., Agrawal, N., Illes, K., Khoshnan, A., Martinez-Vincente, M., Arrasate, M., O'Rourke, J.G., Khashwji, H., et al. (2009). IKK phosphorylates Huntingtin and targets it for degradation by the proteasome and lysosome. J. Cell Biol., in press.

Vonsattel, J.P., and DiFiglia, M. (1998). Huntington disease. J. Neuropathol. Exp. Neurol. *57*, 369–384.

Wang, Y., Meriin, A.B., Zaarur, N., Romanova, N.V., Chernoff, Y.O., Costello, C.E., and Sherman, M.Y. (2009). Abnormal proteins can form aggresome in yeast: aggresome-targeting signals and components of the machinery. FASEB J. *23*, 451–463.

White, J.K., Auerbach, W., Duyao, M.P., Vonsattel, J.P., Gusella, J.F., Joyner, A.L., and MacDonald, M.E. (1997). Huntingtin is required for neurogenesis and is not impaired by the Huntington's disease CAG expansion. Nat. Genet. *17*, 404–410.

Williams, A.J., and Paulson, H.L. (2008). Polyglutamine neurodegeneration: protein misfolding revisited. Trends Neurosci. *31*, 521–528.

Wolfgang, W.J., Miller, T.W., Webster, J.M., Huston, J.S., Thompson, L.M., Marsh, J.L., and Messer, A. (2005). Suppression of Huntington's disease pathology in Drosophila by human single-chain Fv antibodies. Proc. Natl. Acad. Sci. USA *102*, 11563–11568.

Yanai, A., Huang, K., Kang, R., Singaraja, R.R., Arstikaitis, P., Gan, L., Orban, P.C., Mullard, A., Cowan, C.M., Raymond, L.A., et al. (2006). Palmitoylation of huntingtin by HIP14 is essential for its trafficking and function. Nat. Neurosci. *9*, 824–831.

Yang, X.W., and Gong, S. (2005). An overview on the generation of BAC transgenic mice for neuroscience research. Curr. Protoc. Neurosci., Chapter 5, Unit 5 20.

Yang, X.W., Model, P., and Heintz, N. (1997). Homologous recombination based modification in Escherichia coli and germline transmission in transgenic mice of a bacterial artificial chromosome. Nat. Biotechnol. *15*, 859–865.

Zeitlin, S., Liu, J.P., Chapman, D.L., Papaioannou, V.E., and Efstratiadis, A. (1995). Increased apoptosis and early embryonic lethality in mice nullizygous for the Huntington's disease gene homologue. Nat. Genet. *11*, 155–163.

Part II:

Biochemical Characterization of BACHD-ΔN17 and BACWT-ΔN17 Mouse Models

3.1. Introduction

Our previous study described in the first part of this chapter demonstrates the critical importance of the Htt N17 domain and its modifications in HD pathogenesis in mammalian models of HD, and provides a strong rationale to further dissect the normal function of the N17 domain and its role in disease pathogenesis. Although previous studies using cellular models of HD suggest that the N17 domain is essential in cytoplasmic localization of small mHtt N-terminal fragments, thereby preventing mHtt nuclear translocation and aggregation (Atwal et al., 2007; Cornett et al., 2005; Rockabrand et al., 2007), it remains unclear whether the Htt N17 domain acts as a cytoplasmic targeting signal in the mammalian brain, and the significance of this function in mHtt-induced disease pathogenesis *in vivo* has yet to be tested.

To test this hypothesis, the Yang laboratory used a classical genetic approach to delete the N17 domain in the context of the full-length mHtt protein to assess its impact on mHtt subcellular localization, aggregation, and toxicity *in vivo*. This approach has successfully been demonstrated before to study SCA1 pathogenesis in a transgenic mouse model, in which deletion of 100 aa in ataxin-1 in the dimerization domain shows that ataxin-1 aggregation is not required for disease pathogenesis (Klement et al., 1998). We seek to address the question whether abolishing N17 domain function, by deletion of the N17 domain Htt aa 2-16 (ΔN17), can trigger nuclear translocation and aggregation of mHtt (or its toxic fragments) and alter the course of disease pathogenesis in a BAC transgenic mouse model of HD. Dr. Xioafeng Gu, an Assistant Researcher in Dr. X. William Yang's laboratory, generated and characterized the mouse models described in this chapter. However, the focus of this chapter will highlight the

interesting findings from my biochemical investigation on the novel BACHD-ΔN17 and BACWT-ΔN17 mouse models of HD.

3.2. Results

3.2.1. Generation and Characterization of BACHD-ΔN17 and BACWT-ΔN17 Mouse Models

Dr. Xiaofeng Gu in the Yang laboratory re-engineered the original BACHD construct (Gray et al., 2008; Gu et al., 2009) to develop novel BAC transgenic mice expressing fl-mHtt-[97Q] with a deletion of 2-16 aa in the N17 domain (termed BACHD-ΔN17-97Q; Figure 3.1A). He obtained eight founder*s* in an FvB/NJ inbred background; however, only transgenic lines A, L, and N were further analyzed. As a control for polyQ-length-dependent phenotypes, he also created human Htt BAC transgenic mice expressing ΔN17 forms of mHtt 31Q (termed BACWT-ΔN17-31Q; C line analyzed). Most of the data presented in this chapter was performed using longitudinal analyses on the BACHD-ΔN17-97Q-N mice, which will be refereed to as BACHD-ΔN17 (or HDΔN17) throughout this dissertation unless otherwise indicated.

Western blot analyses using cortical extracts and the 1C2 antibody (mAb against expanded polyglutamine) revealed BACHD-ΔN17 mice express full-length mHtt similar to the size of fl-mHtt in BACHD mice (~350 kDa; Figure 3.1B).

3.2.2. BACHD-ΔN17 Transgene Can Rescue Murine htt Knockout Lethality

To assess whether ΔN17 form of mHtt can still function in rescuing murine Htt KO lethality, Dr. Xiaofeng Gu crossed BACHD-ΔN17 onto a Htt KO background (Gu et al., 2009; Zeitlin et al., 1995) and found the BACHD-ΔN17 transgene can completely rescue the Htt KO lethality in in a Mendelian ratio (8 rescue mice among 63 pups total). These rescue mice do not

exhibit any apparent phenotypes up to 4 months of age (data not shown). Western blot analysis using brain extracts from HDΔN17 KO rescue mice demonstrates the lack of endogenous murine Htt and the lack of the N17 domain on mHtt (using an N17-specific antibody), but confirms the presence of the polyQ-expanded form of ΔN17 mHtt (Figure 3.1C). This rescue study is crucial to show that the ΔN17 form of mHtt is still functional and can substitute for the essential function of Htt during development, and also demonstrates that the ΔN17 mutation does not grossly affect the structure and normal function of Htt.

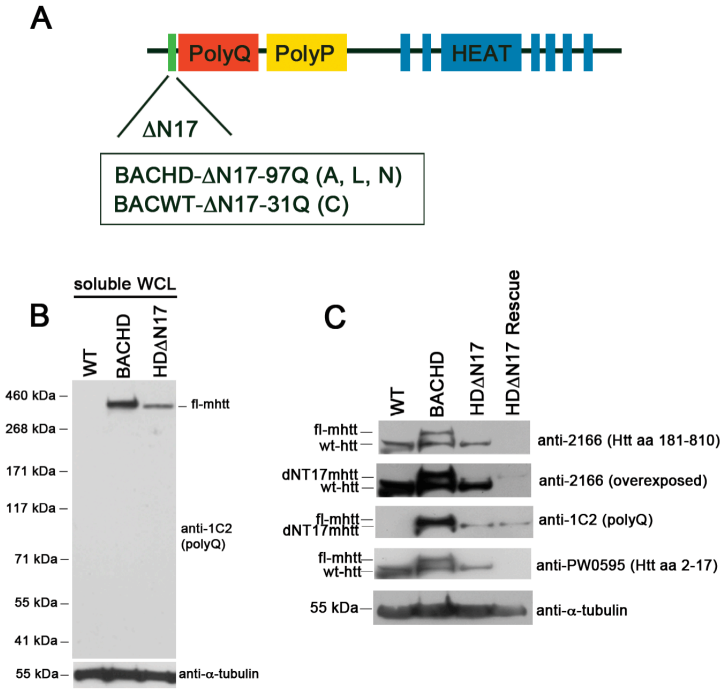


Figure 3.1. Generation and initial biochemical characterization of BACHD-ΔN17 transgenic mice. **(A)** Htt construct designs for BACHD-ΔN17-97Q and BACWT-ΔN17-31Q transgenic mouse models of HD. The transgenic lines that were analyzed in this study are indicated in parenthesis. **(B)** Western blot analyses of 1-month old wildtype, BACHD, and BACHD-ΔN17-97Q-N soluble cortical extracts using the 1C2 antibody. Anti-α-tubulin was used as a loading control. **(C)** Western blot analyses with mAb2166 (Htt aa 181-810; recognizes both mHtt & wildtype Htt), anti-PW0595 (Htt aa 2-17), and anti-1C2 confirm that BACHD-ΔN17-97Q-N KO rescue mice only express fl-mHtt and lack endogenous murine Htt. Anti-α-tubulin was used as a loading control.

3.2.3. Western Blot Analysis of Relative Fl-mHtt Levels in BACHD-ΔN17 and BACWT-ΔN17 Mouse Models

In order to examine the fl-mHtt levels in the BACHD-ΔN17 and BACWT-ΔN17 mouse models, I first had to test various N- and C-terminal Htt antibodies for their ability to bind to the ΔN17 form of mHtt. In Chapter 3, I was able to quantify the levels of fl-mHtt in the SD and SA mouse models using the polyQ specific antibodies 1C2 and 4H7H7, as BACHD, SD, and SA fl-mHtt constructs each have 97Q (Gu et al., 2009). However, in this study I am comparing the fl-mHtt levels in BACHD, BACHD-ΔN17-97Q, and BACWT-ΔN17-31Q mice to one another and therefore had to use the following criteria when selecting Htt antibodies for quantification: 1) Avoid antibodies whose epitope is against expanded polyQ, as antibody binding will differ between the various ΔN17 polyQ tract lengths; 2) Avoid antibodies whose epitope includes the Htt N17 domain (aa 1-17), as antibody binding will differ between BACHD and ΔN17 models; and 3) Choose a human Htt specific antibody, as to avoid murine Htt recognition.

Therefore, I chose to test the following antibodies to quantify fl-mHtt levels in BACHD, BACHD-ΔN17-97Q-N, BACHD-ΔN17-97Q-L, and BACWT-ΔN17-31Q (C-line) mice: 1) N-terminal Anti-Htt aa 1-82 mouse monoclonal antibody (Millipore, MAB5492), which recognizes the proline rich region in human fl-Htt; and 2) Expanded polyQ (1C2) mouse monoclonal antibody (Millipore, MAB1574), which was used as a measure of polyQ-dependence in the ΔN17 mice.

Western blot analysis of young BACHD, BACHD-ΔN17-97Q-N, BACHD-ΔN17-97Q-L, and BACWT-ΔN17-31Q-C forebrain soluble lysates using the 1C2 and 5492 antibodies are shown below in Figure 3.2. Both Htt antibodies detect a significant reduction in the ΔN17 fl-mHtt levels compared to the BACHD mouse model, where the BACHD-ΔN17-97Q-N mice express approximately 43.3% the level of fl-mHtt in the BACHD mice using the 1C2 antibody and 30.7% using the 5492 antibody (data not shown). As shown below in Figure 3.2B, the 1C2 antibody

does detect more fl-mHtt in the BACHD-ΔN17-97Q-N and BACHD-ΔN17-L mice than in the BACHD-ΔN17-97Q-A mice (band barely detected) in both the soluble and 10% SDS solubilized fractions. Interestingly, the N-terminal 5492 polyP antibody did not significantly detect a difference in fl-mHtt expression levels between the HD and WT ΔN17 transgenic lines (Figure 3.2C), and may be the most accurate antibody chosen to quantify fl-mHtt levels in mammalian brain.

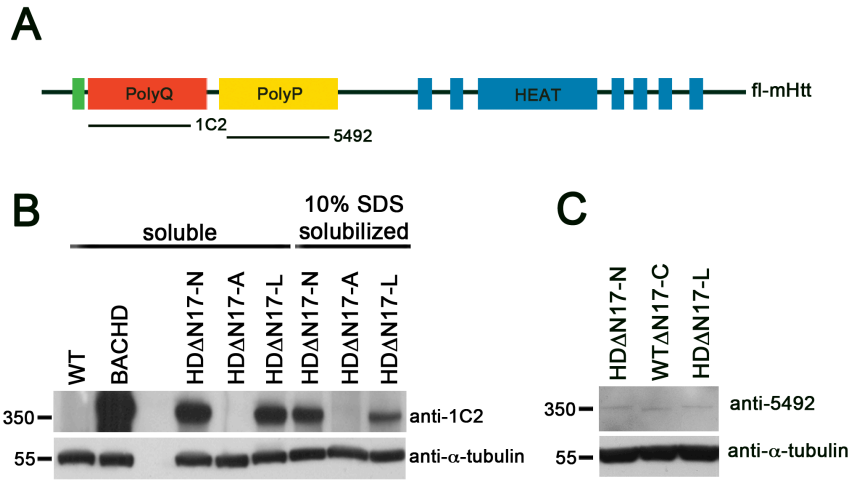


Figure 3.2. Western blot analysis of the fl-mHtt levels in BACHD, BACHD-ΔN17-97Q-N, BACHD-ΔN17-97Q-L, BACHD-ΔN17-97Q-A, and BACWT-ΔN17-31Q-C transgenic mouse models of HD. (A) A schematic diagram of the fl-mHtt protein, where the approximate epitopes for the 1C2 and 5492 antibodies are indicated below. **(B)** Western blot analysis of fl-mHtt levels in young WT, BACHD, BACHD-ΔN17-97Q-N, BACHD-ΔN17-97Q-A, and BACHD-ΔN17-97Q-L soluble and 10% SDS-solubilized forebrain fractions using the 1C2 antibody. Anti-α-tubulin was used as a loading control. **(C)** Western blot analysis of fl-mHtt levels in young BACHD-ΔN17-97Q-N, BACHD-ΔN17-31Q-C, and BACHD-ΔN17-97Q-L soluble forebrain lysates using the 5492 antibody. Anti-α-tubulin was used as a loading control.

To test whether the fl-mHtt protein in the HDΔN17 mice degrades over time, Western blot analysis using young (2m) and old (12m) BACHD and BACHD-ΔN17-97Q (N-line) mice was performed and showed no marked difference in fl-mHtt protein levels in young versus old cortical lysates (Figure 3.3).

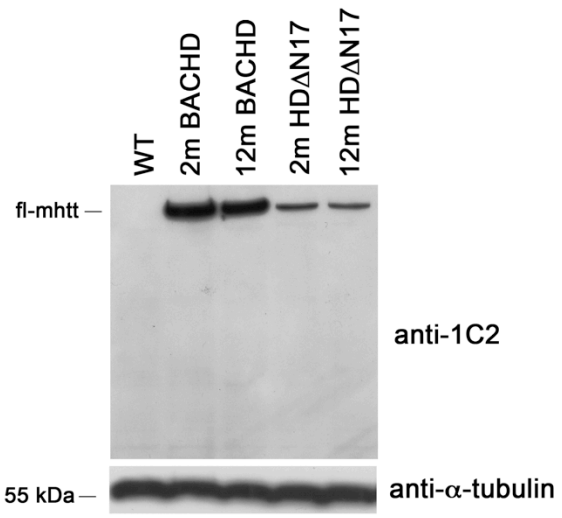


Figure 3.3. Soluble fl-mHtt protein levels in BACHD and BACHD-ΔN17-97Q-N mice do not change between 2- and 12-months of age. Western blot analysis with anti-1C2 reveals that the BACHD and HDΔN17 mice express fl-mHtt protein levels that are comparable between 2 and 12 months of age. This blot suggests there is no aberrant increase in the generation of soluble mHtt polyQ fragments in the HDΔN17 mice compared to the BACHD mice. The same blot was probed with anti-α-tubulin for the loading control.

3.2.4. Mutant Htt Nuclear Localization and Aggregation in BACHD-ΔN17 Mice

A hallmark of HD is nuclear and cytoplasmic aggregation of mHtt N-terminal fragments (Difiglia et al., 1997). To test our hypothesis that the Htt N17 domain plays a cytoplasmic retention role *in vivo*, we predict that BACHD-ΔN17 mice should exhibit earlier nuclear mHtt accumulation and aggregation than BACHD mice, which have predominantly cytoplasmic mHtt aggregates detectable at 12 months of age (Gray et al., 2008). Dr. Xiaofeng Gu performed immunostaining on BACHD and BACHD-ΔN17-97Q (N-line) cortical and striatal tissues using antibodies against mHtt exon 1 (*i.e.,* S830 and EM48) or expanded polyQ (4H7H7) (data not shown). He could readily detect nuclear translocation of mHtt in the cortex and striatum in BACHD-ΔN17, but not WT mice starting at 2 months, and noticed robust nuclear inclusions (NIs) at 6 and 10 months of age (Gray et al., 2008; Gu et al., 2009). The aggregation pattern in the BACHD-ΔN17 mice differs from BACHD mice in that the aggregates appear in the BACHD-ΔN17 mice 10 months earlier than in BACHD mice (2 *vs* 12 months), and the BACHD-ΔN17

mice have almost exclusively nuclear aggregates instead of cytoplasmic aggregates. Importantly, similar to nuclear mHtt aggregates in HD human tissue (Difiglia et al., 1997), those in BACHD-ΔN17 mice can only be detected by N-terminal mHtt antibodies, and not by C-terminal antibodies, and mHtt aggregates co-localize with the polyclonal ubiquitin antibody to suggest the mHtt that accumulates in the HMW species is ubiquitinated (data now shown).

A key biochemical feature of mHtt nuclear aggregates is the presence of high molecular weight (HMW) mHtt species in the nuclear fraction from HD patient and mouse brains (Difiglia et al., 1997; Hoffner et al., 2005; Landles et al., 2010; Nucifora et al., 2012). As shown below in Figure 3.4A, the soluble fl-mHtt in 1m BACHD and BACHD-ΔN17 forebrain lysates is mostly cytosolic, with a small fraction of soluble fl-mHtt in the nuclear fraction. Consistent with these findings, I was able to detect an age-dependent accumulation of HMW mHtt species only in the nuclear (but not cytosolic) fraction of BACHD-ΔN17 mice using mHtt-exon 1 antibodies, S830 and 5492, but not with mHtt C-terminal antibodies (7666). Importantly, these HMW species are not present in HDΔN17 mice at 1 month of age, nor present in BACHD mice at 1 or 10 months of age. Thus, our results suggest that deletion of N17 in the context of fl-mHtt results in an accelerated nuclear translocation and aggregation of mHtt N-terminal fragments.

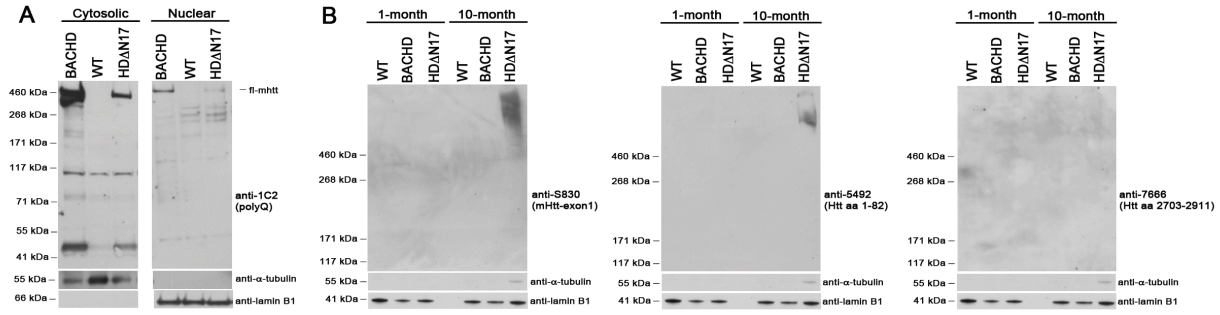


Figure 3.4. Age-dependent N-terminal mHtt HMW nuclear accumulation in HDΔN17 mice. (A) Western blot analysis of 1-month old pure cytosolic and nuclear fractions from wildtype, BACHD, and HDΔN17 mice. The blot was probed with the polyQ-specific 1C2 antibody followed by anti-α-tubulin (cytosolic) and lamin B1 (nuclear) loading controls. **(B)** Western blot analysis of pure nuclear fractions of 1- and 10-month old wildtype, BACHD, and HDΔN17 mice. The blots were probed with the N-terminal mHtt-exon 1 antibodies, S830 and 5492, and the C-terminal Htt antibody, 7666, followed by anti-α-tubulin (cytosolic) and lamin B1 (nuclear) loading controls.

Since BACHD-ΔN17 mice exhibit accelerated nuclear translocation and aggregation of mHtt, we hypothesized that they should exhibit a more severe HD phenotype than the BACHD mouse model. Interestingly, Dr. Xiaofeng Gu determined the BACHD-ΔN17 mice, but not BACWT-ΔN17 mice, exhibit severe motor impairment, significant forebrain weight loss, significant reduction in striatal medium spiny neurons (MSNs), and brain-derived neurotrophic factor (BDNF) transcriptional dysregulation, all key pathogenic features of HD (Reiner et al., 1988; Vonsattel et al., 1985; Zuccato et al, 2001). The remainder of this chapter strives to elucidate the mechanisms underlying the molecular trigger for the onset and progression of these key HD phenotypes in the BACHD-ΔN17 mouse model.

3.2.5. Solubilization of HMW mHtt Nuclear Aggregates in BACHD-ΔN17 Mice Reveals Accumulation of a ~55 to 71 kDa N-terminal mHtt Fragment

In order to determine whether fl-mHtt or an N-terminal fragment of mHtt was the pathogenic species in the BACHD-ΔN17-97Q mouse model of HD, I wanted to solubilize and disrupt the HMW mHtt nuclear aggregates into their smallest proteolytic fragments. Previous work using the Htt-exon 1 R6/2 (Hu Htt aa 1-82 with 190Q) and the *Hdh*Q150 knock-in mouse models of HD demonstrate that the smallest detectable fragment that accumulates in nuclear aggregates is Htt exon-1, which is detected as a ~90-100 kDa fragment by Western blot analysis using polyQ and exon-1 antibodies (Landles et al., 2010). In this study, aggregates in the cytoplasmic and nuclear fractions were dissociated sequentially in 2% SDS detergent and 100% formic acid. My initial attempts to dissociate the BACHD-ΔN17 mHtt aggregates using SDS and formic acid did not result in the detection of any mHtt, neither full-length or fragment. Therefore, I performed a variety of solubilization treatments derived from previously published protocols dissociating polyglutamine aggregates including: 100% formic acid (Landles et al., 2010), 8M urea + 2% SDS (Hazeki et al., 2000), 6N HCl (Hazeki et al., 2000), and 4% sarcosyl

(Mitsui et al., 2006) (Figure 3.5). Interestingly, the HMW mHtt aggregates were slightly solubilized (the HMW species shifted to a lower molecular weight; 5492 antibody epitope was more exposed) in the detergent 8M urea + 2% SDS and 4% sarcosyl conditions, whereas the acidic treatments did not yield any mHtt by Western blot analysis.

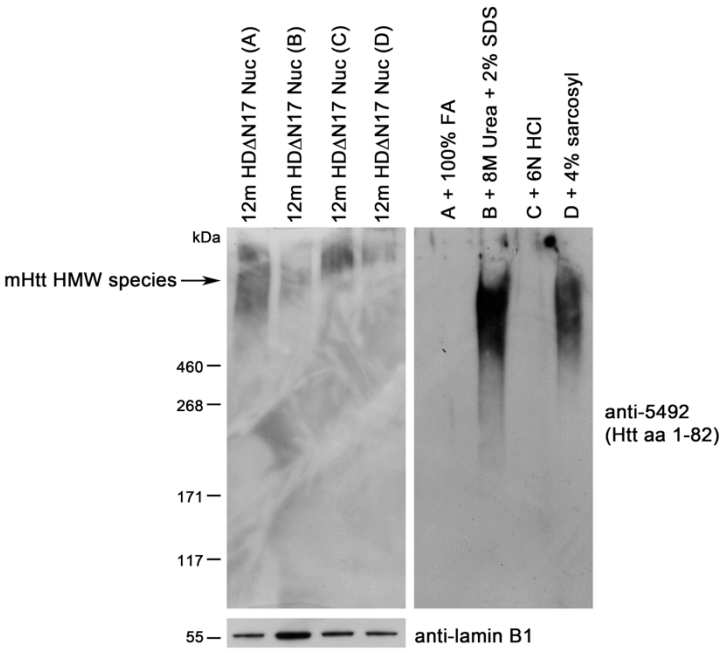


Figure 3.5. Solubilization treatments of BACHD-ΔN17 nuclear mHtt aggregates. Pure nuclear fractions from four BACHD-ΔN17 mice were solubilized with 100% FA (A), 8M urea + 2% SDS (B), 6N HCl (C), or 4% sarcosyl (D). The blot was probed with anti-Htt 5492 and the nuclear loading control lamin B1.

Considering most mHtt nuclear inclusion disaggregation protocols used formic acid (Landles et al., 2010; Lunkes et al., 2002), I decided to further optimize the formic acid treatment conditions by varying the 37° incubation time (30 *vs* 60 minutes) and formic acid concentration (70% - 100%) (Figure 3.6). Interestingly, as the HMW mHtt species is solubilized with increased 37° incubation time and formic acid concentration (as evident after probing with the 5492 Htt antibody), there is a reciprocal increase in the presence of a ~55 to 71 kDa mHtt fragment that is recognized by the N-terminal polyQ 1C2 antibody, but not the C-terminal Htt antibody 7667. These potentially exciting results suggest that a N-terminal mHtt fragment is

accumulating in the nucleus of the BACHD-ΔN17 mice to form the HMW mHtt aggregates during the course of disease.

A recent study analyzing a transgenic mouse model expressing the caspase 6 fragment of Htt with 82 glutamines (N586-82Q) revealed similar solubilized nuclear mHtt fragments sizes (50 to 70 kDa) (Waldron-Roby et al., 2012), which were smaller than the exon-1 detected by Western blot analysis in the R6/2 nuclear fraction (Hu Htt 1-82, 190Q, 90-100 kDa) (Landles et al., 2010). This data suggests that the ΔN17 fl-mHtt in the BACHD-ΔN17 mice may be processed into smaller N-terminal fragments that are less than human Htt aa 1-586 in size.

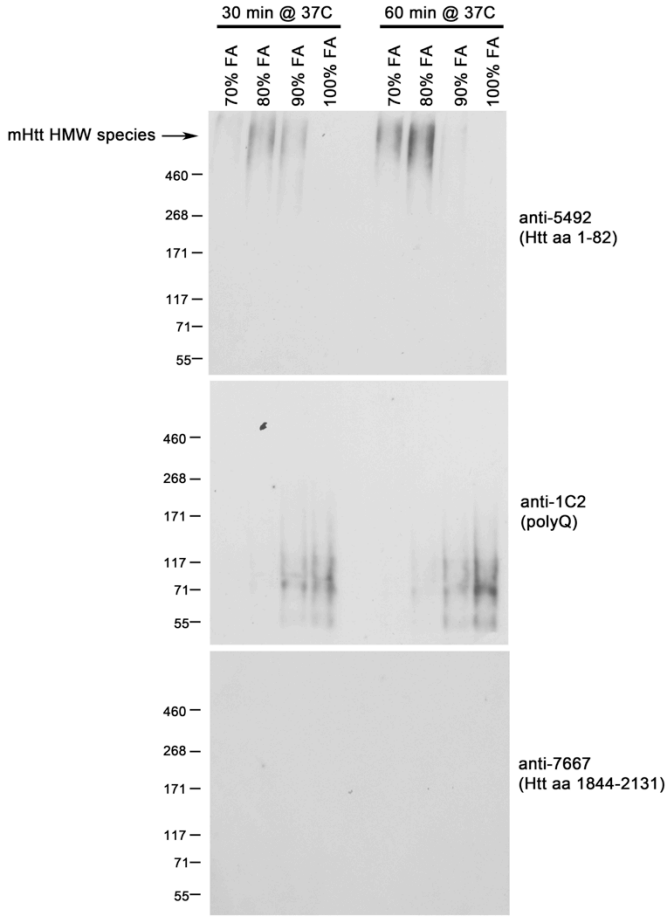


Figure 3.6. Disaggregation of BACHD-ΔN17 nuclear aggregates with formic acid treatment results in a N-terminal ~55 to 71 kDa mHtt fragment. Western blot analysis of BACHD-ΔN17 nuclear fractions (14-ug each) treated with formic acid at various concentrations (70% - 100%) and 37° incubation times (30 *vs* 60 min) using the 5492, 1C2, and 7667 Htt antibodies.

3.2.6. Mass Spectrometry Analysis of BACHD-ΔN17 mHtt HMW Species and Solubilized Fragments

In addition to demonstrating that an N-terminal mHtt fragment accumulates in the nuclear fraction of old BACHD-ΔN17 mice, I also wanted to address the following questions using a mass spectrometry proteomic approach: 1) Is the N-terminal mHtt fragment post-translationally modified?; 2) What is the exact size/sequence of this mHtt N-terminal fragment?; and 3) What are the proteins associated with the mHtt aggregates? The answers to these questions may help to elucidate the molecular trigger of mHtt nuclear aggregation and striatal degeneration in the BACHD-ΔN17 mice.

In order to determine whether the N-terminal mHtt in the HMW species is post-translationally modified and to identify the proteins associated with the mHtt aggregates, I used a traditional in-gel trypsin digestion followed by mass spectrometry approach. The cytosolic and nuclear fractions from 10-month old WT and BACHD-ΔN17 mice were separated by SDS-PAGE followed by staining with GelCode Blue Stain Reagent (Pierce) (Figure 3.7). The approximate size of the HMW mHtt species (or the top four gel bands) were excised and subjected to trypsin digestion in the presence of RapiGest SF surfactant (Waters). The tryptic digests were sequenced by LC-MS/MS using the Waters Xevo-QTof MS, and the data was searched using the ProteinLynx Global SERVER (PLGS v2.4, Waters) against the Swiss-Prot mouse proteome sequence database. The proteins identified with a PLGS score of 100 (indicates high-confidence identification) are listed below in Table 3.1. Interestingly, even though wildtype or mHtt were not identified amongst the short list of proteins, Rps27a (ubiquitin) is the protein identified with the highest score in both the wildtype and BACHD-ΔN17 nuclear fraction. This mass spectrometry data further supports the ubiquitin co-localization immunostaining data in the BACHD-ΔN17 mice.

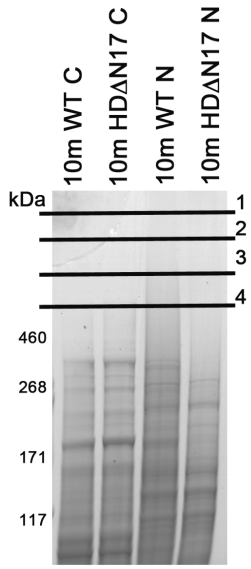


Figure 3.7. Isolation of mHtt HMW species from 10-month old wildtype and BACHD-ΔN17 pure cytosolic and nuclear fractions. A NuPAGE 3-8% Tris-Acetate SDS-PAGE gel of 10-month old wildtype and BACHD-ΔN17 cytosolic (C) and nuclear (N) fractions as visualized by GelCode Blue Stain Reagent. The top four gel bands (#1-4) were excised from the gel, subjected to in-gel trypsin digestion, followed by mass spectrometry protein identification.

Table 3.1. HMW proteins identified in the 10-month old wildtype and BACHD-ΔN17 cytosolic and nuclear fractions. Mass spectrometry data was searched against the Swiss-Prot mouse database using PLGS v2.4 (Waters). Proteins were required to have a PLGS score > 100.

Gel Band #	Genotype	Fraction	Gene ID	Protein Description	Protein Score	Protein MW (Da)	Peptides Identified
1	WT	Cytosolic	Hist1H2ah	Histone H2A	201.3409	13819.0836	3
4	HDΔN17	Cytosolic	Ptprz1	DSD 1 proteoglycan	204.5537	175192.661	12
1	WT	Cytosolic	Hist1h4a	Histone H4	252.7492	11367.3627	5
4	WT	Nuclear	Atp1a3	Sodium potassium transporting ATPase subunit alpha 3	112.7967	111691.8835	9
1	HDΔN17	Nuclear	Col1a2	Collagen, type 1, alpha 2	134.3343	116867.6381	16
1	WT	Nuclear	Hist1h2ah	Histone H2A	507.7774	13819.0836	4
1	WT	Nuclear	Rps27a	Ubiquitin	5009.139	8564.8551	6
1	HDΔN17	Nuclear	Rps27a	Ubiquitin	10316.26	8564.8551	16

Considering only a few proteins were identified from the mHtt HMW species, I reasoned that it might be difficult for the trypsin enzyme to digest proteins in aggregate or oligomer form. Therefore, I solubilized the mHtt aggregates using the 100% formic acid treatment on 12-month old wildtype and BACHD-ΔN17 nuclear fractions, ran a NuPAGE 12% Bis-Tris SDS-PAGE gel to separate smaller molecular weight species (possibly including the mHtt N-terminal fragments), excised the entire gel lane for in-gel trypsin digestion (Figure 3.8), and subjected the tryptic digests to LC-MS/MS sequencing as described above. The 322 high-confidence proteins

identified (PLGS score > 100) from the solubilized BACHD-ΔN17 nuclear fraction are provided in Supplementary Table 3.1. Interestingly, Rps27a (ubiquitin) was identified in both the HMW species and formic acid solubilized BACHD-ΔN17 nuclear fractions.

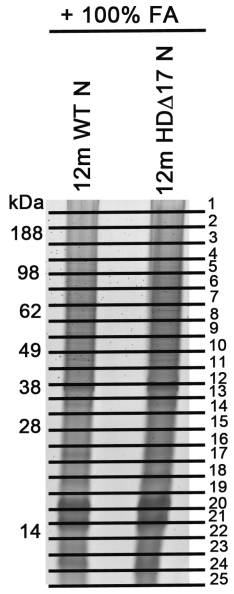


Figure 3.8. Formic acid solubilization of mHtt HMW species from 10-month old wildtype and BACHD-ΔN17 pure nuclear fractions. A NuPAGE 12% Bis-Tris SDS-PAGE gel of 10-month old wildtype and BACHD-ΔN17 nuclear fractions as visualized by GelCode Blue Stain Reagent. The entire gel lane was cut into 25 gel bands and subjected to in-gel trypsin digestion, followed by mass spectrometry protein identification.

Since an anti-1C2 immunoreactive ~50 kDa fragment was detected by Western blot analysis only in the solubilized BACHD-ΔN17 (not wildtype) nuclear fraction (data not shown), I was confident endogenous and/or mutant Htt peptides would be identified by mass spectrometry. However, no endogenous or mutant Htt tryptic peptides were identified using the PLGS search parameters searching against the entire Swiss-Prot mouse (and human Htt) proteome (Supplemental Table 3.1). To increase the likelihood that PLGS will identify Htt peptides, the LC-MS/MS data was searched against only the human Htt protein and keratin homolog (skin contamination) sequences with protein post-translational modifications (K acetylation, STY phosphorylation, M oxidation). The human Htt tryptic peptides identified are listed below in Table 3.2.

Table 3.2. Human Htt tryptic peptides identified in solubilized BACHD-ΔN17 nuclear fraction.
Peptides colored in light blue indicate high-confident Htt peptide (mass accuracy within ± 1.0 ppm).

Gel Band #	Gene ID	Peptide Modification	Peptide m/z	Peptide Sequence	Sequence Start	Peptide Precursor m/z ppm
9	**HTT**		**1064.5843**	**MATLEKLMK**	**0**	**-0.235**
9	HTT		776.4512	KELSATK	91	-53.634
9	HTT		1898.9575	VNHCLTICENIVAQSVR	101	-8.7996
9	HTT		1362.712	MVADECLNKVIK	146	-4.7473
9	HTT		1356.7668	VIKALMDSNLPR	155	11.29
9	HTT		1660.9026	CRPYLVNLLPCLTR	203	-51.6365
9	HTT		1724.9177	RPEESVQETLAAAVPK	220	-29.1835
9	HTT		1543.7758	TAAGSAVSICQHSRR	270	-7.8264
9	HTT		1976.0117	SGSIVELIAGGGSSCSPVLSR	418	5.6603
9	HTT	PhosphoryI+STY(*);PhosphoryI+STY(*)	2264.0393	SGSIVELIAGGGSSCSPVLSRK	418	6.6791
9	HTT		1251.6427	SDVSSSALTASVK	460	-15.2481
9	HTT		1182.6589	NVLVPDRDVR	700	-36.3132
9	HTT		1691.9183	GATAILCGTLICSILSR	767	-26.5215
9	HTT		1834.9731	TLTGNTFSLADCIPLLR	797	-30.7602
9	HTT		1466.7849	EPGEQASVPLSPKK	1190	-21.4306
9	HTT		802.4278	SQGRAQR	1339	5.8284
9	HTT		2073.0725	VNYCLLDSDQVFIGFVLK	1461	-2.6652
9	HTT		2483.3302	LIQYHQVLEMFILVLQQCHK	1579	-39.6053
9	HTT		1081.6187	ILVLQQCHK	1590	-21.7823
9	HTT		1860.857	LRDGDSTSTLEEHSEGK	1715	23.0065
9	HTT		1441.6554	LRDGDSTSTLEEH	1715	47.2544
9	HTT		1272.6371	WWAEVQQTPK	1851	-16.3811
9	HTT		1428.7383	WWAEVQQTPKR	1851	29.1459
9	HTT		1533.8384	SALFEAAREVTLAR	2163	-23.5143
9	HTT		864.4574	SALFEAAR	2163	29.3905
9	HTT		1375.7692	LFEAAREVTLAR	2165	-35.9255
9	HTT		1980.1277	LPSHLHLPPEKEKDIVK	2236	-10.1878
9	HTT		1062.5942	LPLVNSYTR	2403	-54.1318
9	HTT		1047.5582	INTLGWTSR	2454	8.6218
9	**HTT**		**1587.8523**	**GIVEQEIQAMVSKR**	**2553**	**0.4395**
9	HTT		1431.7512	GIVEQEIQAMVSK	2553	28.6424
9	HTT		2077.1553	LGQVSIHSVWLGNSITPLR	2615	-39.9504
9	HTT		1016.5524	WILPSSSAR	2683	-14.6133
9	HTT		1172.6535	WILPSSSARR	2683	17.5959
9	HTT		1756.8938	NQFELMYVTLTELR	2716	7.8365
9	HTT		828.4574	AVAEPVSR	2759	33.6853
9	**HTT**		**831.4934**	**LLESTLR**	**2767**	**0.5494**
9	**HTT**		**813.4829**	**LLESTLR**	**2767**	**0.764**
9	HTT		874.488	LDAESLVK	2895	30.9619
9	HTT		589.3304	LSVDR	2903	-44.7986
9	HTT		2902.4251	TSDPNPAAPDSESVIVAMERVSVLFDR	2939	-4.8622
9	HTT	Oxidation+M(16)	2194.0889	ILPQFLDDFFPPQDIMNK	2980	4.9728
9	HTT		1333.6827	ILPQFLDDFFP	2980	9.7463
9	HTT		2178.094	ILPQFLDDFFPPQDIMNK	2980	33.291
9	HTT		1677.8377	VFQTLHSTGQSSMVR	3020	-45.6022
9	HTT		1596.7839	DWVMLSLSNFTQR	3035	12.0322
9	HTT	PhosphoryI+STY(5)	2164.0699	RAFQSVLEVVAAPGSPYHR	3111	9.9423
9	HTT		1196.6932	LLTCLRNVHK	3130	11.9311
9	HTT		970.5251	TCLRNVHK	3132	14.1221
15	HTT		1064.5843	MATLEKLMK	0	4.086
15	HTT		1210.5984	TLKDESSVTCK	815	-5.3504
15	HTT		1189.6059	ADAGKELETQK	1559	-4.125
15	HTT		932.5047	GKELETQK	1562	3.3928
15	HTT		864.4574	SALFEAAR	2163	26.7299
15	**HTT**		**544.2977**	**LLEST**	**2767**	**-0.5575**
15	HTT		831.4934	LLESTLR	2767	2.8345
15	HTT		813.4829	LLESTLR	2767	3.0997
15	HTT	Oxidation+M(16)	2194.0889	ILPQFLDDFFPPQDIMNK	2980	-4.0058
18	HTT		768.4978	QIIGIPK	1514	2.3407
18	HTT		1189.6059	ADAGKELETQK	1559	-35.9003
18	HTT		1190.6133	LGMCNREIVR	1887	-48.9312
18	HTT		1473.7544	SDSALLEGAELVNR	2113	-47.8113
18	HTT		864.4574	SALFEAAR	2163	27.0769
18	HTT		544.2977	LLEST	2767	-4.0483
18	HTT		831.4934	LLESTLR	2767	-1.8559
18	**HTT**		**813.4829**	**LLESTLR**	**2767**	**0.1494**
22	**HTT**		**1790.829**	**VLLGEEEALEDDSESR**	**444**	**0.2551**
22	HTT		1210.5984	TLKDESSVTCK	815	-4.8547
22	HTT		1626.8962	LVSFLEAKAENLHR	880	3.0634
22	HTT		937.5578	HVAAASLIR	926	-26.3196
22	HTT		1207.5801	QSDTSGPVTTSK	1213	-28.308
22	HTT		845.4727	TNLTSVTK	1404	-9.3515
22	HTT		863.4833	TNLTSVTK	1404	-7.2626
22	HTT		768.4978	QIIGIPK	1514	-4.2956
22	HTT		751.4713	QIIGIPK	1514	-2.3315
22	HTT		640.4392	IIGIPK	1515	-5.0343
22	HTT		357.2496	IPK	1518	-8.7674
22	HTT		703.4097	ITAAATR	1796	-35.7034
22	HTT		428.2504	ITAAA	1796	18.0725
22	HTT		1190.6133	LGMCNREIVR	1887	-44.6477
22	HTT		917.4332	LGMCNREI	1887	16.8203
22	HTT		849.4651	LLCTPFR	1997	51.4204
22	HTT		736.3811	LCTPFR	1998	54.7866
22	HTT		1882.0949	LPLVNSYTRVPPLVWK	2403	-4.3123
22	HTT		1864.0844	LPLVNSYTRVPPLVWK	2403	4.9078
22	HTT		1345.7627	SYTRVPPLVWK	2408	-6.5265
22	HTT		575.3148	ALDTR	2539	17.2929
22	HTT		914.4288	ELGSMSYK	2607	35.1092
22	HTT		831.4934	LLESTLR	2767	-8.23
22	HTT		544.2977	LLEST	2767	-6.9878
22	HTT		813.4829	LLESTLR	2767	-6.8575
22	HTT	Acetyl+K(2)	814.4418	EKVSPGR	2932	-10.1642
22	HTT		1596.7839	DWVMLSLSNFTQR	3035	-44.3311
23	HTT		1016.5193	ALMDSNLPR	158	6.2555
23	HTT		937.5578	HVAAASLIR	926	-19.28
23	HTT		1338.69	EPGEQASVPLSPK	1190	12.6458
23	HTT		1207.5801	QSDTSGPVTTSK	1213	-25.1612
23	HTT		1189.5695	QSDTSGPVTTSK	1213	-22.0411
23	**HTT**		**751.4713**	**QIIGIPK**	**1514**	**-0.7346**
23	**HTT**		**768.4978**	**QIIGIPK**	**1514**	**-0.0015**
23	HTT		640.4392	IIGIPK	1515	1.2114
23	HTT		357.2496	IPK	1518	1.3096
23	HTT		703.4097	ITAAATR	1796	-32.1493
23	HTT		428.2504	ITAAA	1796	26.2452
23	HTT		489.278	AAATR	1798	8.8454
23	HTT		1272.6371	WWAEVQQTPK	1851	34.5368
23	HTT		654.4046	EIVRR	1893	-14.3175
23	HTT		672.4151	EIVRR	1893	-12.9892
23	HTT		864.4574	SALFEAAR	2163	31.7041
23	HTT		1384.7947	NSGVPAFLTPLLR	2382	-16.6892
23	HTT		575.3148	ALDTR	2539	24.5932
23	HTT		914.4288	ELGSMSYK	2607	40.249
23	HTT	Ubiquitination(9)	989.5655	AAAVLGMDK	2750	10.2912
23	HTT		361.2194	VSR	2764	14.4119
23	**HTT**		**544.2977**	**LLEST**	**2767**	**-0.0064**
23	**HTT**		**831.4934**	**LLESTLR**	**2767**	**0.3089**
23	**HTT**		**813.4829**	**LLESTLR**	**2767**	**0.6411**
23	HTT		657.3818	LLESTL	2767	9.0245
23	HTT		835.4672	VSVLFDR	2959	-42.167

While many human Htt tryptic peptides were identified using this lenient search approach, only a few peptides were considered high-confident tryptic peptides (Table 3.2). Even though the predicted mHtt N-terminal fragment is ~50 kDa by Western blot (or near gel band #9 molecular weight), I identified Htt peptides in multiple gel bands (Figure 3.8; gel band #'s 9, 15, 18, 22, 23), and the peptides covered the entire sequence of Htt (*e.g.,* both N- and C-terminal Htt peptides were identified). Considering the human and mouse Htt protein sequence share 90% identity, many of the peptides in Table 3.2 may be derived from endogenous murine Htt in the BACHD-ΔN17 mice. This is the case for gel band #9 peptide MATLEKLMK, since the BACHD-ΔN17 mice lack this domain.

Furthermore, this experiment provided five potentially interesting Htt PTMs in the solubilized nuclear fraction of BACHD-ΔN17 mouse brain (Table 3.2). The first is phosphorylation of the human specific tryptic peptide SDSIVELIAGGSSCSPVLSRK (gel band #9, sequence starting at Htt aa 418), which has two potential STY phosphorylation sites. Phosphorylation at Htt Serine 421 is a well-characterized Htt protein modification that is neuroprotective *in vitro* (Humbert et al., 2002) and significantly reduced in the cortex and striatum *in vivo* (Warby et al., 2005). My preliminary finding suggests that Ser 421 phosphorylation may be a neuroprotective mechanism of mHtt in the nucleus of the BACHD-ΔN17 mice. A second potential phosphorylation site is on the human Htt tryptic peptide, RAFQSVLEVVAAPGSPYHR (gel band #9, sequence starting at Htt aa 3111) at Ser 3116. The third modification, oxidized methionine, was identified on the same human Htt tryptic peptide, lLPQFLDDFFPPQDIMINK at Met 2996, from two separate gel bands (# 9 and #15). While oxidative stress has been implicated in HD pathology (Browne et al., 1999), the role of this modification in mHtt nuclear toxicity remains unclear. The human specific peptide EKVSPGR (gel band #22, sequence starting at Htt aa 2932) was identified as acetylated at Lys 2933, and the mouse/human peptide AAAVLGMDK (gel band #23, sequence starting at Htt aa 2750) was

identified as ubiquitinated at Lys 2759. Again, both these acetylation and ubiquitination post-translational modifications may play a protective role against nuclear mHtt toxicity in the BACHD-N17 mouse model (Jeong et al., 2009; Steffan et al., 2004).

To further enrich for the solubilized mHtt N-terminal fragments, I performed an anti-1C2 IP of 12-month pure cytosolic and nuclear fractions with and without formic acid solubilization treatment from BACHD and BACHD-ΔN17 forebrains (Figure 3.9). Interestingly, in the untreated formic acid fractions, the anti-1C2 IP was able to pull-down the mHtt HMW species in the BACHD-ΔN17 nuclear fraction. Likewise, in the formic acid treated cytosolic and nuclear fractions, the anti-1C2 IP was able to significantly enrich the N-terminal mHtt fragments in the BACHD-ΔN17 nuclear fraction, while no mHtt fragments were detected in the BACHD nuclear fraction.

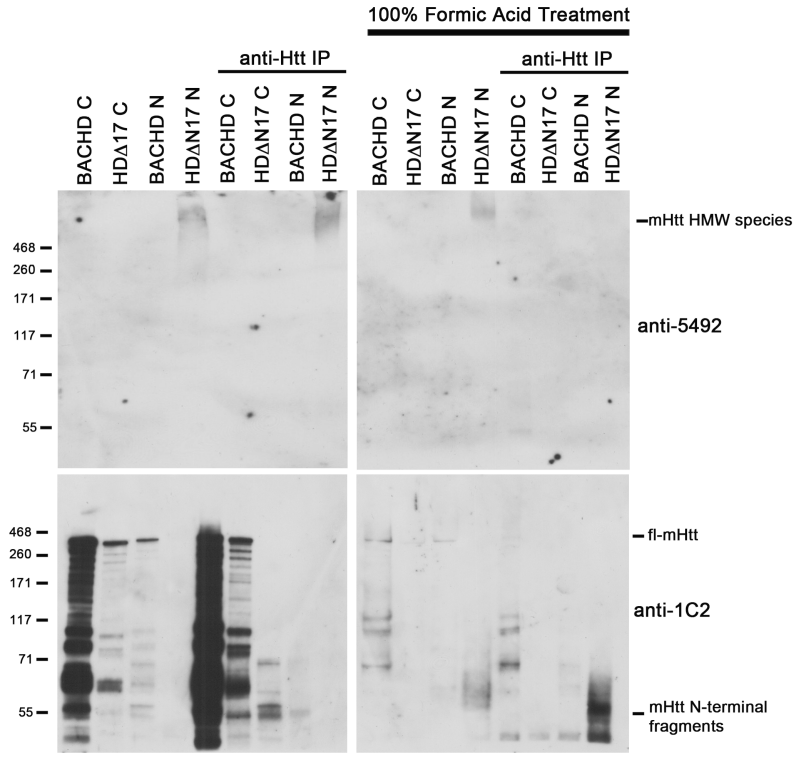


Figure 3.9. Western blot analysis of 1C2-enrichment of N-terminal mHtt fragments in 12-month BACHD-ΔN17 mice. Anti-polyQ (1C2) immunoprecipitation of 12-month old BACHD and BACHD-ΔN17 pure cytosolic and nuclear fractions without (left) and with (right) formic acid treatment. The blots were probed with anti-Htt 5492 and anti-polyQ 1C2.

In order to increase the human Htt tryptic peptide coverage of the N-terminal mHtt fragments, the formic acid solubilized nuclear fractions from 12-month wildtype, BACHD, and BACHD-ΔN17 mice were immunoprecipitated with 1C2. The 1C2 immunoprecipitates were separated on an SDS-PAGE gel (Figure 3.10); the mHtt N-terminal fragment bands were excised; the gel bands were subjected to trypsin digestion; and the tryptic digests were measured by LC-MS/MS on the Xevo-QTof MS. A list of the proteins identified in the 1C2-enriched formic acid solubilized nuclear fractions is provided in Supplemental Table 3.2.

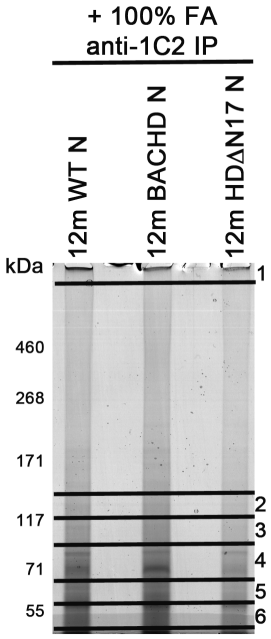


Figure 3.10. 1C2-enrichment of formic acid solubilized 12-month wildtype, BACHD, and BACHD-ΔN17 pure nuclear fractions. A NuPAGE 3-8% Tris-Acetate SDS-PAGE gel of 12-month old wildtype, BACHD, and BACHD-ΔN17 nuclear fractions as visualized by GelCode Blue Stain Reagent. The six gel bands were excised and subjected to in-gel trypsin digestion, followed by mass spectrometry protein identification.

Unfortunately, this 1C2-enrichment experiment did not offer any additional human Htt peptides to further characterize the mHtt N-terminal fragments and its post-translational modifications. However, I was able to compare the mass spectrometry data generated from the solubilized nuclear fraction of BACHD-ΔN17 to the 1C2-enriched solubilized nuclear fraction of BACHD-ΔN17, and 16 proteins were shared amongst the two datasets using different BACHD-ΔN17

biological duplicates (Supplemental Table 3.3). Interestingly, 4/16 proteins are members of the Hsp70 family (Hspa1l, Hspa2, Hspa5, Hspa8), which have previously been identified in polyQ nuclear aggregates (Doi et al., 2004) and have been shown to modulate polyQ aggregation and toxicity both in cell and fly models of HD (Chan et al., 2000). Therefore, the sequestration of these critical molecular chaperones in the nuclear mHtt aggregates may contribute to HD pathogenesis in the BACHD-ΔN17 mouse model.

3.3. Discussion

In this chapter, I present the generation and characterization of the novel BACHD-ΔN17 and BACWT-ΔN17 mouse models. The goal of this research is to better understand the role of the Htt N17 domain in mediating mHtt cytoplasmic retention and nuclear toxicity *in vivo*. We confirmed that deletion of the N17 domain leads to dramatically accelerated nuclear translocation and aggregation of mHtt N-terminal fragments.

More specifically, my contribution to this study has been to apply biochemical approaches to isolate, characterize, and dissociate the nuclear mHtt HMW species in the BACHD-ΔN17 mouse brain. I demonstrate that an N-terminal mHtt fragment (~50 to 70 kDa in size) accumulates in the nucleus as the disease progresses in the BACHD-ΔN17 mice. Furthermore, I use mass spectrometry techniques to identify potential molecular targets (*e.g.,* Hsp 70 proteins) and post-translational modifications (*e.g.,* ubiquitination) that may contribute to the mechanism of mHtt-induced nuclear toxicity demonstrated in this mouse model.

3.4. Experimental Methods

Brain Lysate Preparation

Soluble whole cell protein lysate was prepared as previously described (Gu et al., 2009). Briefly, mouse brains were dissected in ice-cold 100 mM PBS and homogenized in modified RIPA buffer (50mM Tris-HCl, 1% NP-40, 0.25% Na-deoxycholate, 150mM NaCl, pH 7.4) supplemented with 1X Complete Protease Inhibitor Mixture tablets and 1X PhosSTOP Phosphatase Inhibitor tablets (Roche) using 15 strokes from a Potter-Elvehjem homogenizer followed by centrifugation at 4°C for 15 min at 16,000*g*. The resultant supernatant is the soluble whole cell lysate fraction, and the pellet is resuspended in 40-µL 10% SDS solution, boiled for 10 min at 95°C, and briefly spun at 16,000*g* at room temperature; the supernatant is the 10% SDS-solubilized fraction. Protein concentrations were determined using the Bio-Rad Protein Assay (Bio-Rad).

Cytoplasmic and Nuclear Subcellular Fractionation

Pure cytosolic and nuclear fraction were prepared as previously described (Gray et al., 2008). Mouse forebrains were dissected and immediately fresh frozen in dry ice. Tissue was homogenized in 2-mL Buffer A (0.25 M sucrose, 50 mM triethanolamine, pH 7.5, 25 mM KCl, 5 mM $MgCl_2$, supplemented with 0.5 mM DTT and 1X Complete Protease Inhibitor Mixture tablets) using 15 strokes from a Potter-Elvehjem homogenizer followed by centrifugation at 4°C for 15 min at 800*g*. The supernatant was transferred into a new Beckman 2-mL centrifuge tube, balanced, and spun for 1 hour at 100,000g at 4°C; this is the pure cytosolic fraction. The pellet from the initial homogenization was washed in 8-mL Buffer A, followed by another centrifugation at 4°C for 10 min at 800*g*. The resulting supernatant was discarded, and the new pellet was resuspended in 6-mL Buffer B (2.3 M sucrose, 50 mM triethanolamine, pH 7.5, 25 mM KCl, 5

mM $MgCl_2$, supplemented with 0.5 mM DTT and 1X Complete Protease Inhibitor Mixture tablets), homogenized using 5-6 strokes of a ball pestle Dounce homogenizer, then mixed with an additional 2-mL of Buffer A. This mixture was layered onto 4-mL of Buffer B in a Beckman 3.5-inch centrifuge tube, balanced, and spun for 1 hour at 80,000g at 4°C. The supernatant was removed, and the nuclear pellet was resuspended in 1-mL Buffer A, and washed by low-speed centrifugation for 15 min at 1000*g* at room temperature. The pure nuclear pellet was resuspended in ~40-µL Buffer A, and nuclei were lysed using 3 cycles of freeze/thawing on dry ice. After a protein concentration was taken for the cytosolic and nuclear fractions using the Bio-Rad Protein Assay, the pure nuclear fractions were treated with DNase I (1:200 dilution, 50-mg/mL stock) and incubated in 37°C water bath for 5 min. The pure cytosolic and nuclear fractions were prepared for gel loading in 2X Laemmli buffer (100 mM Tris-HCl, pH 7.5, 4% SDS, 0.2% Bromophenol blue, 30% glycerol, 100 mM DTT) and boiled for 10 min at 95°C.

Aggregate Dissociation

Aggregates in BACHD-ΔN17 nuclear fractions were dissociated using the previously published protocols: 100% formic acid (Landles et al., 2010), 8M urea + 2% SDS (Hazeki et al., 2000), 6N HCl (Hazeki et al., 2000), and 4% sarcosyl (Mitsui et al., 2006). Briefly, BACHD-ΔN17 nuclear fraction pellets (30-ug each) were resuspended in 100-µL 100% FA, 20-µL 8M urea + 20-µL 2% SDS buffer, 100-µL 6M HCl, or 20-µL Buffer A + 4% sarcosyl buffer, followed by an hour incubation at 37°C at 300rpm. The FA- and HCl-treated nuclear fractions were dried in a SpeedVac for 4 hours. All samples were prepared for gel loading in 2X Laemmli buffer and boiled for 10 min at 95°C (40-µL total volume). Note that for the FA- and HCl-treated nuclear fractions, 20-µL of 2X Laemmli buffer was added to dried pellet and mixed with 20-µL of 1M Tris-HCl, pH 8.5 buffer to neutralize acid (sample should turn from yellow to purple color).

Immunoprecipitation

The BACHD-ΔN17 (N, A, L) forebrain soluble lysates (500-ug each) were subjected to immunoprecipitation with anti-HDB4E10 (MCA2050, AbD Serotec, 1:500) using Protein G Dynabeads (Invitrogen). Immunoprecipitated proteins (500-ug) were washed, eluted with 4X LDS loading buffer, heated for 10 min at 70°C, and subjected to Western blot analysis. BACHD and BACHD-ΔN17 pure cytosolic and nuclear fractions and FA-treated fractions (dried pellets resuspended in 40-µL Buffer A + 40-µL 1M Tris, pH 8.5; 40-ug each) were subjected to immunoprecipitation with anti-1C2 (MAB1574, Millipore, 1:500) using Protein G Dynabeads (Invitrogen). Immunoprecipitated proteins (40-ug) were washed, eluted with 2X Laemmli buffer, boiled for 10 min at 95°C, and subjected to Western blot analysis.

Gel Electrophoresis and Western Blotting

Protein samples (10- to 60-ug) were run on NuPAGE 12% Bis-Tris gels (Invitrogen; 90 min, 200 V constant, MOPS buffer) and/or NuPAGE 3-8% Tris-Acetate gels (Invitrogen; 2-6 hours, 150 V constant). Gels were dry transferred to PVDF membranes using the iBlot Dry Blotting System (Invitrogen). Blots were blocked in 5% Blotto (Santa Cruz) in 1X PBS/Tween. A list of the antibodies used in this chapter is shown below.

Antibody	Htt Epitope	Host/Clonality	Primary	Secondary	Catalog #	Vendor
2166	aa 181-810	Mouse, monoclonal	1:3000	1:3000	MAB2166	Millipore
1C2	polyQ	Mouse, monoclonal	1:3000	1:3000	MAB1574	Millipore
PW0595	aa 2-17	Rabbit, polyclonal	1:5000	1:5000	PW0595	Enzo Life Sciences
5492	aa 1-82, polyP	Mouse, monoclonal	1:3000	1:3000	MAB5492	Millipore
7667 (HDB4E10)	aa 1844-2131	Mouse, monoclonal	1:3000	1:3000	MCA2050	AbD Serotec
7666	aa 2703-2911	Mouse, monoclonal	1:3000	1:3000	MCA2051	AbD Serotec
S830	hu Htt exon-1	Sheep, polyclonal	1:3000	1:3000	-	Gill Bates
α-tubulin	-	Mouse, monoclonal	1:10,000	1:20,000	T 6074	Sigma
lamin-B1	-	Rabbit, polyclonal	1:1000	1:3000	ab16048	Abcam

In-gel Trypsin Digestion

Gels to be used for mass spectrometry analysis were stained with GelCode Blue Stain reagent (Pierce) according to the manufacturers protocol, destained in ddH_2O, and visualized using the GS-800 Calibrated Densitometer (Bio-Rad). Gel lanes were then cut into gel slices and placed into 100-µL ddH_2O in a 0.5-mL eppendorf tube. The gel slices were washed 3x in alternating solutions of a 50:50 mix of 100 mM $NaHCO_3$ buffer/CH_3CN and 100% CH_3CN. Disulfide bonds were reduced by incubation in 10 mM dithiothreitol (DTT) at 60°C for 1 hour. Free sulfhydryl bonds were blocked by incubating in 50 mM iodoactamide at 45°C for 45 minutes in the dark, followed by washing 3x in alternating solutions of 100 mM $NaHCO_3$ and CH_3CN. The slices were dried, and then incubated in a 20-ng/µL solution of Typsin Gold (Promega, V5280) for 45 minutes at 4°C, followed by incubation at 37°C for 6 to 8 hours. Afterwards, the supernatant was transferred into a fresh collection tube. The gels were incubated for 10 minutes in a solution of 50% CH_3CN/5% trifluoroacetic acid (TFA), in which the supernatant was removed and combined with the previously removed supernatants. This step was repeated a total of 3 times. The supernatant samples containing the peptides were then dried in the SpeedVac for 4 hours and prepared for LC-MS/MS analysis by resuspension in 20-µL of 5% formic acid**.**

Mass Spectrometry Analysis and PLGS Search Parameters

Peptide sequencing was accomplished by nanoACQUITY UPLC coupled with the Xevo-QTof MS (Waters). The nanoACQUITY UPLC was equipped with 180µm x 20mm Symmetry 5µm C18 trap column (Waters) and a C18 BEH130 (particle size 1.7µm, 75µm x 100mm) analytical column (Waters). The eluants used for the LC were 0.1% FA in H_2O (solvent A) and 95% ACN containing 0.1% FA (solvent B). 2-µL of tryptic digestions were injected for analysis at a flow rate of 300 nL/min, and the following gradient was used: 1% B to 40% B in 30 min. The column was finally equilibrated with 3% B for 15 min prior to the next run. Data independent LC-MS^E

acquisition (Geromanos et al., 2009) was performed with lockmass corrected data using [Glu^1]-fibrinopeptide B (785.84 Da) [1-pmol/µL] delivered at 0.3-µL/min and sampled every 60 seconds. Alternate low energy (6 eV) and elevated (15-40 eV) collision energies were applied to the gas cell with MS acquisition of 1.0 s per function over *m/z* 100-2000 Da. Data was processed using the ProteinLynx Global Server version 2.4 (PLGS) and queried against the Swiss-Prot mouse database (with the addition of human huntingtin and keratin sequences). The workflow designer included the following criteria: 1) trypsin was set as the primary digest reagent, and one missed cleavage site was allowed; 2) LC-MS^E peptide and fragment tolerances were set using the following default parameters: min fragments per peptide = 3, min peptides per protein = 1, min fragments per protein = 7, max false positive rate = 4, max protein mass = 600000 Da, min ratio to theoretical = 0.3, min sumProdInten/precInten = 0.03, max ration sumProdInten/precInten = 1, max simultaneous varMods = 3; 3) a minimum of three product ions per peptide were required for peptide identification and one peptide per protein identification; and 4) variable modifications included: (K) ubiquitination, (K) acetylation, (M) oxidation, (STY) phosphorylation, (K) SUMOylation, and (Q) and (E) to pyroE. High-confidence protein identification score criteria for LC-MS^E data required a PLGS protein score >100.

CHAPTER 4

Building the Huntingtin N17- and Phosphorylation-State-Dependent Proteomic Interactome

4.1. Introduction

Previous studies reveal the N17 domain can mediate binding to membranous/cytoplasmic structures (Atwal et al., 2007; Rockabrand et al., 2007), and such cytoplasmic retention appears to override a conventional nuclear localization signal (NLS) in the context of mHtt-exon1 in transgenic mice (Benn et al., 2005). In Chapter 3, we show that compromising the Htt N17 domain function (via a genetic deletion of this domain) leads to dramatic acceleration of nuclear mHtt fragment accumulation and aggregation and HD-like phenotypes *in vivo*. This data suggests that N17 mediated cytoplasmic retention is crucial in delaying the toxicities of mHtt. In this chapter, I investigated the molecular mechanisms through which N17 may mediate Htt cytoplasmic retention, which is currently unknown. Furthermore, in Chapter 3, we demonstrate that the phosphorylation state of fl-Htt Ser13 and Ser16 in the Htt N17 domain are critical determinants of fl-mHtt induced HD pathogenesis *in vivo* (Gu et al., 2009). Since interactions between proteins are often regulated by phosphorylation, it is necessary to determine how changes in the Htt phosphorylation state affect the fl-Htt interactome and protein networks. The goal of this chapter is to identify both the Htt N17- and Htt Ser13 and Ser16 phosphorylation-state-dependent protein interactome using the SD, SA, and BACHD-ΔN17 transgenic mouse models of HD described in Chapter 3 coupled with the spatiotemporal proteomic and network biology approach presented in Chapter 2. I hypothesize that the identification of Htt N17 cytoplasmic/membrane-bound protein(s) and/or Ser13 and Ser16 Htt phosphorylation-state-dependent interactions may prevent translocation of small N-

terminal fragments of mHtt into the nucleus, modify mHtt toxicities *in vivo*, and reveal potential signaling pathways that lead to therapeutic HD drug discovery.

4.2. Results

4.2.1. Confirmation of an N17-Dependent Interacting Protein: Tcp1/Cct1

To test whether we can identify candidate novel N17 domain interactors *in vivo* using differential proteomics with our BACHD and BACHD-ΔN17 mouse models, I first wanted to validate the Htt N17-interacting protein, Tcp1/Cct1, which is able to mediate mHtt aggregation and toxicity *in vitro* (Tam et al., 2009; Tam et al., 2006). Therefore, I immunoprecipitated Tcp1 from WT, BACHD, and BACHD-ΔN17 brains and probed with 1C2 antibody to detect polyQ-expanded mHtt. As shown below in Figure 4.1, Tcp1 efficiently immunoprecipitates mHtt from BACHD, but not BACHD-ΔN17 brains, suggesting the N17-dependent interaction of Tcp1 in mammalian brains.

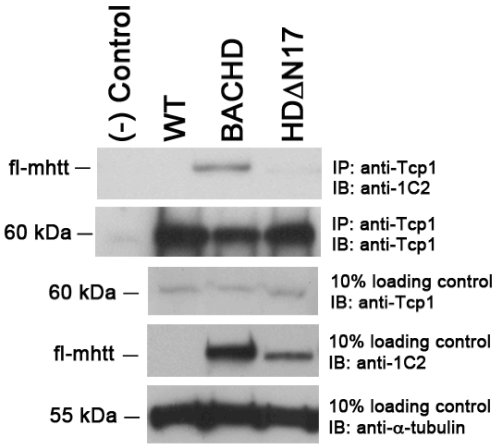
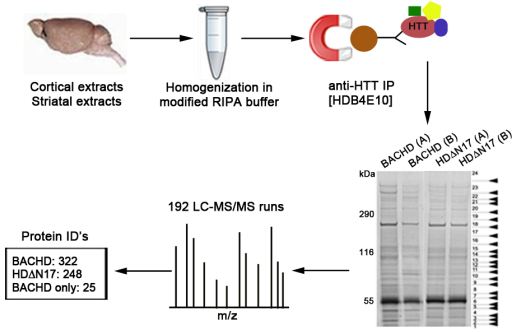


Figure 4.1. Validation of Tcp1 as an Htt N17-dependent interaction. TCP1 was immunoprecipitated from WT, BACHD, and BACHD-ΔN17 brains, and probed with the 1C2 antibody to confirm Tcp1 only pulls-down mHtt in BACHD, not BACHD-ΔN17 mice. The blots were also probed with Tcp1 and anti-α-tubulin as loading controls.

4.2.2. Identification of Htt N17-Dependent Interacting Proteins

To further identify cytosolic proteins that may interact with the Htt N17 domain and mediate mHtt cytoplasmic retention, I performed an unbiased differential proteomic screen using the BACHD and BACHD-ΔN17 mouse models. In Chapter 2, I presented an affinity purification approach using the human-selective Htt C-terminal antibody (HDB4E10, AbD Serotec, human Htt aa 1844-2131), which selectively immunoprecipitates human mHtt, while pulling-down very little murine Htt from mouse brain. I used this same approach to profile Htt protein-protein interactions from 2-month old BACHD and BACHD-ΔN17 cortical and striatal extracts (n=2 per each brain region/genotype), followed by mass spectrometry protein identification (Figure 4.2A; Supplemental Tables 4.1 and 4.2). Among the 322 proteins identified in the BACHD IP samples, and the 248 proteins identified in the BACHD-ΔN17 IP samples, only 25 proteins reproducibly co-immunoprecipitated with fl-mHtt in an N17-dependent manner (*i.e.,* at least 5 unique peptides identified in both BACHD samples, and 0 peptides in both BACHD-ΔN17 IP samples; see Figure 4.2B). I used the semi-quantitative readout of protein abundance in this mass spectrometry experiment (*i.e.,* unique tryptic peptide counts) to identify several proteins that have striking binding differences between the BACHD and BACHD-ΔN17 IP samples (Figure 4.2B). For example, 152 alpha-tubulin 1a (Tuba1a) peptides were identified in the BACHD IP samples, and 0 peptides were identified in the BACHD-ΔN17 IP samples.

A



B

Cytoplasm	Membrane	Mitochondrion
Tuba1a (152)	Atp2b3 (25)	Hspd1 (23)
Tuba8 (55)	Atl1 (17)	Acsl6 (21)
Tubb1 (25)	Lgi1 (17)	Acat1 (18)
Pkfl (24)	Plp1 (12)	Slc25a31 (18)
Acta2 (16)	Slc12a7 (11)	Vdac1 (10)
Dync1li1 (13)	Slc1a3 (10)	
Ywhaq (13)	Gnaz (10)	
Sept11 (11)	Napb (10)	
Prkacb (11)		
Sept9 (11)		

Figure 4.2. A proteomic strategy to profile Htt N17-dependent interactions. (A) Full-length mHtt was immunoprecipitated from cortical and striatal BACHD and BACHD-ΔN17 soluble lysates (n=2), IPs were separated on a NuPAGE 3-8% Tris-Acetate gel (Invitrogen), gel lanes were cut into 24 gel bands, gel bands were subjected to in-gel trypsin digestion, digests were sequenced using the nanoAcquity UPLC coupled to the Xevo-QTof MS (Waters), and data was searched using PLGS. The number of proteins identified in the BACHD, BACHD-ΔN17, and BACHD only IP samples are indicated. **(B)** The subcellular localization of the 25 putative N17-dependent Htt-interacting proteins identified, where the difference in unique tryptic peptide counts between the BACHD and BACHD-ΔN17 IP samples are indicated in parenthesis.

There is additional evidence to support that this differential proteomic experiment yields a candidate pool of mHtt N17-dependent interactors for further validation. First, our collaborator Ray Truant (McMaster University, unpublished data) has previously performed an *in vitro* proteomic experiment in which he used a synthesized N17 peptide to pull-down putative N17-binding proteins from mouse brain extracts. Impressively, among a dozen or so proteins he had identified using mass spectrometry, three of the proteins overlapped with our list (Tuba1a, Ywhaq, and Hspd1). Second, consistent with the idea that an N17 interactor can anchor mHtt to membranous or cytoskeletal structures in the cytosol (Atwal et al., 2007; Rockabrand et al., 2007), our 25 putative N17 interactors are all cytosolic, membrane, or mitochondrial proteins (Figure 4.2B). I further validated Tuba1a as an N17-dependent interactor *in vivo* by reciprocal co-IP/immunoblot analysis using the 1C2 and Tuba1a (clone DM1A) antibodies (Figure 4.3A-B).

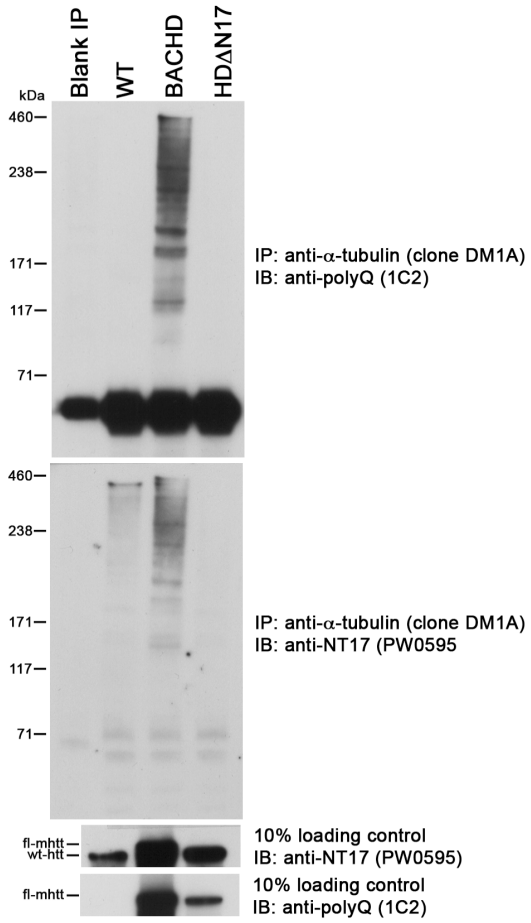


Figure 4.3. Validation of Tuba1a as an N17-dependent Htt interactor *in vivo*. Immunoprecipitation of Tuba1a (clone DM1A) from WT, BACHD, and BACHD-ΔN17 mouse brain. As shown, Tuba1a is unable to pull-down human (1C2, anti-polyQ) or murine (PW0595, anti-N17) Htt from the BACHD-ΔN17 lysates, only fl-Htt from WT and BACHD brains. A 10% loading control blot was probed with 1C2 and PW0595 antibodies as loading controls for the IP.

I used an alternative proteomic approach to verify Htt N17-dependent interactors, in which I immunoprecipitated fl-mHtt from (n=2) BACHD cortical extracts using the N17 antibody (PW0595, Enzo Life Sciences, Htt aa 2-16) and Protein G Dynabeads (Invitrogen). My rationale behind this experiment was that a set of "missing" N17-depedent interactors might be revealed after comparison between the C-terminal (HDB4E10) BACHD IP and the N17 (PW0595) BACHD IP datasets since the Htt N17 epitope will be blocked by antibody during immunoprecipitation. As shown in Figure 4.4, the majority of duplicated Htt interactors (108) are shared between the two separate IP's, where only 15 Htt interactors are selectively pulled down with the N-terminal antibody and 12 Htt interactors are selectively pulled down with the C-terminal antibody (which may represent a list of potential Htt N17-binding proteins)

(Supplemental Table 4.3). Interestingly, four proteins (Napb, Matr3, Efta, and Atl1) were identified as putative N17-dependent interactors, whereas three proteins (Eef1g, Pygb, and Tuba1c) were identified as more C-terminal Htt-binding proteins using both experimental proteomic approaches (Figure 4.2, Supplemental Tables 4.1 and 4.2). Further validation is required to determine the specific binding of these proteins, their cytoplasmic retention, neuroprotective and/or toxic effects on fl-mHtt.

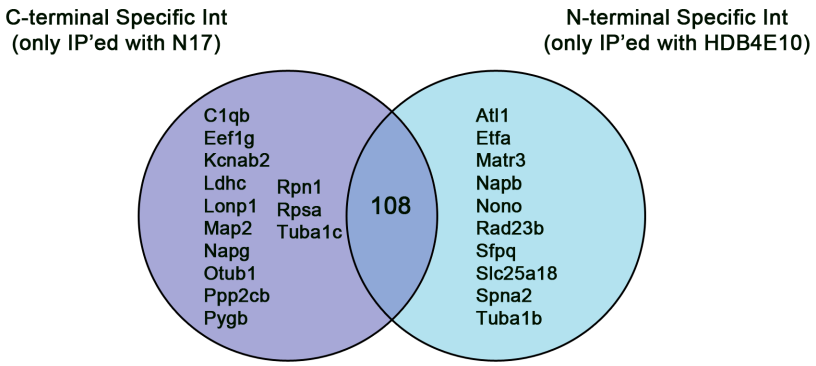


Figure 4.4. Htt N17-binding proteins identified by comparing BACHD anti-N17 and anti-HDB4E10 immunoprecipitations. A Venn diagram comparison of the potential C-terminal (left) and N-terminal (right) Htt-interacting proteins by immunoprecipitation from BACHD cortical extracts using the N17 and HDB4E10 antibodies.

4.2.3. Building the Phosphorylation-State-Dependent Interactome

Previous studies suggest that Htt acts as a scaffolding protein, bringing together multiple protein signaling complexes to modulate cellular functions such as clathrin-mediated endocytosis, vesicle-transport, and transcriptional regulation (Harjes and Wanker, 2003; Kaltenbach et al., 2007). It is postulated that Htt PTMs play a major role in regulating Htt's subcellular localization, conformational changes, and protein-protein interactions to drive these cellular processes. In Chapter 3, I present one example of how "mimicking" phosphorylation at Htt Ser13 and Ser16 acts as a neuroprotective molecular switch *in vivo* (Gu et al., 2009). However, the mechanism behind this neuroprotection remains unclear.

Large-scale proteomic studies have strived to understand protein phosphorylation at the systems level to build networks of kinases and their substrates (Linding et al., 2007). In this study, I used an affinity purification-mass spectrometry (AP-MS) approach to profile phosphorylation-state-dependent Htt interactions using the SD and SA mouse models previously described in Chapter 3. While the phosphorylation of proteins can be detected using this approach, the most useful information extracted from this experiment will be the proteins specifically associated with the Htt Ser13 and Ser16 phosphomimetic “non-toxic” form of fl-mHtt (SD mice) and/or the phosphoresistant “toxic” form of fl-mHtt (SA mice). I hypothesize that these Htt-interacting proteins will provide a candidate list of kinases, phosphatases, and signaling molecules involved in pathways that may lead to therapeutic HD drug discovery.

Initial anti-Htt IP experiments using equivalent amounts of SD and SA cortical lysate for input (2.5-mg) resulted in the differential pull-down of fl-mHtt from the BACHD, SD, and SA mouse models. As shown in Figure 4.5A, both the protein stain and Western blot analysis using the 1C2 antibody show significantly more fl-mHtt IP’ed from the BACHD and SA mouse models compared to the SD mice. This is expected considering the fl-mHtt expression level in the BACHD and SA mice is slightly greater than the fl-mHtt expression level in SD mice (Gu et al., 2009). Furthermore, after protein identification by mass spectrometry, both SD cortical biological duplicate IP samples identified zero human Htt peptides. Therefore, I decided to optimize the SD anti-Htt IP conditions to pull-down approximately equivalent amounts of fl-mHtt from the SD and SA mice for easier comparison of phosphorylation-state-dependent Htt protein interactors between samples. I determined that it requires ~1.6x more SD lysate as an input for the anti-Htt IP compared to the SA brain lysate (Figure 4.5B).

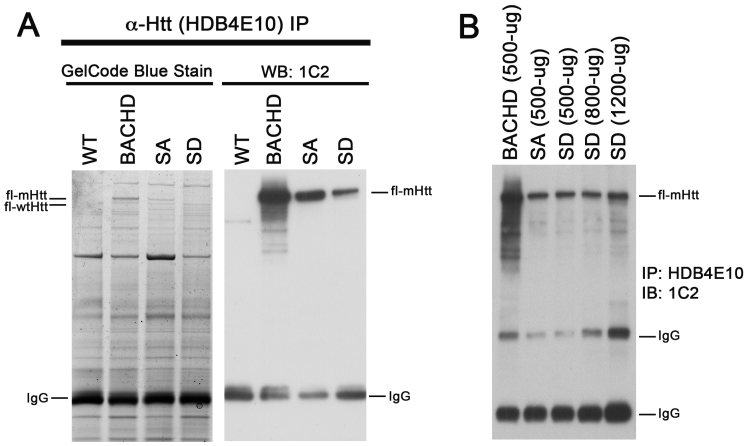


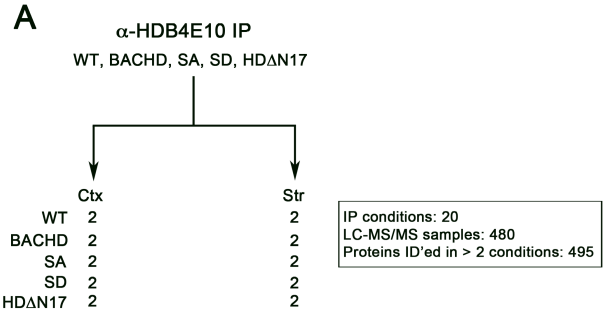
Figure 4.5. Optimization of anti-HDB4E10 immunoprecipitation of fl-mHtt from SD and SA mouse models. (A) Anti-Htt IP of equivalent inputs from WT, BACHD, SA, and SD cortical extracts followed by GelCode Blue protein stain (left) and Western blot analysis using the 1C2 antibody (right). **(B)** Anti-Htt IP of BACHD, SA, and various input levels of SD cortical extracts followed by Western blot analysis using the 1C2 antibody. As shown, 800-ug of SD lysate pulls-down approximately the same amount of fl-mHtt as 500-ug of SA lysate.

To identify BACHD Ser13 and Ser16 phosphomimetic and phosphoresistant fl-Htt interactions *in vivo*, I immunoprecipitated endogenous Htt and fl-mHtt from the cortex and striatum of young (2m) WT, BACHD, SD, and SA mice using the Htt C-terminal antibody, clone HDB4E10 (AbD Serotec) and Protein G Dynabeads. All immunoprecipitations and control assays (no antibody) were performed in duplicate. The immunoprecipitates were separated on NuPAGE 3-8% Tris-Acetate gels (Invitrogen), in which the entire lane of each sample was divided into 24 gel pieces, and each gel slice will be subjected to in-gel trypsin digestion. Each digestion sample was subjected to peptide sequencing by LC-MS/MS using the Waters nanoAcquity UPLC-Xevo QTof MS system. Sequences were searched against the Swiss-Prot mouse and mammalian genomes using Waters ProteinLynx Global Server (PLGS).

An overview of the N17- and phosphorylation-state-dependent IP experiments performed is summarized below in Figure 4.6A and Supplemental Table 4.1. Of the 887 proteins identified in this study, only 495 proteins appeared in more than 2 independent IP conditions. As shown below in Figure 4.6B, the number of Htt peptides (combined murine and human unique

tryptic peptides) and the number of putative interactors (> 2 IP conditions; see Supplemental Tables 4.3 and 4.4) varied between genotype and brain regions. For example, 1.6x more SD cortical lysate was required to IP any Htt peptides, whereas the SD striatal lysate did not need any extra input for the IP to identify Htt peptides. Furthermore, a biological replicate for WT Str and HDΔN17 Str samples failed to identify any Htt peptides (Figure 4.6B). A caveat to this study, unlike the Htt interactome presented in Chapter 2, is that I am comparing the interactors from different HD transgenic mouse models (BACHD, SD, SA, HDΔN17) which all have various levels of fl-mHtt expression. Therefore, if the Htt-binding proteins are dependent on the amount of Htt pulled-down, then this may skew the semi-quantitative nature of this experiment and prove the comparison of interactors across samples more challenging.

A



B

Cortical IP Samples	2mW1Ctx	2mW2Ctx	2mD1Ctx	2mD2Ctx	2mA1Ctx	2mA2Ctx	2mB1Ctx	2mB2Ctx	2mNT1Ctx	2mNT2Ctx
# of Unique Htt Peptides	30	46	73	80	95	42	139	149	67	22
# of Interactors	214	158	162	228	191	217	205	291	183	206
Duplicated Interactors	*128/244 = 52.4%*		*134/256 = 52.3%*		*148/260 = 56.9%*		*174/322 = 54.0%*		*142/247 = 57.4%*	

Striatal IP Samples	2mW1Str	2mW2Str	2mD1Str	2mD2Str	2mA1Str	2mA2Str	2mB1Str	2mB2Str	2mNT1Str	2mNT2Str
# of Unique Htt Peptides	0	27	84	55	28	14	80	131	0	21
# of Interactors	127	195	266	190	403	296	168	108	211	89
Duplicated Interactors	*107/215 = 49.7%*		*173/283 = 61.1%*		*284/415 = 68.4%*		*92/184 = 50.0%*		*76/224 = 33.9%*	

Figure 4.6. Experimental overview of the Htt N17- and phosphorylation-state-dependent interactome. (A) A schematic diagram of the 20 IP experiments performed to build the Htt interactome, where each IP was performed with n=2 biological duplicates. **(B)** A table summarizing the number of unique Htt tryptic peptides identified (combined murine and human peptides), the number of interactors identified (>2 IP conditions), and the number of duplicated interactors between biological replicates for each IP sample condition.

I was able to compare the 2-month cortical and striatal BACHD IP proteins identified in the Chapter 2 (n = 437) with the same IP conditions in this current study (n = 384), to determine an overlap of ~33% (204 intersection/617 union) between datasets. The number of shared interactors is low, but this is expected since the data in Chapter 2 and Chapter 4 were acquired

on different QTof-MS instruments (QSTAR *vs* Xevo QTof), under different LC-MS/MS acquisition modes (DDA *vs* LC-MS^E) (Geromanos et al., 2009), and different search engines and parameters (Mascot *vs* PLGS). See 'Experimental Methods' section from each chapter for more experimental details.

4.2.4. Comparison of Reproducible Htt Interactors Identified in the BACHD, BACHD-ΔN17, SD, and SA Mouse Models of HD Reveals Interesting N17 Htt Biology

The strongest information derived from this study is the identification of specific fl-Htt-interacting proteins from the various BAC transgenic mice analyzed. The highly reproducible fl-Htt interactors from the BACHD, BACHD-ΔN17, SD, and SA IP experiments (defined as proteins identified in both cortical and striatal IP samples, with reproducibly identified WT IP sample proteins removed) were compared below in Figure 4.7 (see also Supplemental Table 4.5). In the following section, I highlight the putative proteins that specifically interact with only the SD, SA, and BACHD-ΔN17 forms of mHtt and their implications to N17 biology and HD pathogenesis.

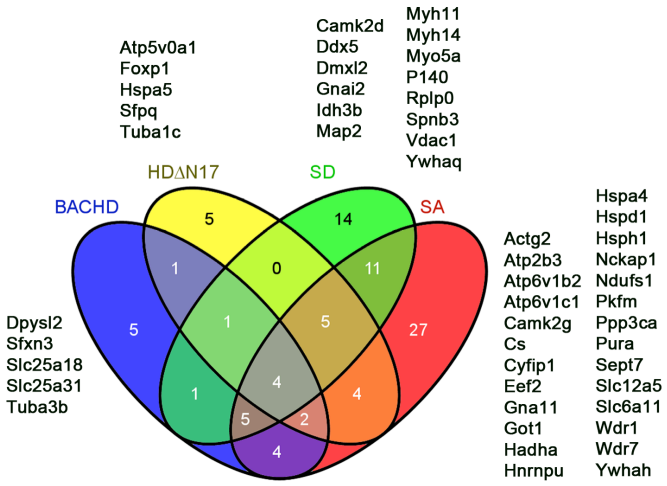


Figure 4.7. Venn diagram comparison of the reproducible fl-Htt interactors identified in the BACHD, BACHD-ΔN17, SD, and SA IP samples. Proteins which were identified in both n=2 cortical and striatal IP samples from the BACHD, BACHD-ΔN17, SD, and SA mice (with WT proteins removed from dataset; see Supplemental Table 4.5) were compared to one another, where the unique protein identifications for each genotype are listed.

SD-specific Htt interactors are enriched with cytoskeletal organization proteins

Interestingly, the SD-only highly reproducible Htt interactors include proteins involved in calcium signaling and actin cytoskeleton remodeling including: calcium/calmodulin-dependent protein kinase II delta (Camk2d), the microtubule-associated protein 2 (Map2), spectrin beta III (Spnb3), and members of the myosin superfamily (Myh11, Myh14, and Myo5a). Previous studies have shown that Htt acts as a scaffold to facilitate vesicular transport along the actin and microtubule cytoskeleton (Caviston and Holzbaur, 2009). More specifically, it is well known that huntingtin enhances the transport of brain-derived neurotrophic factor (BDNF) along microtubules, in which striatal neurons depend on the transport of cortex-derived BDNF for survival (Gauthier et al., 2004). However, the role of Htt and its ability to switch vesicles from actin (short-range transport) to microtubules (long-distance transport), and the mechanism by which Htt facilitates bidirectional vesicle transport (retrograde *vs* anterograde) remains unclear.

Phosphorylation of Htt at Ser421 acts as a molecular switch for this process. Htt phosphorylation at Ser421 is able to recruit kinesin to vesicles to promote anterograde vesicle transport (plus-end direction; towards the axon tip); however, unphosphorylated Htt is no longer able to stabilize kinesin binding, and the dynein-dynactin complex predominates in retrograde vesicle transport (minus-end direction; towards the cell body) (Colin et al., 2008). Furthermore, there is evidence to suggest that Htt and its interaction with the small GTPase Rab5 via the adaptor protein Hap40 (F8a1) mediates vesicle attachment of myosin VI to actin via a myosin adapter protein (*i.e.,* optineurin, Optn) to enhance retrograde actin-based vesicle transport (Pal et al., 2006; Sahlender et al., 2005). Interestingly, myosin VI is the only identified myosin that moves towards the minus end of the actin microfilament (*i.e.,* retrograde transport). Therefore, mimicking phosphorylation of Htt at Ser13 and Ser16 in the SD mice may enhance binding to other myosins (Myh11, Myh14, and Myo5a) to potentially promote anterograde axonal transport.

There is evidence to support actin or actin-binding proteins play a role in regulating mHtt polyQ aggregation (Angeli et al., 2010). Y-27632, a rho-kinase (ROCK) inhibitor has been shown to reduce mHtt exon-1 aggregation *in vitro* (Shao et al., 2008a), decrease toxicity in a fly model of HD (Pollitt et al., 2003), and improve motor performance in R6/2 mice (Li et al., 2009). Y-27632 works by blocking phosphorylation of profilin, an actin-binding protein, that binds directly to mHtt to mediate its aggregation and toxicity effects (Shao et al., 2008b). Additional work has shown that Htt aa 1-14 in the N17 domain mediates Htt exon-1 binding to filamentous actin (F-actin) and increases its aggregation, as deletion of these residues decrease Htt exon-1 aggregation *in vitro* (Angeli et al., 2010). Therefore, I postulate that Htt Ser13 and Ser16 phosphorylation may mediate Htt's N17 interaction with F-actin, profilin, and help play a role in actin remodeling.

SA-specific Htt interactors are enriched with Rho GTPases, WW-domain proteins, and heat shock proteins

The SA-only highly reproducible Htt-interactors include Rho family GTPase signaling proteins (Cyfip1, Sept7, Gna11, Gnal1, Actg2), Protein kinase A signaling molecules (Ywhah, Camk2g, Ppp3ca, Gna11, Gnal1), molecular chaperones (Hspd1, Hsph1, Hspa4), and WW-domain proteins (Wdr1, Wdr7) (Figure 4.7). Previous studies have shown that mHtt contributes to HD pathogenesis by interacting directly or indirectly with signaling pathways abnormally regulated by Rho GTPases, which are small proteins involved in maintaining actin cytoskeletal organization and the microtubule network (Holbert et al., 2003; Song et al., 2002; Sun et al., 2001). Furthermore, our previous *in vitro* SA exon-1 Htt peptide findings suggest the biophysical properties of the more hydrophobic SA version of mHtt results in a "toxic mHtt conformation" that is prone to faster aggregation into amyloid-like fibrils compared to normal exon-1 Htt peptides (Gu et al., 2009). The identification of molecular chaperones and WW-domain proteins

in the SA-specific IP samples supports the idea that SA fl-mHtt is improperly folded, which may lead to aberrant polyP protein-protein interactions and increased association with protein folding machinery.

Htt differentially interacts with 14-3-3 proteins in SD and SA IP conditions

Interestingly, both the SA and SD mice reproducibly interact with a member of the 14-3-3 family of proteins. As previously discussed in Chapter 2, the Htt-containing Red Module from our network analysis of the fl-Htt interactome contained six (Ywhab, Ywhae, Ywhag, Ywhah, Ywhaq, Ywhaz) of the nine possible 14-3-3 family member proteins. Considering 14-3-3 proteins are phospho-serine/phospho-threonine binding proteins (Morrison, 2009) and have been shown to physically or genetically interact with Htt N-terminal fragments (Kaltenbach et al., 2007; Omi et al., 2008), this study offers novel insight into the *in vivo* phosphorylation-state dependent context in which Ywhaq (SD-specific interactor) and Ywhah (SA-specific interactor) may play a neuroprotective or detrimental role in HD pathogenesis.

ΔN17-specific Htt interactors include Foxp1 and Hspa5

The BACHD-ΔN17 mice reproducibly interact with the Hsp70 family protein (Hspa5) and transcription factor, Forkhead box protein p1 (Foxp1) (Figure 4.7). A previous study suggests Foxp1 plays a neuroprotective effect under normal physiological conditions as a transcriptional repressor against glial activation. However, in the presence of mHtt, Foxp1 is sequestered into mHtt nuclear aggregates in the striatum of R6/1 mice resulting in a loss of repression of immune-related genes (Tang et al., 2012). Furthermore, Hsp70 proteins have shown to have a suppressive effect on mHtt aggregation and toxicity both *in vitro* (Jana et al, 2000; Muchowski et al., 2000) and *in vivo* (Wacker et al., 2009). Considering the propensity of the BACHD-ΔN17 to form nuclear aggregates as the disease progresses, I presume that the mHtt in the young BACHD-ΔN17 sequesters these proteins at an early age, which leads to transcriptional

dysregulation and HD pathogenesis.

4.2.5. Functional Annotation of the N17- and Phosphorylation-State-Dependent Interactome

To gain further biological insight into the Htt N17- and phosphorylation-state-dependent interactome, the proteins that were reproducibly identified in both biological duplicate cortical and striatal WT, BACHD, SD, SA, and BACHD-ΔN17 IP samples (see Supplemental Table 4.5) were subjected to gene ontology (GO) term enrichment (Supplemental Table 4.6) and Ingenuity Pathway Analysis (IPA) (Supplemental Table 4.7). The most overrepresented GO terms and IPA canonical pathways are displayed below in Table 4.1.

Table 4.1. The most significant GO terms and IPA canonical pathways enriched for the reproducible proteins identified in the BACHD, BACHD-ΔN17, SA, SD, and WT IP samples. The GO terms enriched for each biological process (BP), cellular compartment (CC), and molecular function (MF) and IPA canonical pathways with corresponding p-values and protein identifications provided.

IP Sample	P-Value	Gene ID
BACHD		
GO Term Enrichment		
BP: protein polymerization	3.68E-15	TUBB2B, TUBB2A, TUBA3B, TUBB2C, TUBB5, TUBA4A, TUBB6, TUBA1A, TUBA1B, TUBB3, TUBB4
CC: microtubule	6.24E-10	TUBB2B, TUBB2A, TUBA3B, TUBB2C, TUBB5, TUBB6, TUBA4A, DYNC1H1, TUBA1A, TUBA1B, TUBB3, DNM1, DNM2, TUBB4
MF: GTPase activity	5.08E-23	TUFM, EEF1A1, GNAO1, DNM1L, TUBB2B, TUBB2A, TUBA3B, TUBB2C, GNAL, GNB2
		TUBB5, TUBA4A, TUBB6, GNAS, TUBA1A, TUBA1B, TUBB3, DNM1, DNM2, TUBB4
IPA Canonical Pathway		
Gap Junction Signaling	1.26E-12	TUBB3,GNAS,TUBB4B,ACTB,TUBB2A,TUBA4A,TUBB4A,ACTG1,TUBA1B,TUBB2B,TUBA1A,TUBB6,GNAL
Clathrin-mediated Endocytosis Signaling	1.48E-10	HSPA8,DNM1,AP2B1,AP2A1,ACTB,CLTC,AP1B1,DNM1L,AAK1,ACTG1,AP2A2,DNM2
HDΔN17		
GO Term Enrichment		
BP: ATP biosynthetic process	9.10E-11	ATP2B1, ATP1B1, ATP5B, ATP5C1, ATP1A3, ATP6V0A1, ATP1A1, ATP5A1, ATP1A2, ATP6V0D1
CC: microtubule	3.44E-07	TUBB2A, TUBB2C, TUBB5, TUBA4A, TUBB6, DYNC1H1, TUBA1B, TUBB3, DNM1, TUBA1C, TUBB4
MF: GTPase activity	2.57E-17	EEF1A1, GNAO1, DNM1L, TUBB2A, EEF1A2, TUBB2C, GNB2, GNB1, TUBB5, TUBA4A, TUBB6, TUBA1B, TUBB3, DNM1, TUBA1C, TUBB4
IPA Canonical Pathway		
Huntington's Disease Signaling	4.07E-10	GNB1,HSPA8,DNM1,NSF,ATP5B,HSPA1L,HSPA9,CLTC,GNB2,HSPA5,HSPA2,AP2A2
14-3-3-mediated Signaling	8.13E-08	TUBB3,TUBB6,TUBB4B,TUBB2A,TUBA4A,TUBA1C,TUBB4A,TUBA1B
SA		
GO Term Enrichment		
BP: ATP metabolic process	2.11E-13	ATP1B1, ATP5B, ATP1A3, ATP1A1, ATP6V1B2, ATP1A2, ATP6V1C1, ATP2B1, ATP2B2, ATP2B3, ATP2B4, ATP5C1, ATP5A1, NDUFS1
CC: mitochondrial inner membrane	3.05E-09	UQCRC2, TUFM, SLC25A4, SLC25A5, PHB, GLUD1, ATP5B, HADHA, SLC25A12, GOT2, SLC25A22, ATP5C1, SLC25A3, HSPD1, ATP5A1, BDH1, NDUFS1
MF: ribonucleotide binding	1.22E-26	HSP90AB1, SEPT5, SEPT3, TUBB2B, TUBB2A, GNA11, ATP5B, TUBB2C, CCT3, ATP2B1
		ACTG1, ACTG2, HSPH1, ATP2B2, ATP2B3, ATP2B4, AAK1, TUBB5, TUBB6, TUBA1A, SUCLA2, DYNC1H1, TUBA1B,
IPA Canonical Pathway		
14-3-3-mediated Signaling	5.01E-14	TUBB3,YWHAG,YWHAE,YWHAH,TUBB4B,GNA11,TUBB2A,GNAQ,YWHAZ,TUBA4A,TUBB4A,TUBA1B,TUBB2B,TUBA1A,TUBB6
Clathrin-mediated Endocytosis Signaling	3.98E-11	AP2B1,AP2M1,AP2A1,ACTB,CLTC,AP1B1,ACTG1,AP2A2,HSPA8,DNM1,ACTG2,DNM1L,AAK1,PPP3CA,DNM2
SD		
GO Term Enrichment		
BP: protein polymerization	7.04E-12	TUBB2A, TUBB2C, TUBB5, TUBA4A, TUBB6, TUBA1B, TUBB3, TUBA1C, TUBB4
CC: actomyosin	7.65E-07	MYO5A, MYH11, MYH14, MYH9, MYH10
MF: nucleotide binding	3.23E-12	SEPT5, MYO5A, SEPT3, GNAI2, GLUD1, HK1, CCT3, ATP2B1, ATP2B4, CAMK2D
		TUBB6, DYNC1H1, EEF1A2, IDH3B, ACLY, DDX5, MYH9, VDAC1, GNAQ, MYH11, GNAS, MYH14, DNM2, MDH1, MYH10
IPA Canonical Pathway		
Calcium Signaling	2.14E-07	MYH10,CAMK2D,ATP2B1,MYH14,MYH9,MYH11,ATP2B4
14-3-3-mediated Signaling	2.24E-04	YWHAQ,YWHAG,TUBB6,GNAQ
WT		
GO Term Enrichment		
BP: protein polymerization	1.20E-11	TUBB2B, TUBB2A, TUBB2C, TUBB5, TUBA4A, TUBA1A, TUBA1B, TUBB3, TUBB4
CC: mitochondrial inner membrane	2.64E-10	UQCRC2, TUFM, SLC25A4, SLC25A5, ATP5B, SLC25A12, GOT2, SLC25A11, PHB2, SLC25A22, CKMT1, ATP5C1, SLC25A3, ATP5O, ATP5A1
MF: GTPase activity	6.90E-17	TUFM, EEF1A1, GNAO1, TUBB2B, TUBB2A, TUBB2C, GNAL, GNB2, GNB1, TUBB5, TUBA4A, TUBA1A, TUBA1B, TUBB3, DNM1, TUBB4
IPA Canonical Pathway		
14-3-3-mediated Signaling	2.95E-10	TUBB3,TUBA1A,YWHAE,TUBB4B,TUBB2A,YWHAZ,TUBA4A,TUBB4A,TUBA1B,TUBB2B
Huntington's Disease Signaling	1.15E-07	GNB1,HSPA8,DNM1,NSF,ATP5B,HSPA1A/HSPA1B,CLTC,GNB2,HSPA2,AP2A2

Interestingly, the BACHD, SD, and WT mouse models are highly significant for the GO biological process 'protein polymerization', which is composed of alpha and beta tubulin family proteins and may represent a normal function of Htt involved in maintaining the microtubule and cytoskeletal network. However, the SA and BACHD-ΔN17 mice are enriched with energy production signaling pathways such as 'ATP metabolic' and 'ATP biosynthetic' processes, as actin-ATP hydrolysis, actin remodeling, and protein folding processes are a major energy drain for neurons (Bernstein and Bamburg, 2003). The GO cellular compartment term most significantly enriched in BACHD and BACHD-ΔN17 mice are 'microtubule' proteins, whereas the SD samples are enriched with 'actomyosin' complex proteins, which further support the differential roles of mHtt in cytoskeletal organization.

The IPA signaling pathways, either directly or indirectly affected in HD, were compared between the BACHD, SD, SA, and BACHD-ΔN17 genotypes (Figure 4.8). Interestingly, both the SA and BACHD-ΔN17 were significantly enriched for 'HD Signaling' and 'Protein Ubiquitination Pathway' proteins more than the BACHD and SD mouse models. However, both the SD and SA mice were more significantly enriched for 'Calcium Signaling' and 'Actin Cytoskeleton Signaling' proteins to further elicit the function of the N17 domain in cytoskeletal organization as previously elicited in Section 4.2.4.

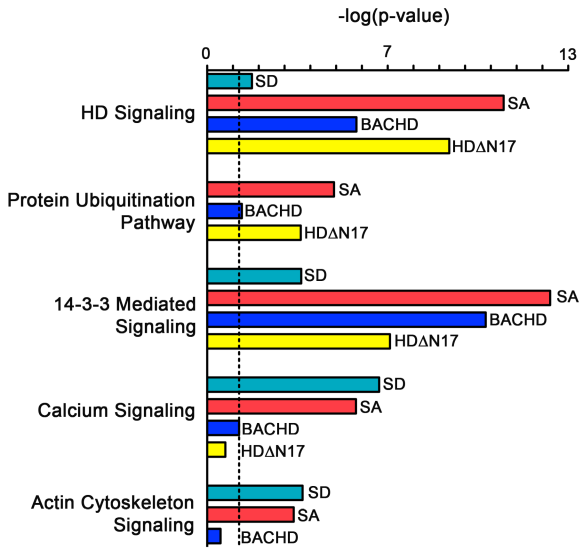


Figure 4.8. IPA canonical pathway comparison of the reproducible proteins identified in the BACHD, BACHD-ΔN17, SA, and SD IP samples. The dashed line indicates p-value significance ($p < 0.05$).

4.2.6. Preliminary Weighted Gene Correlation Network Analysis of the Htt N17- and Phosphorylation-State-Dependent Interactome

To facilitate an unbiased, quantitative analysis of our proteomic dataset and help identify high value molecular targets and protein networks relevant to Htt N17 biology and HD, in collaboration with Dr. Giovanni Coppola (UCLA) we applied Weighted Gene Correlation Network Analysis (WGCNA) to our dataset (Horvath and Dong, 2008; Langfelder and Horvath, 2008). Unlike the network analysis of the fl-Htt interactome described in Chapter 2, this application of WGCNA will potentially reveal Htt N17- and phosphorylation-state-dependent protein interactions and networks to provide insight into the cytoplasmic retention and neuroprotective function of the Htt N17 domain *in vivo*. WGCNA is able to provide two valuable types of information: first, an unbiased ranking of the proteins based on their strength of correlation with Htt across all 20 experimental conditions; and second, distinct protein modules/networks consisting of highly correlated protein-protein interactions.

In our current N17 interactome study, the number of samples we generated (20 distinct IP experimental conditions) represents the lower limit that can be used for WGCNA analyses (suggested minimum is 12 independent conditions). However, we noticed an experimental outlier in one of the 2-month SA striatum anti-Htt IP samples (labeled 2mA1Str). Out of the 887 Htt-interacting proteins identified in this study, the 2mA1Str sample identified 261 protein-protein interactions that were unique only to this IP condition (see Supplemental Table 4.1). This outlier had skewed our initial network results (data not shown) and was therefore removed prior to WGCNA analysis.

We calculated the a pairwise Pearson correlation between the 625 Htt-interacting proteins (dataset not including 2mA1Str sample) and the Htt protein using unique tryptic peptide counts as an entry point (Supplemental Table 4.8). Therefore, if a protein has a high correlation value with Htt, then that protein would demonstrate a similar peptide profile across samples

when compared to Htt. Interestingly, we determined that 52 proteins are significantly correlated to the Htt protein ($p < 0.05$), and the top ten proteins most significantly correlated with Htt include the previously identified Htt-interacting proteins Napb, Dync1h1, and Ywhag (see also Chapter 2; Kaltenbach et al., 2007).

WGCNA identified eight modules of highly correlated proteins in the Htt interactome by hierarchical clustering of the proteins based on their topological overlap using the criterion that a protein had to be identified in at least three IP conditions (Figure 4.9, Supplemental Table 4.9, see Supplemental Figure 4.1). Each module was assigned a color: Black (20 proteins), Blue (54), Brown (18), Green (29), Navy (71), Purple (24), Red (101), and Yellow (15). In WGCNA, all of the 336 proteins were assigned to one module, and proteins that did not clearly belong to a module were colored Grey. The Htt protein was assigned to the Purple Module.

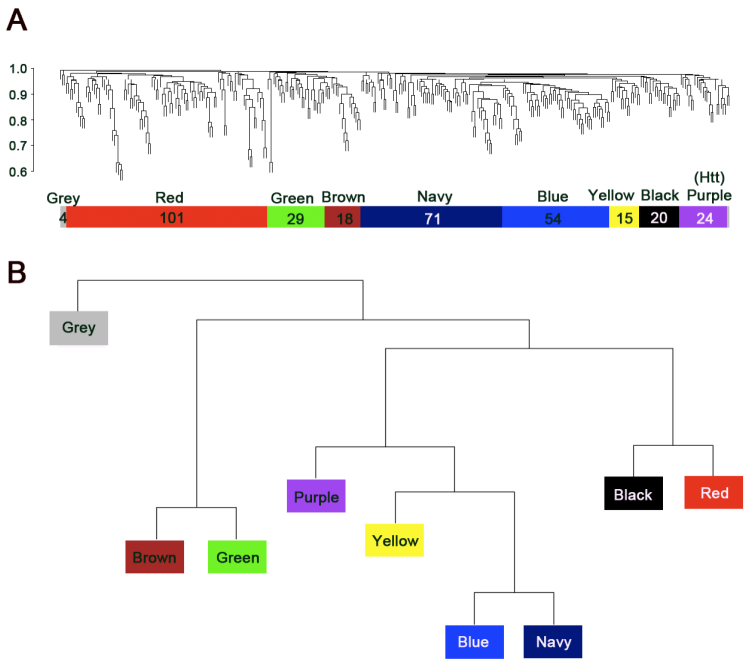


Figure 4.9. Weighted Gene Correlation Network Analysis of the Htt N17- and phosphorylation-state-dependent interactome. (A) Cluster dendrogram generated by hierarchical clustering of proteins on the basis of topological overlap. Modules of correlated proteins were assigned colors and are indicated by the horizontal bar beneath the dengrogram, where all unassigned proteins were placed in the Grey Module. The number in the color modules represents the number of proteins assigned to each module. **(B)** Meta-network organization of the WGCNA module eigenproteins

4.2.7. WGCNA Modules Reveals Distinct Htt N17 Biology

Even though WGCNA assigns proteins to one color module, *in vivo* protein expression data and protein-protein interactions can differ according to tissue, age, or genotype conditions and thus proteins may actually belong or fit into more than one module. Therefore, each module was also defined as single representative peptide correlation profile or the module eigenprotein (MP). A Pearson correlation was then calculated between each of the proteins in the network and each module eigenprotein to yield a module membership value (MM) with an associated p-value (Supplemental Table 4.10). The MM value is a "fuzzy" measure to describe the extent to which a protein conforms to the characteristic peptide correlation profile of a module.

The underlying organization of the modules and their biological relationships (for example, functional, pathway, tissue specific, direct or indirect PPI) must be defined following WGCNA analysis by other independent means. Therefore, we performed gene ontology (GO) term enrichment (Supplemental Table 4.11) and IPA on the individual color modules (Supplemental Table 4.12) of our N17 Htt interactome. To identify age, tissue, or genotype specific organization among the modules, each module and the unique peptide counts across the 19 experimental conditions were graphed as a heat map in which proteins with high peptides counts (red) and low peptide counts (green) are represented (see WGCNA report in Supplemental Figure 4.1).

After the above analyses were performed, three modules in particular (the Htt-containing Purple Module, Brown Module, and Yellow Module) stood out as potential networks of proteins that demonstrate relevance to N17-mediated mHtt biology, whereas the remaining WGCNA modules were enriched with proteins/signaling pathways previously implicated in HD and normal Htt function (Table 4.2, see also Chapter 2).

Table 4.2. A summary of the top IPA canonical pathways for each WGCNA color module.

Module	IPA Canonical Pathway	P-value	Protein IDs
Black	Oxidative Phosphorylation	4.27E-05	NDUFS1, ATP5A1, ATP6V0D1, ATP6V1A
Blue	Glycolysis/Gluconeogenesis	3.98E-11	PKM2, PGK1, DLAT, ALDOA, PFKP, PFKL, PDHB, PFKM, ALDOC
Brown	Actin Cytoskeleton Signaling	1.48E-06	MYH10,MYH14,MYH9,MYH11,ARPC1A
Green	Clathrin-mediated Endocytosis Signaling	4.90E-07	ACTR3, RAB4A, ACTB, ACTG2, AAK1, ACTG1
Navy	G Beta Gamma Signaling	6.17E-09	GNAI3, GNB4, GNAT2, GNA11, PRKACA, GNAQ, GNAZ, GNA13
Purple	Protein Kinase A Signaling	1.35E-06	YWHAG, CAMK2D, CAMK2A, YWHAE, CAMK2B, CAMK2G
Red	14-3-3-mediated Signaling	5.25E-07	TUBB3, TUBA1A, TUBB2C, YWHAB, TUBB2A, TUBA4A, VIM, TUBB4
Yellow	Huntington's Disease Signaling	1.26E-11	HSPA8, DNM1, HSPA1L, HSPA1A, HSPA9, DNM3, HSPA2, DNM2

The Htt-containing Purple Module is overrepresented in the 2-month BACHD and BACHD-ΔN17 mice cortical extracts (Supplemental Figure 4.1) and is significantly enriched in IPA 'Protein Kinase A Signaling' proteins ($p = 1.35 \times 10^{-6}$, Table 4.2). Furthermore, the most significant Purple Module Membership proteins ($p < 0.05$, Supplemental Table 4.10) include the well known Htt-interactors Camk2b, Cct3, Cntn1, Hsp90aa1, and Ywhag. This module overlaps with the fl-Htt Red Module (Chapter 2), and may represent a small network of 24 proteins that are core mHtt-interacting proteins, critical for HD pathogenesis, and putative therapeutic targets for the disease.

The proteins assigned to the Yellow Module are highly overrepresented in the 2-month BACHD-ΔN17 cortical samples and are the most significantly enriched module for IPA 'Huntington's Disease Signaling' ($p = 1.25 \times 10^{-11}$). The top Yellow Module Membership proteins ($p < 0.05$, Supplemental Table 4.10) include many members of the Hsp 70 family (Hspa8, Hsapa9, Hspa2, Hspa1l, Hspa1a, Hspa5, Hspa4l), which were also specifically enriched in the SA-only and BACHD-ΔN17-only IP samples. The Yellow Module contains a network of proteins involved in SA and BACHD-ΔN17 mHtt toxicity, and targeting the molecular chaperones that help fold these aberrant conformations of mHtt may improve HD pathogenesis.

The Brown Module is overrepresented in WT, SD, SA, and BACHD cortical samples, and underrepresented in the BACHD and BACHD-ΔN17 striatal samples (Supplemental Figure 4.1). The Brown Module is highly enriched for 'Actin Cytoskeleton Signaling' ($p = 1.35 \times 10^{-6}$) proteins, which have previously been identified as highly reproducible SD Htt-interacting proteins. Top Brown Module Membership proteins ($p < 0.05$, Supplemental Table 4.10) include

the myosin superfamily proteins (Myh10, Myo5a, Myh9, Myh11, Myo5b, Myh14, Myo5c), spectrins (Spbn1, Spta1, Spnb3, Spna2, Spnb4), debrin (Dbn1), and ankyrin (Ank3). This module represents a network of proteins that elicit the neuroprotective role of Htt Ser13 and Ser16 phosphorylation *in vivo*.

4.3. Discussion

The work presented in this chapter is the culmination of my thesis, as I investigate the role of the Htt N17 domain and its Ser13 and Ser16 phosphorylation modifications in mediating HD pathogenesis *in vivo*. My goal was to identify putative Htt N17- and phosphorylation-state-dependent interactors using the spatiotemporal proteomic approach developed in Chapter 2 on the novel SD, SA, and BACHD-ΔN17 BAC transgenic mouse models of HD described in Chapter 3. This study offers a rich resource of potential therapeutic targets for HD drug discovery.

We demonstrate in Chapter 3, how deletion of the Htt N17 domain *in vivo* leads to accelerated nuclear mHtt aggregation and toxicity and more severe HD pathogenesis. Therefore, my motivation for identifying Htt N17-binding proteins was to find potential cytoplasmic retention targets that will keep mHtt in the cytosol (attached to membranous structures), and out of the nucleus. I used two separate differential proteomic strategies to profile Htt N17-dependent protein-protein interactions using the BACHD and BACHD-ΔN17 mouse models of HD. The proteins that were identified between the two proteomic approaches (Napb, Matr3, Efta, and Atl1) and the validated interactors from the *in vitro* N17-peptide pull-down experiments provided by the Truant Lab at McMaster University (Tuba1a, Ywhaq, and Hspd1), provides an initial subset of proteins to map their specific interaction with the Htt N17 domain, and test their mHtt cytoplasmic retention ability *in vitro*.

Furthermore in Chapter 3, we demonstrate the neuroprotective effect of mimicking Htt phosphorylation at Ser13 and Ser16, and the opposing detrimental effect of inhibiting these sites for potential phosphorylation *in vivo*. Therefore, my goal was to profile phosphorylation-state-specific Htt protein-protein interactions using the SD and SA mouse models of HD in order to identify proteins and signaling pathways that specifically interact with SD, SA, or BACHD-ΔN17 mouse models that can provide mechanistic insight into the function of the N17 domain in modulating mHtt toxicity and HD pathogenesis. By comparing the highly reproducible fl-Htt interactors identified in the BACHD, SD, SA, and BACHD-ΔN17 mice, I determined that the SD-specific interactors are enriched for myosins and actin cytoskeleton organizational proteins, the SA- specific interactors are enriched for WW-domain proteins and molecular chaperones, and the HDΔN17-specific interactors are enriched in HD signaling proteins. Therefore, phosphorylation of Htt Ser13 and Ser16 residues may enhance mHtt's "protective" role in cytoskeletal organization and vesicle anterograde axonal transport, while deletion, dysfunction, or inhibition of Ser13 and Ser16 phosphorylation in this neuroprotective N17 domain may cause abnormal Htt protein folding, and the need for increased association with molecular chaperones and aberrant interactions with polyP WW-domain proteins.

To gain an unbiased network interpretation of the N17- and phosphorylation-state-dependent interactome, we applied Weighted Gene Correlation Network Analysis (WGCNA) to our dataset as previously described in Chapter 2. This application of WGCNA was imperfect, as only 19/20 of our conditions were used for the analysis due to an experimental outlier (2mA1Str sample), and the amount of Htt pulled-down was inconsistent between genotype, brain region, and biological duplicate IP samples. Nonetheless, WGCNA revealed three potentially interesting modules (or highly correlated networks of proteins) relevant to Htt N17 biology: the Htt-containing Purple Module, Yellow Module, and Brown Module. The Purple Module contains the Htt protein and well-known Htt interactors that were also identified in our fl-Htt interactome

presented in Chapter 2 (Camk2b, Cct3, Cntn1, Hsp90aa1, and Ywhag). This small network of 24 double-validated proteins represents critical mHtt interactors necessary for HD pathogenesis, and thus may be putative therapeutic targets for the disease. The Yellow Module is enriched with IPA 'HD Signaling' molecules and many members of the Hsp 70 family. This module overlaps with the SA- and BACHD-ΔN17-specific interacting proteins and provides mechanistic insights into SA and HDΔN17 mHtt toxicity. The Brown Module is heavily enriched for IPA 'Actin Cytoskeleton Signaling' proteins, which have been identified as highly reproducible SD Htt-interacting proteins. This small network of 15 proteins provides insight into the potential neuroprotective role of Htt Ser13 and Ser16 phosphorylation *in vivo*. This study reveals novel N17- and phosphorylation-state-dependent Htt-interacting proteins to further validate as genetic modifiers in a fly model of HD.

4.4. Experimental Methods

Validation of Tcp1/Cct1 and Tuba1a as N17-Dependent Htt Interactors

Soluble cortical lysates were prepared as previously described in Chapter 3 Experimental Methods. Young WT, BACHD, and BACHD-N17 cortical soluble lysates (500-ug each) were subjected to immunoprecipitation with anti-Tcp1/Cct1 (sc-13869, Santa Cruz, 1:50) and anti-α-tubulin (clone DM1A, 05-829, Millipore, 1:500) using Protein G Dynabeads (Invitrogen). Immunoprecipitated proteins (500-ug) were washed, eluted with 4X LDS loading buffer, heated for 10 min at 70°C, and subjected to Western blot analysis. Please refer to Chapter 3 Experimental Methods for SDS-PAGE and Western blotting protocols. A list of the antibodies used in this chapter is shown below.

Antibody	Host/Clonality	Primary	Secondary	Catalog #	Vendor
Tcp1	Goat, polyclonal	1:200	1:3000	sc-13869	Santa Cruz
1C2	Mouse, monoclonal	1:3000	1:3000	MAB1574	Millipore
PW0595	Rabbit, polyclonal	1:5000	1:5000	PW0595	Enzo Life Sciences
α-tubulin	Mouse, monoclonal	1:10,000	1:20,000	T 6074	Sigma
α-tubulin (clone DM1A)	Mouse, monoclonal	1:1000	1:3000	05-829	Millipore

Immunoprecipitation

2-month WT, BACHD, SAA (SA), CH (SD), and BACHD-ΔN17-97Q-N forebrain soluble lysates (2500-ug each) were subjected to immunoprecipitation with either anti-HDB4E10 (MCA2050, AbD Serotec, 1:500) or anti-N17 (PW0595, Enzo Life Sciences, 1:500) using Protein G Dynabeads (Invitrogen), as previously described in Chapter 2. Immunoprecipitated proteins (2500-ug) were washed, eluted with 4X LDS loading buffer, heated for 10 min at 70°C, and subjected to Western blot or SDS-PAGE analysis. Protein samples (2000-ug) were run on NuPAGE 3-8% Tris-Acetate gels (Invitrogen; 2-6 hours, 150 V constant). Gels were dry transferred to PVDF membranes using the iBlot Dry Blotting System (Invitrogen). Blots were blocked in 5% Blotto (Santa Cruz) in 1X PBS/Tween.

In-gel Trypsin Digestion, Mass Spectrometry, PLGS Search Parameters

Please refer to Chapter 3 Experimental Methods section for detailed procedures.

Weighted Gene Correlation Network Analysis of Htt N17- and Phosphorylation-State-Dependent Interactome

Proteins with unique tryptic peptides identified in 3 independent IP conditions were used for WGCNA, and the 2mA1Str IP sample was removed prior to WGCNA. Please see Chapter 2 Experimental Methods section for complete procedures.

CHAPTER 5

Conclusions and Future Directions

5.1. Overview

My work presented in this thesis strives to better understand the function of full-length mHtt in disease, and determine how its N17 domain and modifications mediate protein-protein interactions, toxicity, aggregation, and HD pathogenesis *in vivo*. In Chapter 2, we applied a novel spatiotemporal proteomic and network biology approach (WGCNA) to profile endogenous fl-Htt-interacting proteins from WT and BACHD mouse brains. This study revealed a verifiable rank of Htt-correlated proteins and a robust network of Htt-interacting protein modules. In Chapter 3, I present the work done in collaboration with Dr. Xiaofeng Gu in the Yang laboratory in which we investigate the role of the Htt N17 domain as a neuroprotective molecular switch and cytoplasmic retention signal *in vivo*. In the first part of Chapter 3, we demonstrate that mimicking Htt Ser13 and Ser16 phosphorylation in the context of fl-mHtt is neuroprotective (SD mice), while preventing these phosphorylation sites leads to fl-mHtt induced HD pathogenesis *in vivo* (SA mice) (Gu et al., 2009). In the second part of Chapter 3, we show that the Htt N17 domain is a cytoplasmic retention signal *in vivo*, as deletion of Htt aa 2-16 (BACHD-ΔN17 mice) leads to dramatic nuclear accumulation, increased mHtt aggregation and toxicity of a small N-terminal mHtt fragment. Finally in Chapter 4, I integrate the techniques and mouse models presented in the previous chapters to further investigate the function of the Htt N17 by performing differential proteomics on the WT, BACHD, SD, SA, and BACHD-ΔN17 mouse models of HD to determine N17- and phosphorylation-state-dependent mHtt protein interactions. This study revealed a new possible role for N17 phosphorylation in regulating actin

cytoskeleton organization and remodeling, and provided insight into why the phosphoresistant and ΔN17 form of mHtt leads to increased toxicity *in vivo*.

5.2. WGCNA of Fl-Htt Interactome Reveals New Htt Biology and Genetic Modifiers of HD

In Chapter 2, we used a spatiotemporal affinity-purification followed by mass spectrometry approach to obtain the first compendium of 747 *in vivo* full-length Htt-interacting proteins in the WT and BACHD mammalian brains. Furthermore, we applied for the first time to a proteomic dataset, Weighted Gene Correlation Network Analysis (WGCNA) to construct *in vivo* protein interaction networks. WGCNA identified six significant Htt-correlated modules with brain region- or age-specific overrepresentation that reveal distinct aspects of Htt biology. One module in particular, the Htt-containing Red Module, is significantly enriched with HD signaling proteins, is the most significantly correlated with the Htt protein across samples, and contains many well-known Htt interactors and genetic modifiers of HD. We were able to validate 6 Red Module proteins as novel *in vivo* Htt interactors by co-IP, and 12 as novel genetic modifiers of Htt toxicity in a fly model of HD.

This study is a rich resource not only to the HD field, as it provides a spatiotemporal view of the fl-Htt interactome in mammalian brain, an unbiased ranking of proteins for future pharmacological drug testing, and generates tightly correlated protein networks that define specific aspects of Htt biology, but this powerful application of systems biology to proteomics can be readily applied to other complex diseases. Future HD studies using this type of approach may include: 1) A comparison of fl-Htt interactors from different cellular compartments (*i.e.,* mitochondria, nucleus, post-synaptic density, etc.) of WT and BACHD mice to further investigate the subcellular function of mHtt during disease progression, 2) A comparison fl-Htt interactors from the knock-in *Hdh* allelic series mouse models to better understand the role of polyQ-dependent interactors during disease, and 3) A comparison of fl-Htt interactors following

enrichment for post-translational modifications such as phosphorylation or ubiquitination in WT and BACHD mouse brains to elucidate possible neuroprotective or pathological signaling cascades.

5.3. Phosphorylation at Htt Ser13 and Ser16 Acts as a Neuroprotective Molecular Switch *In Vivo*

Many studies have shown that the first 17 aa of Htt is a critical domain in modulating mHtt toxicity, aggregation, PTMs, and subcellular localization (Greiner and Yang, 2011). While Htt Ser13 and Ser16 are phosphorylated *in vitro*, the effect of these modifications on fl-mHtt induced toxicity *in vivo* remained unclear. In the first part of Chapter 3, we demonstrate that mimicking phosphorylation of Htt at Ser13 and Ser16 in the SD fl-mHtt mouse model of HD abolishes mHtt aggregation and HD-like phenotypes *in vivo*, whereas the phosphoresistant control (SA mice) have a similar mHtt aggregation pattern, pathology, and HD behavior phenotype to the BACHD fl-mHtt mouse model (Gu et al., 2009). While a few studies have attempted to validate the IKKβ kinase (Thompson et al., 2009), casein kinase-2 (CK2) inhibitors (Atwal et al., 2011), and the ganglioside GM1 (Di Pardo et al., 2012) as potential molecular targets for Ser13 and Ser16 phosphorylation, further *in vivo* testing in a full-length mouse model of HD is required.

5.4. The Htt N17 Domain Acts as a Cytoplasmic Retention Signal *In Vivo*

Previous *in vitro* studies suggest that the N17 domain is an essential cytoplasmic localization signal that prevents the nuclear translocation, aggregation, and toxicity of a small N-terminal mHtt fragment (Atwal et al., 2007; Cornett et al., 2005; Rockabrand et al., 2007). However, whether the Htt N17 domain acts as a cytoplasmic retention signal in the context of fl-mHtt in the mammalian brain, and the significance of such function has yet to be determined. In

the second part of Chapter 3, we demonstrate that deletion Htt aa 2-16 in the fl-mHtt-97Q BAC transgenic mouse model of HD (BACHD-ΔN17) results in accelerated nuclear accumulation of a N-terminal mHtt fragment (55 to 71 kDa) which leads to severe HD-like phenotype. I determined that the BACHD-ΔN17 mice accumulate a nuclear mHtt high molecular weight (HMW) species as the disease progresses that is recognized by only N-terminal, but not C-terminal antibodies, and is solubilized into a 55 to 71 kDa fragment after treatment with 100% formic acid.

I used mass spectrometry and proteomic approaches to identify the proteins that associate with the mHtt HMW species, identify novel mHtt post-translational modifications, and map the specific size of the N-terminal mHtt fragment in hope of gaining insight into the mechanism behind BACHD-ΔN17 HD pathogenesis. The results generated were very preliminary, but suggest BACHD-ΔN17 mHtt sequesters Hsp70 family proteins (Hspa1l, Hspa2, Hspa5, Hspa8) in the solubilized BACHD-ΔN17 nuclear fraction, and may deplete these essential molecular chaperones from the cellular pool. Further co-localization and Western blot validation experiments are required to verify if these proteins are indeed associated with the mHtt HMW species *in vivo*. Additional studies on the BACHD-ΔN17 mice include enrichment of mHtt post-translational modifications, mapping the fragment size of N-terminal mHtt using cell culture transfection experiments using various N-terminal mHtt-97Q construct sizes and Western blot analysis with N-terminal Htt antibodies.

While investigation of the BACHD-ΔN17 mice may offer potentially interesting new biology into the role of a small N-terminal mHtt fragment-induced nuclear toxicity, in order to truly understand the role of the N17 domain in modulating HD pathogenesis, it is important to ask whether there is an N17-dependent mechanism by which fl-mHtt in HD human patients accumulates in the nucleus during disease? We hypothesize that either the function of the N17 domain is compromised by aberrant protein-protein interactions or PTMs, or the domain may be cleaved by an N-terminal aminopeptidase. Future studies to test these ideas include nuclear

fractionation of human HD and control tissue, identification of mHtt HMW species by Western blot, followed by mass spectrometry analysis to probe for protein interactions, PTMs, and proteomic strategies to enrich for sequencing the N-terminus of fl-mHtt.

5.5. Htt N17- and Phosphorylation-State-Dependent Interactors Reveal New Htt N17 Biology and Disease Implications

In Chapter 4, I applied the spatiotemporal proteomic and network strategy presented in Chapter 2 to profile fl-mHtt interactions in the SA, SD, and BACHD-ΔN17 mouse models of HD described in Chapter 3. My goal was to identify Htt N17- and phosphorylation-state-dependent interactions to better understand the function of the N17 domain *in vivo*. I hypothesize that these putative interactors may mediate the cytoplasmic retention of mHtt and/or Ser13 and Ser16 phosphorylation.

I used two separate differential proteomic strategies to profile Htt N17-dependent protein-protein interactions using the BACHD and BACHD-ΔN17 mouse models of HD to identify seven double-validated cytoplasmic, membrane, or mitochondrial proteins (Napb, Matr3, Efta, Atl1, Tuba1a, Ywhaq, and Hspd1) that may regulate the cytoplasmic retention of mHtt *in vivo*. Future validation studies include: 1) Validating the N17 candidate interactors using mHtt fragments, 2) Reducing the expression of the putative interactors in cell models to trigger N17-dependent nuclear translocation, aggregation, and toxicity, 3) Overexpressing the putative interactors in cell models to induce N17-dependent suppression of nuclear translocation, aggregation, and toxicity, and 4) Testing whether overexpression of a confirmed N17-depedent interactor can suppress mHtt-induced nuclear toxicity in R6/2 mice.

Furthermore, I profiled the fl-mHtt interactions in the SD, SA, and BACHD-ΔN17 mouse models of HD and performed WGCNA network analysis to identify proteins and signaling pathways that specifically associate with the phosphomimetic SD form of fl-mHtt, the

phosphoresistant SA form of fl-mHtt, or the ΔN17 form of mHtt to unravel mechanistic insight into the function of the N17 domain in modulating mHtt toxicity and HD pathogenesis. I highlight the interesting findings from this study below in Figure 5.1

I determined that SD-specific interactors and proteins assigned to the Brown Module are highly enriched for myosin and actin cytoskeleton organizational proteins. This module suggests the potential neuroprotective role of Htt Ser13 and Ser16 phosphorylation *in vivo* involves cytoskeletal organization. However, the SA- and BACHD-ΔN17-specific interactors and proteins assigned to the Yellow Module reveal proteins involved in HD pathogenesis and members of the Hsp 70 family. This data implies that if the Htt N17 domain is compromised or the sites for Htt Ser13 or Ser16 are blocked for phosphorylation (*i.e.,* interaction with polyP WW-domain proteins), then mHtt is more likely to misfold, translocate into the nucleus, and form toxic mHtt nuclear inclusions. Lastly, proteins associated with the BACHD and BACHD-ΔN17 mice and the Purple Module include the Htt protein, as well as previously identified Htt interactors from our fl-Htt interactome presented in Chapter 2 (Camk2b, Cct3, Cntn1, Hsp90aa1, and Ywhag). These critical mHtt interactors represent a short list of putative therapeutic targets for the disease, and should be further tested for their genetic modifier effects *in vivo*.

A few experimental factors affected the outcome and interpretation of this differential proteomic study, and should be considered for future fl-Htt interactome studies. First, the amount of fl-mHtt pulled pulled-down was too variable between the different genotype comparisons, considering the BACHD, SD, SA, and BACHD-ΔN17 mice have different fl-mHtt expression levels. It would have been easier to compare the interactors across the twenty IP conditions if the fl-mHtt levels were first normalized prior to IP. Second, in pulling-down fl-mHtt using the C-terminal Htt antibody HDB4E10, we assume that each of the native BACHD, SD, SA, and BACHD-ΔN17 fl-mHtt conformations are the same and for IP, and this may not be correct since the N17 mutations could affect fl-mHtt structure. Third, an additional biological

sample (n=3 total) for each IP should be performed to increase sample reproducibility and data confidence.

5.6. Concluding Remarks

The goal of this dissertation was to investigate the role of the Htt N17 domain and its modifications in modulating mHtt protein-protein interactions, aggregation, and toxicity *in vivo*. This study is a valuable resource to the HD community, as it provides insight into the biological function of Htt and its N17 domain in the brain and identifies novel molecular targets critical to HD pathogenesis and therapy. We demonstrate the application of a powerful, yet simple proteomic and systems biology approach to profile endogenous interactors that can help elucidate complex biological processes in the mammalian brain.

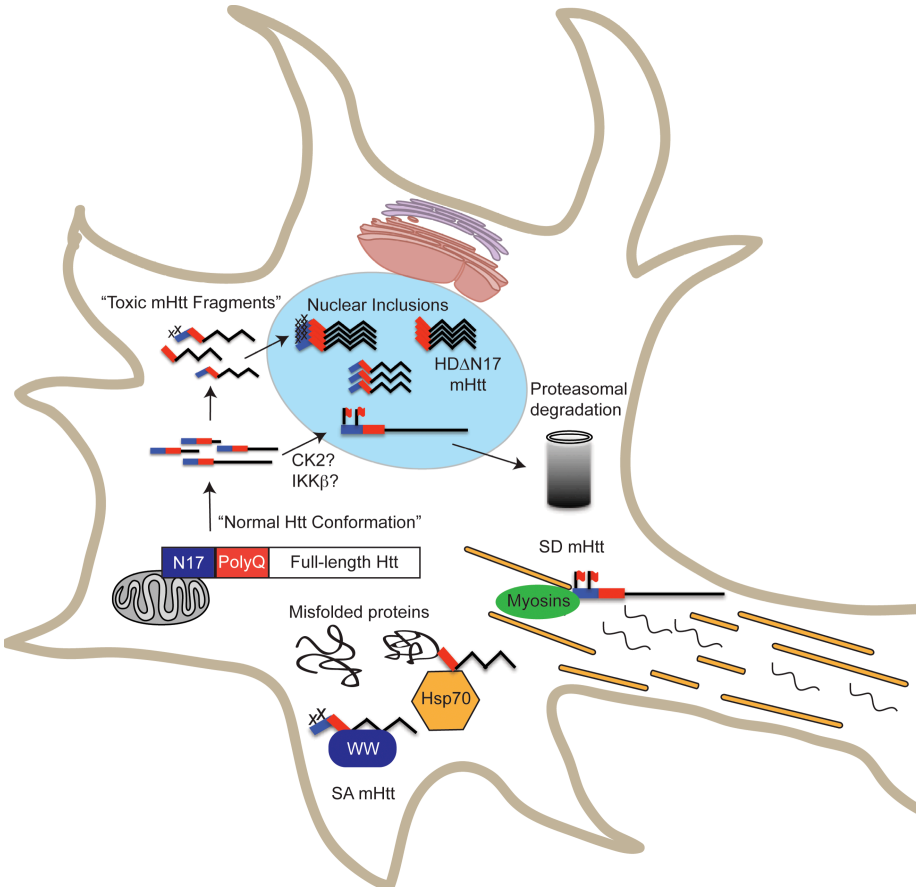


Figure 5.1. A schematic diagram illustrating the putative neuroprotective or toxic roles of the Htt N17 domain in HD pathogenesis. Full-length mutant Htt normally associates with membranous structures in the cytosol via the N17 domain. During disease, mutant Htt is cleaved into smaller N-terminal mHtt fragments by caspases and calpains that are able to accumulate in the nucleus as nuclear inclusions. However, upon Ser13 and Ser16 phosphorylation, the mHtt is able to easily degrade by the degradation machinery and renders mHtt non-toxic, whereas the ΔN17 and SA form of the mHtt readily aggregate in the nucleus. The work from this thesis suggests the SD form of mHtt plays a role in cytoskeletal organization, whereas the SA form of mHtt interacts with WW-domain proteins, and the ΔN17 form of mHtt interacts with the Hsp 70 protein folding machinery and HD Signaling molecules.

REFERENCES

Aiken, C., Steffan, J., Guerrero, C., Khashwji, H., Lukacsovich, T., Simmons, D., Purcell, J., et al. (2009b). Phosphorylation of threonine 3: implications for Huntingtin aggregation and neurotoxicity. *J Biol Chem*, *284*(43).

Allen, J. D., Xie, Y., Chen, M., Girard, L., & Xiao, G. (2012). Comparing statistical methods for constructing large scale gene networks. *PLoS ONE*, *7*(1), e29348.

Andrade, M. A., & Bork, P. (1995). HEAT repeats in the Huntington's disease protein. *Nat Genet*, *11*(2), 115–116.

Angeli, S., Shao, J., & Diamond, M. I. (2010). F-actin binding regions on the androgen receptor and huntingtin increase aggregation and alter aggregate characteristics. *PLoS ONE*, *5*(2), e9053.

Anne, S. L., Saudou, F., & Humbert, S. (2007). Phosphorylation of huntingtin by cyclin-dependent kinase 5 is induced by DNA damage and regulates wild-type and mutant huntingtin toxicity in neurons. *J Neurosci*, *27*(27), 7318–7328.

Attar, N., & Cullen, P. J. (2010). The retromer complex. *Advances in enzyme regulation*, *50*(1), 216–236.

Atwal, R. S., Desmond, C. R., Caron, N., Maiuri, T., Xia, J., Sipione, S., & Truant, R. (2011). Kinase inhibitors modulate huntingtin cell localization and toxicity. *Nat Chem Biol*, *7*(7), 453–460.

Atwal, R. S., Xia, J., Pinchev, D., Taylor, J., Epand, R. M., & Truant, R. (2007). Huntingtin has a membrane association signal that can modulate huntingtin aggregation, nuclear entry and toxicity. *Hum Mol Genet*, *16*(21), 2600–2615.

Balch, W. E., Morimoto, R. I., Dillin, A., & Kelly, J. W. (2008). Adapting proteostasis for disease intervention. *Science*, *319*(5865), 916–919.

Bates, G., & Harper, P. (2002). *Huntington's disease*.

Benn, C. L., Landles, C., Li, H., Strand, A. D., Woodman, B., Sathasivam, K., Li, S. H., et al. (2005). Contribution of nuclear and extranuclear polyQ to neurological phenotypes in mouse models of Huntington's disease. *Hum Mol Genet*, *14*(20), 3065–3078.

Bernstein, B. W., & Bamburg, J. R. (2003). Actin-ATP hydrolysis is a major energy drain for neurons. *J Neurosci*, *23*(1), 1–6.

Browne, S. E., Ferrante, R. J., & Beal, M. F. (1999). Oxidative stress in Huntington's disease. *Brain Pathol*, *9*(1), 147–163.

Caviston, J. P., & Holzbaur, E. L. F. (2009). Huntingtin as an essential integrator of intracellular vesicular trafficking. *Trends Cell Biol*, *19*(4), 147–155.

Caviston, J. P., Ross, J. L., Antony, S. M., Tokito, M., & Holzbaur, E. L. F. (2007). Huntingtin facilitates dynein/dynactin-mediated vesicle transport. *Proc Natl Acad Sci U S A*, *104*(24), 10045–10050.

Chan, H. Y., Warrick, J. M., Gray-Board, G. L., Paulson, H. L., & Bonini, N. M. (2000). Mechanisms of chaperone suppression of polyglutamine disease: selectivity, synergy and modulation of protein solubility in Drosophila. *Hum Mol Genet*, *9*(19), 2811–2820.

Chen, H. K., Fernandez-Funez, P., Acevedo, S. F., Lam, Y. C., Kaytor, M. D., Fernandez, M. H., Aitken, A., et al. (2003). Interaction of Akt-phosphorylated ataxin-1 with 14-3-3 mediates neurodegeneration in spinocerebellar ataxia type 1. *Cell*, *113*(4), 457–468.

Choo, Y. S., Johnson, G. V., MacDonald, M., Detloff, P. J., & Lesort, M. (2004). Mutant huntingtin directly increases susceptibility of mitochondria to the calcium-induced permeability transition and cytochrome c release. *Hum Mol Genet*, *13*(14), 1407–1420.

Colin, E., Zala, D., Liot, G., Rangone, H., Borrell-Pagès, M., Li, X.-J., Saudou, F., et al. (2008). Huntingtin phosphorylation acts as a molecular switch for anterograde/retrograde transport in neurons. *EMBO J*, *27*(15), 2124–2134.

Cong, X., Held, J. M., DeGiacomo, F., Bonner, A., Chen, J. M., Schilling, B., Czerwieniec, G. A., et al. (2011). Mass spectrometric identification of novel lysine acetylation sites in huntingtin. *Mol Cell Proteomics*, *10*(10), M111.009829.

Cornett, J., Cao, F., Wang, C. E., Ross, C. A., Bates, G. P., Li, S. H., & Li, X. J. (2005). Polyglutamine expansion of huntingtin impairs its nuclear export. *Nat Genet*, *37*(2), 198–204.

Davies, S. W., Turmaine, M., Cozens, B. A., Difiglia, M., Sharp, A. H., Ross, C. A., Scherzinger, E., et al. (1997). Formation of neuronal intranuclear inclusions underlies the neurological dysfunction in mice transgenic for the HD mutation. *Cell*, *90*(3), 537–548.

Di Pardo, A., Maglione, V., Alpaugh, M., Horkey, M., Atwal, R. S., Sassone, J., Ciammola, A., et al. (2012). Ganglioside GM1 induces phosphorylation of mutant huntingtin and restores normal motor behavior in Huntington disease mice. *Proc Natl Acad Sci U S A*, *109*(9), 3528–3533.

Difiglia, M., Sapp, E., Chase, K. O., Davies, S. W., Bates, G. P., Vonsattel, J. P., & Aronin, N. (1997). Aggregation of huntingtin in neuronal intranuclear inclusions and dystrophic neurites in brain. *Science*, *277*(5334), 1990–1993.

Doi, H., Mitsui, K., Kurosawa, M., Machida, Y., Kuroiwa, Y., & Nukina, N. (2004). Identification of ubiquitin-interacting proteins in purified polyglutamine aggregates. *FEBS Lett*, *571*(1-3), 171–176.

Doi, H., Okamura, K., Bauer, P. O., Furukawa, Y., Shimizu, H., Kurosawa, M., Machida, Y., et al. (2008). RNA-binding protein TLS is a major nuclear aggregate-interacting protein in huntingtin exon 1 with expanded polyglutamine-expressing cells. *J Biol Chem*, *283*(10), 6489–6500.

Dorsey, R. E., & Shoulson, I. (2012). *Neurobiology of Huntington's Disease: Applications to Drug Discovery*. (D. C. Lo & R. E. Hughes, Eds.)Chapter 12 Huntington's Disease: Clinical Experimental Therapeutics. Boca Raton, FL: CRC Press.

Dragatsis, I., Levine, M., & Zeitlin, S. (2000). Inactivation of Hdh in the brain and testis results in progressive neurodegeneration and sterility in mice. *Nature Genetics*, *26*(3), 300–306.

Emamian, E., Kaytor, M., Duvick, L., Zu, T., Tousey, S., Zoghbi, H., Clark, H., et al. (2003). Serine 776 of ataxin-1 is critical for polyglutamine-induced disease in SCA1 transgenic mice. *Neuron*, *38*(3), 375–387.

Faber, P. W., Barnes, G. T., Srinidhi, J., Chen, J., Gusella, J. F., & MacDonald, M. E. (1998). Huntingtin interacts with a family of WW domain proteins. *Hum Mol Genet*, *7*(9), 1463–1474.

Fan, J., Cowan, C. M., Zhang, L. Y. J., Hayden, M. R., & Raymond, L. A. (2009). Interaction of postsynaptic density protein-95 with NMDA receptors influences excitotoxicity in the yeast artificial chromosome mouse model of Huntington's disease. *J Neurosci*, *29*(35), 10928–10938.

Fernández, E., Collins, M. O., Uren, R. T., Kopanitsa, M. V., Komiyama, N. H., Croning, M. D. R., Zografos, L., et al. (2009). Targeted tandem affinity purification of PSD-95 recovers core postsynaptic complexes and schizophrenia susceptibility proteins. *Molecular systems biology*, *5*, 269.

Gafni, J., Hermel, E., Young, J. E., Wellington, C. L., Hayden, M. R., & Ellerby, L. M. (2004). Inhibition of calpain cleavage of huntingtin reduces toxicity: accumulation of calpain/caspase fragments in the nucleus. *J Biol Chem*, *279*(19), 20211–20220.

Gauthier, L. R., Charrin, B. C., Borrell-Pagès, M., Dompierre, J. P., Rangone, H., Cordelières, F. P., De Mey, J., et al. (2004). Huntingtin controls neurotrophic support and survival of neurons by enhancing BDNF vesicular transport along microtubules. *Cell*, *118*(1), 127–138.

Geromanos, S. J., Vissers, J. P., Silva, J. C., Dorschel, C. A. et al. (2009). The detection, correlation, and comparison of peptide precursor and product ions from data independent LC-MS with data dependent LC-MS/MS. *Proteomics*, *9*(6)*,* 1683-1695.

Godin, J. D., Poizat, G., Hickey, M. A., Maschat, F., & Humbert, S. (2010). Mutant huntingtin-impaired degradation of beta-catenin causes neurotoxicity in Huntington's disease. *EMBO J*, *29*(14), 2433–2445.

Goehler, H., Lalowski, M., Stelzl, U., Waelter, S., Stroedicke, M., Worm, U., Droege, A., et al. (2004). A protein interaction network links GIT1, an enhancer of huntingtin aggregation, to Huntington's disease. *Mol Cell*, *15*(6), 853–865.

Graham, R. K., Deng, Y., Slow, E. J., Haigh, B., Bissada, N., Lu, G., Pearson, J., et al. (2006). Cleavage at the caspase-6 site is required for neuronal dysfunction and degeneration due to mutant huntingtin. *Cell*, *125*(6), 1179–1191.

Gray, M., Shirasaki, D. I., Cepeda, C., Andre, V. M., Wilburn, B., Lu, X. H., Tao, J., et al. (2008). Full-length human mutant huntingtin with a stable polyglutamine repeat can elicit progressive and selective neuropathogenesis in BACHD mice. *J Neurosci*, *28*(24), 6182–6195.

Greiner, E. R., & Yang, X. W. (2011). Huntington's disease: flipping a switch on huntingtin. *Nat Chem Biol*, *7*(7), 412–414.

Gu, X., Greiner, E., Mishra, R., Kodali, R., Osmand, A., Finkbeiner, S., Steffan, J., et al. (2009). Serines 13 and 16 are critical determinants of full-length human mutant huntingtin induced disease pathogenesis in HD mice. *Neuron*, *64*(6), 824–840.
Gutekunst, C. A., Li, S. H., Yi, H., Mulroy, J. S., Kuemmerle, S., Jones, R., Rye, D., et al. (1999). Nuclear and neuropil aggregates in Huntington's disease: relationship to neuropathology. *J Neurosci*, *19*(7), 2522–2534.
Harjes, P., & Wanker, E. E. (2003). The hunt for huntingtin function: interaction partners tell many different stories. *Trends Biochem Sci*, *28*(8), 425–433.
Hazeki, N., Tukamoto, T., Goto, J., & Kanazawa, I. (2000). Formic acid dissolves aggregates of an N-terminal huntingtin fragment containing an expanded polyglutamine tract: applying to quantification of protein components of the aggregates. *Biochem Biophys Res Commun*, *277*(2), 386–393.
Herbst, M., & Wanker, E. E. (2007). Small molecule inducers of heat-shock response reduce polyQ-mediated huntingtin aggregation. A possible therapeutic strategy. *Neurodegener Dis*, *4*(2-3), 254–260.
Hersch, S. M., Gevorkian, S., Marder, K., Moskowitz, C., Feigin, A., Cox, M., Como, P., et al. (2006). Creatine in Huntington disease is safe, tolerable, bioavailable in brain and reduces serum 8OH2'dG. *Neurology*, *66*(2), 250–252.
Hodgson, J. G., Agopyan, N., Gutekunst, C. A., Leavitt, B. R., LePiane, F., Singaraja, R., Smith, D. J., et al. (1999). A YAC mouse model for Huntington's disease with full-length mutant huntingtin, cytoplasmic toxicity, and selective striatal neurodegeneration. *Neuron*, *23*(1), 181–192.
Hoffner, G., Island, M. L., & Djian, P. (2005). Purification of neuronal inclusions of patients with Huntington's disease reveals a broad range of N-terminal fragments of expanded huntingtin and insoluble polymers. *J Neurochem*, *95*(1), 125–136.
Hoffner, G., Kahlem, P., & Djian, P. (2002). Perinuclear localization of huntingtin as a consequence of its binding to microtubules through an interaction with beta-tubulin: relevance to Huntington's disease. *J Cell Sci*, *115*(Pt 5), 941–948.
Holbert, S., Dedeoglu, A., Humbert, S., Saudou, F., Ferrante, R. J., & Neri, C. (2003). Cdc42-interacting protein 4 binds to huntingtin: neuropathologic and biological evidence for a role in Huntington's disease. *Proc Natl Acad Sci U S A*, *100*(5), 2712–2717.
Horvath, S., & Dong, J. (2008). Geometric interpretation of gene coexpression network analysis. *PLoS computational biology*, *4*(8), e1000117.
Huang, K., Yanai, A., Kang, R., Arstikaitis, P., Singaraja, R. R., Metzler, M., Mullard, A., et al. (2004). Huntingtin-interacting protein HIP14 is a palmitoyl transferase involved in palmitoylation and trafficking of multiple neuronal proteins. *Neuron*, *44*(6), 977–986.
Humbert, S., Bryson, E. A., Cordelieres, F. P., Connors, N. C., Datta, S. R., Finkbeiner, S., Greenberg, M. E., et al. (2002). The IGF-1/Akt pathway is neuroprotective in Huntington's disease and involves Huntingtin phosphorylation by Akt. *Dev Cell*, *2*(6), 831–837.
Husi, H., Ward, M. A., Choudhary, J. S., Blackstock, W. P., & Grant, S. G. (2000). Proteomic analysis of NMDA receptor-adhesion protein signaling complexes. *Nat Neurosci*, *3*(7), 661–669.
Jana, N. R., Tanaka, M., Wang, G., & Nukina, N. (2000). Polyglutamine length-dependent interaction of Hsp40 and Hsp70 family chaperones with truncated N-terminal huntingtin: their role in suppression of aggregation and cellular toxicity. *Hum Mol Genet*, *9*(13), 2009–2018.
Jeong, H., Then, F., Melia, T. J., Mazzulli, J. R., Cui, L., Savas, J. N., Voisine, C., et al. (2009). Acetylation targets mutant huntingtin to autophagosomes for degradation. *Cell*, *137*(1), 60–72.
Kalchman, M. A., Graham, R. K., Xia, G., Koide, H. B., Hodgson, J. G., Graham, K. C., Goldberg, Y. P., et al. (1996). Huntingtin is ubiquitinated and interacts with a specific ubiquitin-conjugating enzyme. *J Biol Chem*, *271*(32), 19385–19394.
Kaltenbach, L. S., Romero, E., Becklin, R. R., Chettier, R., Bell, R., Phansalkar, A., Strand, A., et al. (2007). Huntingtin interacting proteins are genetic modifiers of neurodegeneration. *PLoS Genet*, *3*(5), e82.
Kim, Y. J., Sapp, E., Cuiffo, B. G., Sobin, L., Yoder, J., Kegel, K. B., Qin, Z. H., et al. (2006). Lysosomal proteases are involved in generation of N-terminal huntingtin fragments. *Neurobiol Dis*, *22*(2), 346–356.

Kim, Y. J., Yi, Y., Sapp, E., Wang, Y., Cuiffo, B., Kegel, K. B., Qin, Z. H., et al. (2001). Caspase 3-cleaved N-terminal fragments of wild-type and mutant huntingtin are present in normal and Huntington's disease brains, associate with membranes, and undergo calpain-dependent proteolysis. *Proc Natl Acad Sci U S A*, *98*(22), 12784–12789.

Kleiman, R. J., Kimmel, L. H., Bove, S. E., Lanz, T. A., Harms, J. F., Romegialli, A., Miller, K. S., et al. (2011). Chronic suppression of phosphodiesterase 10A alters striatal expression of genes responsible for neurotransmitter synthesis, neurotransmission, and signaling pathways implicated in Huntington's disease. *J Pharmacol Exp Ther*, *336*(1), 64–76.

Klement, I. A., Skinner, P. J., Kaytor, M. D., Yi, H., Hersch, S. M., Clark, H. B., Zoghbi, H. Y., et al. (1998). Ataxin-1 nuclear localization and aggregation: role in polyglutamine-induced disease in SCA1 transgenic mice. *Cell*, *95*(1), 41–53.

Krüger, M., Moser, M., Ussar, S., Thievessen, I., Luber, C. A., Forner, F., Schmidt, S., et al. (2008). SILAC mouse for quantitative proteomics uncovers kindlin-3 as an essential factor for red blood cell function. *Cell*, *134*(2), 353–364.

Kuemmerle, S., Gutekunst, C. A., Klein, A. M., Li, X. J., Li, S. H., Beal, M. F., Hersch, S. M., et al. (1999). Huntington aggregates may not predict neuronal death in Huntington's disease. *Ann Neurol*, *46*(6), 842–849.

Landles, C., Sathasivam, K., Weiss, A., Woodman, B., Moffitt, H., Finkbeiner, S., Sun, B., et al. (2010). Proteolysis of mutant huntingtin produces an exon 1 fragment that accumulates as an aggregated protein in neuronal nuclei in Huntington disease. *J Biol Chem*, *285*(12), 8808–8823.

Langfelder, P., & Horvath, S. (2008). WGCNA: an R package for weighted correlation network analysis. *BMC Bioinformatics*, *9*, 559.

Langfelder, P., Zhang, B., & Horvath, S. (2008). Defining clusters from a hierarchical cluster tree: the Dynamic Tree Cut package for R. *Bioinformatics*, *24*(5), 719–720.

Lecerf, J. M., Shirley, T. L., Zhu, Q., Kazantsev, A., Amersdorfer, P., Housman, D. E., Messer, A. et al. (2001). Human single-chain Fv intrabodies counteract in situ huntingtin aggregation in cellular models of Huntington's disease. *Proc Natl Acad Sci U S A*, *98*(8), 4764–4769.

Li, M., Huang, Y., Ma, A. A. K., Lin, E., & Diamond, M. I. (2009). Y-27632 improves rotarod performance and reduces huntingtin levels in R6/2 mice. *Neurobiol Dis*, *36*(3), 413–420.

Li, S., & Li, X.-J. (2006). Multiple pathways contribute to the pathogenesis of Huntington disease. *Molecular neurodegeneration*, *1*, 19.

Liao, L., McClatchy, D. B., & Yates, J. R. (2009). Shotgun proteomics in neuroscience. *Neuron*, *63*(1), 12–26.

Lim, J., Crespo-Barreto, J., Jafar-Nejad, P., Bowman, A. B., Richman, R., Hill, D. E., Orr, H. T., et al. (2008). Opposing effects of polyglutamine expansion on native protein complexes contribute to SCA1. *Nature*, *452*(7188), 713–718.

Lim, J., Hao, T., Shaw, C., Patel, A. J., Szabó, G., Rual, J.-F., Fisk, C. J., et al. (2006). A protein-protein interaction network for human inherited ataxias and disorders of Purkinje cell degeneration. *Cell*, *125*(4), 801–814.

Linding, R., Jensen, L. J., Ostheimer, G. J., van Vugt, M. A. T. M., Jørgensen, C., Miron, I. M., Diella, F., et al. (2007). Systematic discovery of in vivo phosphorylation networks. *Cell*, *129*(7), 1415–1426.

Liu, H., Sadygov, R. G., & Yates, J. R. (2004). A model for random sampling and estimation of relative protein abundance in shotgun proteomics. *Anal Chem*, *76*(14), 4193–4201.

Liu, Y. F., Deth, R. C., & Devys, D. (1997). SH3 domain-dependent association of huntingtin with epidermal growth factor receptor signaling complexes. *J Biol Chem*, *272*(13), 8121–8124.

Lunkes, A., & Mandel, J. L. (1998). A cellular model that recapitulates major pathogenic steps of Huntington's disease. *Hum Mol Genet*, *7*(9), 1355–1361.

Lunkes, A., Lindenberg, K. S., Ben-Haiem, L., Weber, C., Devys, D., Landwehrmeyer, G. B., Mandel, J. L., et al. (2002). Proteases acting on mutant huntingtin generate cleaved products that differentially build up cytoplasmic and nuclear inclusions. *Mol Cell*, *10*(2), 259–269.

Luthi-Carter, R., Taylor, D. M., Pallos, J., Lambert, E., Amore, A., Parker, A., Moffitt, H., et al. (2010). SIRT2 inhibition achieves neuroprotection by decreasing sterol biosynthesis. *Proc Natl Acad Sci U S A*, *107*(17), 7927–7932.

Major, M. B., Camp, N. D., Berndt, J. D., Yi, X., Goldenberg, S. J., Hubbert, C., Biechele, T. L., et al. (2007). Wilms tumor suppressor WTX negatively regulates WNT/beta-catenin signaling. *Science*, *316*(5827), 1043–1046.
Mangiarini, L., Sathasivam, K., Seller, M., Cozens, B., Harper, A., Hetherington, C., Lawton, M., et al. (1996). Exon 1 of the HD gene with an expanded CAG repeat is sufficient to cause a progressive neurological phenotype in transgenic mice. *Cell*, *87*(3), 493–506.
Martindale, D., Hackam, A., Wieczorek, A., Ellerby, L., Wellington, C., McCutcheon, K., Singaraja, R., et al. (1998). Length of huntingtin and its polyglutamine tract influences localization and frequency of intracellular aggregates. *Nat Genet*, *18*(2), 150–154.
Masuda, N., Peng, Q., Li, Q., Jiang, M., Liang, Y., Wang, X., Zhao, M., et al. (2008). Tiagabine is neuroprotective in the N171-82Q and R6/2 mouse models of Huntington's disease. *Neurobiol Dis*, *30*(3), 293–302.
Maxwell, M. M., Tomkinson, E. M., Nobles, J., Wizeman, J. W., Amore, A. M., Quinti, L., Chopra, V., et al. (2011). The Sirtuin 2 microtubule deacetylase is an abundant neuronal protein that accumulates in the aging CNS. *Hum Mol Genet*, *20*(20), 3986–3996.
Menalled, L., El-Khodor, B., M, P., Suarez-Farinas, M., Orenstein, S., B, Z., Leahy, C., et al. (2009). Systematic behavioral evaluation of Huntington's disease transgenic and knock-in mouse models. *Neurobiology of Disease*, *35*(3), 319–336.
Mende-Mueller, L. M., Toneff, T., Hwang, S. R., Chesselet, M. F., & Hook, V. Y. (2001). Tissue-specific proteolysis of Huntingtin (htt) in human brain: evidence of enhanced levels of N- and C-terminal htt fragments in Huntington's disease striatum. *J Neurosci*, *21*(6), 1830–1837.
Miller, J. A., Oldham, M. C., & Geschwind, D. H. (2008). A systems level analysis of transcriptional changes in Alzheimer's disease and normal aging. *J Neurosci*, *28*(6), 1410–1420.
Miller, J. P., Holcomb, J., Al-Ramahi, I., de Haro, M., Gafni, J., Zhang, N., Kim, E., et al. (2010). Matrix metalloproteinases are modifiers of huntingtin proteolysis and toxicity in Huntington's disease. *Neuron*, *67*(2), 199–212.
Mitsui, K., Doi, H., & Nukina, N. (2006). Proteomics of polyglutamine aggregates. *Methods Enzymol*, *412*, 63–76.
Mitsui, K., Nakayama, H., Akagi, T., Nekooki, M., Ohtawa, K., Takio, K., Hashikawa, T., et al. (2002). Purification of polyglutamine aggregates and identification of elongation factor-1alpha and heat shock protein 84 as aggregate-interacting proteins. *J Neurosci*, *22*(21), 9267–9277.
Morrison, D. K. (2009). The 14-3-3 proteins: integrators of diverse signaling cues that impact cell fate and cancer development. *Trends Cell Biol*, *19*(1), 16–23.
Muchowski, P. J., Schaffar, G., Sittler, A., Wanker, E. E., Hayer-Hartl, M. K., & Hartl, F. U. (2000). Hsp70 and hsp40 chaperones can inhibit self-assembly of polyglutamine proteins into amyloid-like fibrils. *Proc Natl Acad Sci U S A*, *97*(14), 7841–7846.
Nollen, E. A. A., Garcia, S. M., van Haaften, G., Kim, S., Chavez, A., Morimoto, R. I., & Plasterk, R. H. A. (2004). Genome-wide RNA interference screen identifies previously undescribed regulators of polyglutamine aggregation. *Proc Natl Acad Sci U S A*, *101*(17), 6403–6408.
Nucifora, L. G., Burke, K. A., Feng, X., Arbez, N., Zhu, S., Miller, J., Yang, G., et al. (2012). Identification of novel potentially toxic oligomers formed in vitro from mammalian-derived expanded huntingtin exon-1 protein. *J Biol Chem*.
Oldham, M. C., Konopka, G., Iwamoto, K., Langfelder, P., Kato, T., Horvath, S., & Geschwind, D. H. (2008). Functional organization of the transcriptome in human brain. *Nat Neurosci*, *11*(11), 1271–1282.
Omi, K., Hachiya, N. S., Tanaka, M., Tokunaga, K., & Kaneko, K. (2008). 14-3-3zeta is indispensable for aggregate formation of polyglutamine-expanded huntingtin protein. *Neurosci Lett*, *431*(1), 45–50.
Orr, H. T., & Zoghbi, H. Y. (2007). Trinucleotide repeat disorders. *Annu Rev Neurosci*, *30*, 575–621.
Pal, A., Severin, F., Lommer, B., Shevchenko, A., & Zerial, M. (2006). Huntingtin-HAP40 complex is a novel Rab5 effector that regulates early endosome motility and is up-regulated in Huntington's disease. *J Cell Biol*, *172*(4), 605–618.
Pallos, J., Bodai, L., Lukacsovich, T., Purcell, J. M., Steffan, J. S., Thompson, L. M., & Marsh, J. L. (2008). Inhibition of specific HDACs and sirtuins suppresses pathogenesis in a Drosophila model of Huntington's disease. *Hum Mol Genet*, *17*(23), 3767–3775.

Passani, L. A., Bedford, M. T., Faber, P. W., McGinnis, K. M., Sharp, A. H., Gusella, J. F., Vonsattel, J. P., et al. (2000). Huntingtin's WW domain partners in Huntington‘s disease post-mortem brain fulfill genetic criteria for direct involvement in Huntington’s disease pathogenesis. *Hum Mol Genet*, *9*(14), 2175–2182.

Peters, M. F., & Ross, C. A. (2001). Isolation of a 40-kDa Huntingtin-associated protein. *J Biol Chem*, *276*(5), 3188–3194.

Pollitt, S. K., Pallos, J., Shao, J., Desai, U. A., Ma, A. A. K., Thompson, L. M., Marsh, J. L., et al. (2003). A rapid cellular FRET assay of polyglutamine aggregation identifies a novel inhibitor. *Neuron*, *40*(4), 685–694.

Rangone, H., Poizat, G., Troncoso, J., Ross, C. A., MacDonald, M. E., Saudou, F., & Humbert, S. (2004). The serum- and glucocorticoid-induced kinase SGK inhibits mutant huntingtin-induced toxicity by phosphorylating serine 421 of huntingtin. *Eur J Neurosci*, *19*(2), 273–279.

Ratovitski, T., Gucek, M., Jiang, H., Chighladze, E., Waldron, E., D'Ambola, J., Hou, Z., et al. (2009). Mutant huntingtin N-terminal fragments of specific size mediate aggregation and toxicity in neuronal cells. *J Biol Chem*, *284*(16), 10855–10867.

Ratovitski, T., Nakamura, M., D'Ambola, J., Chighladze, E., Liang, Y., Wang, W., Graham, R., et al. (2007). N-terminal proteolysis of full-length mutant huntingtin in an inducible PC12 cell model of Huntington's disease. *Cell Cycle*, *6*(23), 2970–2981.

Ravasz, E., Somera, A. L., Mongru, D. A., Oltvai, Z. N., & Barabási, A. L. (2002). Hierarchical organization of modularity in metabolic networks. *Science*, *297*(5586), 1551–1555.

Raymond, L. A., Andre, V. M., Cepeda, C., Gladding, C. M., Milnerwood, A. J., & Levine, M. S. (2011). Pathophysiology of Huntington's disease: time-dependent alterations in synaptic and receptor function. *Neuroscience*, *198*, 252–273.

Reiner, A., Albin, R. L., Anderson, K. D., D'Amato, C. J., Penney, J. B., & Young, A. B. (1988). Differential loss of striatal projection neurons in Huntington disease. *Proc Natl Acad Sci U S A*, *85*(15), 5733–5737.

Rockabrand, E., Slepko, N., Pantalone, A., Nukala, V., Kazantsev, A., Marsh, J., PG, S., et al. (2007). The first 17 amino acids of Huntingtin modulate its sub-cellular localization, aggregation and effects on calcium homeostasis. *Human Molecular Genetics*, *16*(1), 61–77.

Ross, C. A., & Poirier, M. A. (2004). Protein aggregation and neurodegenerative disease. *Nat Med*, *10 Suppl*, S10–7.

Sahlender, D. A., Roberts, R. C., Arden, S. D., Spudich, G., Taylor, M. J., Luzio, J. P., Kendrick-Jones, J., et al. (2005). Optineurin links myosin VI to the Golgi complex and is involved in Golgi organization and exocytosis. *J Cell Biol*, *169*(2), 285–295.

Scherzinger, E., Lurz, R., Turmaine, M., Mangiarini, L., Hollenbach, B., Hasenbank, R., Bates, G. P., et al. (1997). Huntingtin-encoded polyglutamine expansions form amyloid-like protein aggregates in vitro and in vivo. *Cell*, *90*(3), 549–558.

Schilling, B., Gafni, J., Torcassi, C., Cong, X., Row, R. H., LaFevre-Bernt, M. A., Cusack, M. P., et al. (2006). Huntingtin phosphorylation sites mapped by mass spectrometry. Modulation of cleavage and toxicity. *J Biol Chem*, *281*(33), 23686–23697.

Schilling, G., Becher, M. W., Sharp, A. H., Jinnah, H. A., Duan, K., Kotzuk, J. A., Slunt, H. H., et al. (1999). Intranuclear inclusions and neuritic aggregates in transgenic mice expressing a mutant N-terminal fragment of huntingtin. *Hum Mol Genet*, *8*(3), 397–407.

Schilling, G., Klevytska, A., Tebbenkamp, A. T., Juenemann, K., Cooper, J., Gonzales, V., Slunt, H., et al. (2007). Characterization of huntingtin pathologic fragments in human Huntington disease, transgenic mice, and cell models. *J Neuropathol Exp Neurol*, *66*(4), 313–320.

Shao, J., Welch, W. J., & Diamond, M. I. (2008a). ROCK and PRK-2 mediate the inhibitory effect of Y-27632 on polyglutamine aggregation. *FEBS Lett*, *582*(12), 1637–1642.

Shao, J., Welch, W. J., Diprospero, N. A., & Diamond, M. I. (2008b). Phosphorylation of profilin by ROCK1 regulates polyglutamine aggregation. *Mol Cell Biol*, *28*(17), 5196–5208.

Sherman, M. Y., & Goldberg, A. L. (2001). Cellular defenses against unfolded proteins: a cell biologist thinks about neurodegenerative diseases. *Neuron*, *29*(1), 15–32.

Sieradzan, K. A., Mechan, A. O., Jones, L., Wanker, E. E., Nukina, N., & Mann, D. M. (1999). Huntington's disease intranuclear inclusions contain truncated, ubiquitinated huntingtin protein. *Exp Neurol*, *156*(1), 92–99.

Silva, M. C., Fox, S., Beam, M., Thakkar, H., Amaral, M. D., & Morimoto, R. I. (2011). A genetic screening strategy identifies novel regulators of the proteostasis network. *PLoS Genet*, *7*(12), e1002438.
Sittler, A., Walter, S., Wedemeyer, N., Hasenbank, R., Scherzinger, E., Eickhoff, H., Bates, G. P., et al. (1998). SH3GL3 associates with the Huntingtin exon 1 protein and promotes the formation of polygln-containing protein aggregates. *Mol Cell*, *2*(4), 427–436.
Smith, R., Klein, P., Koc-Schmitz, Y., Waldvogel, H. J., Faull, R. L., Brundin, P., Plomann, M., et al. (2007). Loss of SNAP-25 and rabphilin 3a in sensory-motor cortex in Huntington's disease. *J Neurochem*, *103*(1), 115–123.
Snyder-Keller, A., McLear, J. A., Hathorn, T., & Messer, A. (2010). Early or late-stage anti-N-terminal Huntingtin intrabody gene therapy reduces pathological features in B6.HDR6/1 mice. *J Neuropathol Exp Neurol*, *69*(10), 1078–1085.
Song, C., Perides, G., & Liu, Y. F. (2002). Expression of full-length polyglutamine-expanded Huntingtin disrupts growth factor receptor signaling in rat pheochromocytoma (PC12) cells. *J Biol Chem*, *277*(8), 6703–6707.
Southwell, A. L., Khoshnan, A., Dunn, D. E., Bugg, C. W., Lo, D. C., & Patterson, P. H. (2008). Intrabodies binding the proline-rich domains of mutant huntingtin increase its turnover and reduce neurotoxicity. *J Neurosci*, *28*(36), 9013–9020.
Steffan, J. S., Agrawal, N., Pallos, J., Rockabrand, E., Trotman, L. C., Slepko, N., Illes, K., et al. (2004). SUMO modification of Huntingtin and Huntington's disease pathology. *Science*, *304*(5667), 100–104.
Subramaniam, S., Sixt, K. M., Barrow, R., & Snyder, S. H. (2009). Rhes, a striatal specific protein, mediates mutant-huntingtin cytotoxicity. *Science*, *324*(5932), 1327–1330.
Sugars, K. L., Brown, R., Cook, L. J., Swartz, J., & Rubinsztein, D. C. (2004). Decreased cAMP response element-mediated transcription: an early event in exon 1 and full-length cell models of Huntington's disease that contributes to polyglutamine pathogenesis. *J Biol Chem*, *279*(6), 4988–4999.
Suhr, S. T., Senut, M. C., Whitelegge, J. P., Faull, K. F., Cuizon, D. B., & Gage, F. H. (2001). Identities of sequestered proteins in aggregates from cells with induced polyglutamine expression. *J Cell Biol*, *153*(2), 283–294.
Sun, Y., Savanenin, A., Reddy, P. H., & Liu, Y. F. (2001). Polyglutamine-expanded huntingtin promotes sensitization of N-methyl-D-aspartate receptors via post-synaptic density 95. *J Biol Chem*, *276*(27), 24713–24718.
Tam, S., Geller, R., Spiess, C., & Frydman, J. (2006). The chaperonin TRiC controls polyglutamine aggregation and toxicity through subunit-specific interactions. *Nat Cell Biol*, *8*(10), 1155–1162.
Tam, S., Spiess, C., Auyeung, W., Joachimiak, L., Chen, B., Poirier, M., & Frydman, J. (2009). The chaperonin TRiC blocks a huntingtin sequence element that promotes the conformational switch to aggregation. *Nat Struct Mol Biol*, *16*(12), 1279–1285.
Tanaka, Y., Igarashi, S., Nakamura, M., Gafni, J., Torcassi, C., Schilling, G., Crippen, D., et al. (2006). Progressive phenotype and nuclear accumulation of an amino-terminal cleavage fragment in a transgenic mouse model with inducible expression of full-length mutant huntingtin. *Neurobiol Dis*, *21*(2), 381–391.
Tang, B., Becanovic, K., Desplats, P. A., Spencer, B., Hill, A. M., Connolly, C., Masliah, E., et al. (2012). Forkhead box protein p1 is a transcriptional repressor of immune signaling in the CNS; implications for transcriptional dysregulation in Huntington disease. *Hum Mol Genet*.
Thakur, A., Jayaraman, M., Mishra, R., Thakur, M., Chellgren, V., Byeon, I., Anjum, D., et al. (2009). Polyglutamine disruption of the huntingtin exon 1 N terminus triggers a complex aggregation mechanism. *Nat Struc Mol Biol*, *16*(4), 380–389.
The Huntington's Disease Collaborative Research Group. (1993). A novel gene containing a trinucleotide repeat that is expanded and unstable on Huntington's disease chromosomes. *Cell*, *72*(6), 971–983.
Thompson, L., Aiken, C., Kaltenbach, L., Agrawal, N., Illes, K., Khoshnan, A., Martinez-Vicente, M., et al. (2009). IKK phosphorylates Huntingtin and targets it for degradation by the proteasome and lysosome. *J Cell Biol*, *187*(7), 1083–1099.
Toledo, E. M., Colombres, M., & Inestrosa, N. C. (2008). Wnt signaling in neuroprotection and stem cell differentiation. *Prog Neurobiol*, *86*(3), 281–296.
Vidal, M., Cusick, M. E., & Barabási, A.-L. (2011). Interactome networks and human disease. *Cell*, *144*(6), 986–998.

Vis, J. C., Nicholson, L. F., Faull, R. L., Evans, W. H., Severs, N. J., & Green, C. R. (1998). Connexin expression in Huntington's diseased human brain. *Cell Biol Int*, *22*(11-12), 837–847.
Voineagu, I., Wang, X., Johnston, P., Lowe, J. K., Tian, Y., Horvath, S., Mill, J., et al. (2011). Transcriptomic analysis of autistic brain reveals convergent molecular pathology. *Nature*, *474*(7351), 380–384.
Vonsattel, J. P., & Difiglia, M. (1998). Huntington disease. *J Neuropathol Exp Neurol*, *57*(5), 369–384.
Vonsattel, J. P., Myers, R. H., Stevens, T. J., Ferrante, R. J., Bird, E. D., & Richardson, E. P. J. (1985). Neuropathological classification of Huntington's disease. *J Neuropathol Exp Neurol*, *44*(6), 559–577.
Wacker, J. L., Huang, S.-Y., Steele, A. D., Aron, R., Lotz, G. P., Nguyen, Q., Giorgini, F., et al. (2009). Loss of Hsp70 exacerbates pathogenesis but not levels of fibrillar aggregates in a mouse model of Huntington's disease. *J Neurosci*, *29*(28), 9104–9114.
Waldron-Roby, E., Ratovitski, T., Wang, X., Jiang, M., Watkin, E., Arbez, N., Graham, R. K., et al. (2012). Transgenic mouse model expressing the caspase 6 fragment of mutant huntingtin. *J Neurosci*, *32*(1), 183–193.
Wang, Yan, Meriin, A. B., Zaarur, N., Romanova, N. V., Chernoff, Y. O., Costello, C. E., & Sherman, M. Y. (2009). Abnormal proteins can form aggresome in yeast: aggresome-targeting signals and components of the machinery. *FASEB J*, *23*(2), 451–463.
Wang, Yu, Steimle, P. A., Ren, Y., Ross, C. A., Robinson, D. N., Egelhoff, T. T., Sesaki, H., et al. (2011). Dictyostelium huntingtin controls chemotaxis and cytokinesis through the regulation of myosin II phosphorylation. *Mol Biol Cell*, *22*(13), 2270–2281.
Warby, S. C., Chan, E. Y., Metzler, M., Gan, L., Singaraja, R. R., Crocker, S. F., Robertson, H. A., et al. (2005). Huntingtin phosphorylation on serine 421 is significantly reduced in the striatum and by polyglutamine expansion in vivo. *Hum Mol Genet*, *14*(11), 1569–1577.
Waza, M., Adachi, H., Katsuno, M., Minamiyama, M., Sang, C., Tanaka, F., Inukai, A., et al. (2005). 17-AAG, an Hsp90 inhibitor, ameliorates polyglutamine-mediated motor neuron degeneration. *Nat Med*, *11*(10), 1088–1095.
Wellington, C. L., & Hayden, M. R. (2000). Caspases and neurodegeneration: on the cutting edge of new therapeutic approaches. *Clin Genet*, *57*(1), 1–10.
Wellington, C. L., Ellerby, L. M., Gutekunst, C. A., Rogers, D., Warby, S., Graham, R. K., Loubser, O., et al. (2002). Caspase cleavage of mutant huntingtin precedes neurodegeneration in Huntington's disease. *J Neurosci*, *22*(18), 7862–7872.
Wetzel, R. (2012). Physical Chemistry of Polyglutamine: Intriguing Tales of a Monotonous Sequence. *J Mol Biol*.
Wexler, E. M., Rosen, E., Lu, D., Osborn, G. E., Martin, E., Raybould, H., & Geschwind, D. H. (2011). Genome-wide analysis of a Wnt1-regulated transcriptional network implicates neurodegenerative pathways. *Sci Signal*, *4*(193), ra65.
Yanai, A., Huang, K., Kang, R., Singaraja, R. R., Arstikaitis, P., Gan, L., Orban, P. C., et al. (2006). Palmitoylation of huntingtin by HIP14 is essential for its trafficking and function. *Nat Neurosci*, *9*(6), 824–831.
Yip, A. M., & Horvath, S. (2007). Gene network interconnectedness and the generalized topological overlap measure. *BMC Bioinformatics*, *8*, 22.
Zeitlin, S., Liu, J. P., Chapman, D. L., Papaioannou, V. E., & Efstratiadis, A. (1995). Increased apoptosis and early embryonic lethality in mice nullizygous for the Huntington's disease gene homologue. *Nat Genet*, *11*(2), 155–163.
Zeron, M. M., Hansson, O., Chen, N., Wellington, C. L., Leavitt, B. R., Brundin, P., Hayden, M. R., et al. (2002). Increased sensitivity to N-methyl-D-aspartate receptor-mediated excitotoxicity in a mouse model of Huntington's disease. *Neuron*, *33*(6), 849–860.
Zhang, B., & Horvath, S. (2005). A general framework for weighted gene co-expression network analysis. *Stat Appl Genet Molec Biol*, *4*, Article17.
Zhang, S., Binari, R., Zhou, R., & Perrimon, N. (2010). A genomewide RNA interference screen for modifiers of aggregates formation by mutant Huntingtin in Drosophila. *Genetics*, *184*(4), 1165–1179.
Zoghbi, H. Y., & Orr, H. T. (2000). Glutamine repeats and neurodegeneration. *Annu Rev Neurosci*, *23*, 217–247.

Zuccato, C., Ciammola, A., Rigamonti, D., Leavitt, B. R., Goffredo, D., Conti, L., MacDonald, M. E., et al. (2001). Loss of huntingtin-mediated BDNF gene transcription in Huntington's disease. *Science*, *293*(5529), 493–498.